

# H $\alpha$ emitters from the Southern Photometric Local Universe Survey (S-PLUS)

L. A. Gutiérrez-Soto,<sup>1</sup>  R. Lopes de Oliveira<sup>1,2,3</sup>

<sup>1</sup>Departamento de Astronomia, IAG, Universidade de São Paulo, Rua do Matão, 1226, 05509-900, São Paulo, Brazil

<sup>2</sup>Departamento de Física, Universidade Federal de Sergipe, Av. Marechal Rondon, S/N, 49100-000, São Cristóvão, SE, Brazil

<sup>3</sup>Observatório Nacional, Rua Gal. José Cristino 77, 20921-400, Rio de Janeiro, RJ, Brazil

Accepted XXX. Received YYY; in original form ZZZ

## ABSTRACT

In the way to map 9000 deg<sup>2</sup> of the Southern hemisphere, the S-PLUS project is also surveying the sky in a proxy of a myriad of astrophysical processes: the H $\alpha$  transition. Here we explore such a capability from its DR3 to make H $\alpha$  emitters in evidence from the ( $r - J$ 0660) versus ( $r - i$ ) color-color diagram and distinguish the red from the blue ones by exploring the ( $r - i$ ) and ( $g - z$ ) diagram. Our catalog is composed of 9,200 objects that exhibit excess in the narrow J0660 band which is consistent with H $\alpha$  in emission. Unsupervised, clustering machine learning approach revealed two distinct populations: one with an intense blue continuum and another with a red one. The hierarchical clustering algorithm was compared with the HDBSCAN. By adopting a “soft” clustering approach, we assigned the probability of each emitter belonging to a given population, blue or red clusters. We use synthetic and observed (SDSS) spectra to emphasize the potential of color-color diagrams to distinguish several classes of emission line emitters that include planetary nebulae, H II regions, young stellar objects, symbiotic stellar systems, cataclysmic variables, blue compact galaxies, star-forming galaxies, and quasars, and trace the way to reveal new ones with S-PLUS data.

**Key words:** surveys – stars: emission-line, Be – novae, cataclysmic variables – galaxies: dwarf – quasars: emission lines

## 1 INTRODUCTION

Atomic excitation followed by recombination in Balmer hydrogen emission lines may be ignited in many different ways, from thermal and non-thermal collisional excitation in shock-heated gas, and from energetic photons acting over a diffuse gas. As a practical result, and the Universe being Hydrogen abundant, the observation of those electronic transitions offer an important window into the study of astrophysical objects. Among them, the Balmer lines represent extremely useful tools in Astronomy and in particular the red H $\alpha$  line (which has rest-frame wavelength of @6564.614 Å at vacuum), that corresponds to the electron transition from the  $n = 3$  to the  $n = 2$  energy level, is the most widely used to identify astronomical systems, given that it is the strongest. They are common in the spectra of star-forming regions and around extended planetary nebulae and supernova remnants, allowing the investigation of these and a number of other systems.

Emission lines trace discs (Schwöpe et al. 2000; Ratti et al. 2012) in stellar and extragalactic systems, including their geometrical characteristics from line profiles (Horne & Marsh 1986). Some short-lived evolutionary stages of stars may also be marked by emission lines. This category includes young stellar (YSOs) and Herbig-Haro (HH) objects surrounded by a nebula-like structure, evolved systems like post-asymptotic and some asymptotic giant branch (AGB), some red giant stars (RGB), active late-type dwarfs, and supernova remnants.

Amongst massive stars, emission lines are observed, for example, in Be stars when circumstellar decretion disks are present and in Wolf-Rayet (WR) stars, which are marked by strong winds. Interacting binary systems experiencing mass exchange, like symbiotic stars (SySt) in which a white dwarf (WD) or a neutron star accretes matter from a supergiant star, and Cataclysmic Variables (CVs), pairs of white dwarf plus a low mass star, may be added to this category. Emission lines in Planetary Nebulae (PNe) allow the study of the remnant envelope of dying stars, illuminated by their residual white dwarf.

At much larger scales, emission line objects such as H II regions, around regions with young stars, allow us to map and study the star formation history of the far reaches of our Galaxy and of distant galaxies. Emission lines in general (not necessarily Halpha) in starburst galaxies and QSOs, the most luminous objects, allow us to probe conditions when the Universe was young, in particular the first generations of stars and the primordial formation of heavy elements.

Most of the classes mentioned above are not homogeneous and far from complete even in the local Universe, with some being highly populated while others less so. For example, there are ~320 SySt known, with only ~65 out of them harbored in galaxies other than the Milky Way (Akras et al. 019a). The number of known PNe in our Galaxy is higher, with 3500 objects listed in catalogs (Parker et al. 2016), but it is argued that it represents only about 15-30% of the total expected in the Galaxy (Frew, 2008; Jacoby et al., 2010).

Many H $\alpha$  surveys in a variety of angular resolution, sky coverage, and sensitivity have been carried out. Some of them, with modest spa-

\* E-mail: gsoto.angel@gmail.com

tial resolutions, revealed spatially resolved, extended nebular emission to study supernova remnants, galaxy groups, and star forming regions (e.g. Davies et al. 1976). Others with higher spatial resolution disclosed compact emission-line sources in the Galaxy and sources in nearby galaxies. Examples are the INT Photometric H $\alpha$  survey (IPHAS; Drew et al. 2005; Barentsen et al. 2014), the SuperCOSMOS H $\alpha$  Survey with the UK Schmidt Telescope (UKST) of the Anglo-Australian Observatory (Parker et al. 2005), and the ongoing VST Photometric H $\alpha$  Survey (VPHAS+; Drew et al. 2014).

Traditionally, H $\alpha$  emitters are revealed directly from images and in color-color diagrams from photometric surveys observing the sky with at most five - generally broad-band or H $\alpha$  - filters. For example, the ( $r$  - H $\alpha$ ) versus ( $r$  -  $i$ ) colour-colour diagram or similar was used to find new CVs (Witham et al. 2006, 2007), YSOs (Vink et al. 2008), SySt (Corradi et al. 2008; Corradi & Giammanco 2010; Corradi et al. 2011), early-type emission-line stars (Drew et al. 2008), and PNe (Viironen et al. 2009; Sabin et al. 2010).

There are two new ongoing multi-band surveys observing the sky in a systematic, complementary way, with 5 broad and 7 narrow-band filters, including H $\alpha$ : the Javalambre Photometric Local Universe Survey (J-PLUS<sup>1</sup>; Cenarro et al. 2018), covering the Northern celestial hemisphere, and the Southern-Photometric Local Universe Survey (S-PLUS<sup>2</sup>; Mendes de Oliveira et al. 2019), doing the same to the Southern sky with a twin 80 cm telescope. They are paving the way for an even more ambitious survey, the Javalambre Physics of the Accelerating Universe Astrophysical Survey (J-PAS), which will observe the Northern sky with 56 narrow-band filters. As source hunters, the spectral energy distribution provided by these surveys also provide an unprecedented classification from photometry. However, as part of the new era of big data, efficient investigation tools are required to deal with their massive data sets and machine learning techniques have been increasingly used.

Here we present H $\alpha$  emitters from the S-PLUS iDR3 by using color-color diagrams and unsupervised machine learning techniques, classifying them as blue or red fonts and also proposing a class to which they belong. Section 2.1 describes the observations related to S-PLUS project, as well as important information of the third data release, section 2 presents the technique implemented to select the H $\alpha$  emitters and machine learning approaches used to divide the sample in two populations based in their colors, in section 3 the results and our findings are discussed and finally section 4 discusses our study and conclusions.

## 2 METHODOLOGY

### 2.1 Observations: The S-PLUS project

This paper uses data from S-PLUS, a photometric sky map being carried out since end of 2017 using a 0.83m robotic telescope located at Cerro Tololo, Chile (Mendes de Oliveira et al. 2019). The project is surveying the Southern sky with 12 filters from the Javalambre filter system (Marín-Franch et al. 2012) spanning the wavelength range from 3000Å to 10000Å. The filters used are seven narrow-band filters ( $J0378$ ,  $J0395$ ,  $J0410$ ,  $J0430$ ,  $J0515$ ,  $J0660$ , and  $J0861$ ) and five broad-band Sloan-like (Fukugita et al. 1996) filters ( $u$ ,  $g$ ,  $r$ ,  $i$  and  $z$ ). The narrow-band  $J0660$  filter covers the H $\alpha$  plus the [N II] spectral lines for sources up to redshift of approximately 0.02 (see Fig. 1 after Marín-Franch et al. 2012).

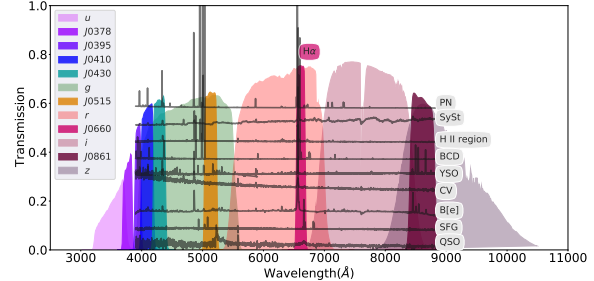


**Figure 1.** Transmission curves of the S-PLUS filter set. The narrow-band filter  $J0660$  includes the H $\alpha$  emission line. Over-plotted are spectra of different classes of emission line objects. From top to bottom: a PN, a symbiotic star, an extragalactic H II region, a blue compact/H II galaxy, a YSO, a CV star, a B[e] star, a star forming galaxy and a QSO with a redshift of XX.

The S-PLUS data used here are those of the third data release (DR3). It is composed by about 60 million objects distributed over  $\sim 2,000 \text{ deg}^2$  (out of the  $\sim 8,000 \text{ deg}^2$  of sky, at high Galactic latitudes,  $> 30 \text{ deg}$ , that are planned to be done by S-PLUS by its completion). No area from the Galactic disk and bulge were included in this study (S-PLUS plans to cover  $\sim 1,300 \text{ deg}^2$  of such areas), given that these will be available only in Dr4. In order to ensure that the best data are used, we consider only objects which were detected at least in the  $r$ ,  $i$  and  $J0660$  bands, with errors less than 0.2 mag.

The first goal of this paper is to identify objects that may be bona-fide H $\alpha$  emitters among sources detected in the S-PLUS DR2. For this, we applied an iterative and automatic technique to select objects with an excess in the  $J0660$  band, which is consistent with the detection of the H $\alpha$  line in emission. Next, the selected objects were separated into two groups, one having redder and the other bluer emission. This classification was done by using optical colors in combination with unsupervised machine learning/statistical tools. These procedures are described in the following sections.

### 2.2 Finding the main stellar locus and selecting the H $\alpha$ emitters

Before applying the method, which is based on the excess in the  $J0660$ -band magnitude with respect to that in the  $r$ -band, we first divided our sample into four sub-samples, splitting the systems according to their magnitudes in the  $r$ -band. In this way, we avoid mixing up bright and faint objects that tend to have low and high uncertainties, respectively, in the same color-color diagram. Otherwise, the selection criteria would be potentially affected by the intrinsic scatter in the measurement of faint objects. We considered the following four sub-samples: (i)  $r$ -band  $< 16$ , (ii)  $16 \leq r < 18$ , (iii)  $18 \leq r < 20$ , and  $20 \leq r < 21$ .

The identification of H $\alpha$  emitters was based on the method applied successfully by (IPHAS Witham et al. 2008) to create the INT/WFC Photometric H $\alpha$  Survey, given that they use filters that are also available in our survey:  $r$ ,  $J0660$ , and  $i$  filters. The same technique was also used by Scaringi et al. (2013) and Wevers et al. (2017) to reveal H $\alpha$  emitters.

We first generated the ( $r$  -  $J0660$ ) versus ( $r$  -  $i$ ) diagram for each magnitude bin and attempted to put in evidence the loci mainly occupied by main-sequence and giant stars with a linear regression fit. We then implemented an iterative  $\sigma$ -clipping technique so that, by construction, H $\alpha$  emitters should satisfy the condition:

$$r - J0660_{\text{obs}} - r - J0660_{\text{fit}} \geq C \times \sqrt{\sigma_s^2 - \sigma_{\text{phot}}^2} \quad (1)$$

<sup>1</sup> <https://www.j-plus.es>

<sup>2</sup> <http://www.splus.iag.usp.br>

where  $\sigma_s$  is the root mean squared value of the residuals around the fit and  $\sigma_{\text{phot}}$  is the error on the observed  $r - J0660$  colour index.  $C$  is a constant which has the value 4 following Wevers et al. (2017). The fits were carried out with the aid of the python library `astropy.modeling`<sup>3</sup>

Figure 2 illustrates the procedure applied. The continuous black lines represent the initial fit and the dashed lines indicate the 4- $\sigma$  clipping fit lines. The dotted lines are the cut selection criteria for the H $\alpha$  emitters – the 4- $\sigma$  above of the final fit. Note that these cut lines are only an approximations because only the residual around the fit is taken into account. Note that the approach includes the photometric uncertainties of the ( $r - J0660$ ) color for each individual data source (see Equation 1).

Once having selected H $\alpha$  emitters, we proceed with a visual inspection of their spectral energy distributions as seen from the whole S-PLUS coverage, namely S-spectra, and their false-color images. For illustration, Figure 3 shows how an H $\alpha$  emitter looks like from the S-PLUS data.

Figure 4 exhibits the distribution of the H $\alpha$  emitters on the ( $r - J0660$ ) versus ( $r - i$ ) color-color plane. It also present the main-sequence and giant stars loci as derived from synthetic spectra collected of Pickles (1998) convolved with the transmission of S-PLUS filters, and defined in the AB magnitude system (Oke & Gunn 1983).

At this point, we can say that the algorithm implemented here worked well because the sources are located above of the loci of the main and giant stars. The wide distribution of fonts across the ( $r - J060$ ) and ( $r - i$ ) colours indicates that several types of objects were selected. For instance, higher values on the ( $r - J0660$ ) color of some sources could be indicating that they are H II regions or/and blue compact galaxies and PNe. On the other hand, the ( $r - i$ ) color indicates the reddened nature of sources such as SySt and young stellar objects or in the opposite case, sources with a strong blue continuum as cataclysm variables and QSOs.

Figure 5 displays the distribution of all emitters in Galactic latitude and longitude. The density map regions represent the spatial positions of the objects on the sky. The surface density of  $J0660$ -excess objects is highest near the Galactic plane.

Once, we felt confident of our sample of H $\alpha$  emission lines sources, we proceeded to classify the objects into two groups; one group containing those objects with a strong blue continuum and another formed by sources with intense emission of the continuum on the red part of the spectra.

### 2.3 Unsupervised machine learning/clustering techniques

Objects of our sample were divided into two groups, distinguishing the bluer from the redder population. To do this, we apply an unsupervised machine learning approach to implement two clustering techniques: hierarchical clustering and hierarchical density-based cluster selection, both based on the  $g - r$  and  $z - g$  colors, whose results were mutually compared.

#### 2.3.1 Hierarchical agglomerative clustering

“Hierarchical clustering” (HC) belongs to the family of clustering algorithms of which clusters are constructed by recursively grouping and splitting the sources. It is an unsupervised algorithm in the sense that it does not require a training sample or pre-conceived hypotheses. From it, individuals are grouped based on patterns in a given space

of parameters and on the levels of similarity at which the groupings change (Jain et al. 1999). In the end, HC allows a diagrammatic representation of groups as a tree diagram, a dendrogram, and thus following a hierarchical structure.

There are two types of hierarchical clustering: the *hierarchical agglomerative clustering* (HAC; the one used in this work), which is “bottom-up” approach, and the *hierarchical divisive clustering*, with a “top-down” approach. The HAC consists of building a binary merge tree, starting from each data element stored at the leaves (interpreted as individual clusters) and proceed by merging two by two the “closest” sub-sets (stored at nodes) until it reaches the root – unique cluster – of the tree that contains all the elements of the data set. The agglomerative term is used because individual data are successively aggregated into higher-level. In each iteration, two “nearby” clusters are selected and collapsed them into a new, more populated group (Mann & Kaur 2013; Aggarwal 2015). Thus, each merging step reduces the number of clusters. The procedure may be summarized in three steps:

- (i) Initially, each individual data point represents one cluster, i.e. “leaves of the tree”. This means that at the beginning, the number of total the clusters is the number of elements of the data set.
- (ii) Through a looping process, the clusters or nodes are merged into groups that have the maximum similarity between them.
- (iii) At the end of the process, all the nodes belong to an unique cluster, “the root of the tree” structure.

In the opposite direction is the other type of hierarchical clustering, the *hierarchical divisive clustering*. Following its “top-down” approach, the investigation starts from data as being in one only cluster then moving down recursively in the hierarchy to small groups. In simple words, hierarchical (agglomerative and divisive) clustering algorithms intend to gather similar objects into groups called clusters or nodes in the space of parameters which is investigated.

#### 2.3.2 Hierarchical density-based cluster selection

Hierarchical density-based cluster selection (HDBSCAN; Campello et al. 2013) is another unsupervised machine learning algorithm that relies on clustering. It is based on a slightly modified version of density-based spatial clustering of applications with noise (DBSCAN; Ester et al. 1996) which declares points as noise. It is an algorithm that assumes clusters that are characterized by “islands” of high density in the sea of the parameter space. Such clusters constitute data partitions that have a higher density than their neighbors (Ntwaetsile & Geach 2021). HDBSCAN takes forward the DBSCAN concept by introducing a hierarchy to the clustering, with “persistent” clusters finally extracted from the hierarchical tree. The main advantage of HDBSCAN in comparison with the predecessor consists in the possibility in finding clusters of variables densities and different shapes. Following Malzer & Baum (2021) and Ntwaetsile & Geach (2021), it works as follows:

- (i) HDBSCAN define the “core” distance for a point  $x$ ,  $\text{core}_k x$ , as the distance of an object to its  $k$ th nearest neighbor. This mean that lower values of  $\text{core}_k x$  represent higher densities and vice-versa.
- (ii) The “mutual readability distance” between two points  $a$  and  $b$  is defined as  $d_{ma,b} \min\{\text{core}_k a, \text{core}_k b, da, db\}$ , where  $da, db$  is the distance between  $a$  and  $b$  according, for instance, Euclidean metric. The mutual readability distance allows points in dense regions to stay close together and those that are in less dense regions to move away.
- (iii) The mutual readability plot is used to construct the minimum spanning tree, and sorting its edges by the mutual readability distance

<sup>3</sup> <https://docs.astropy.org/en/stable/modeling/index.html>

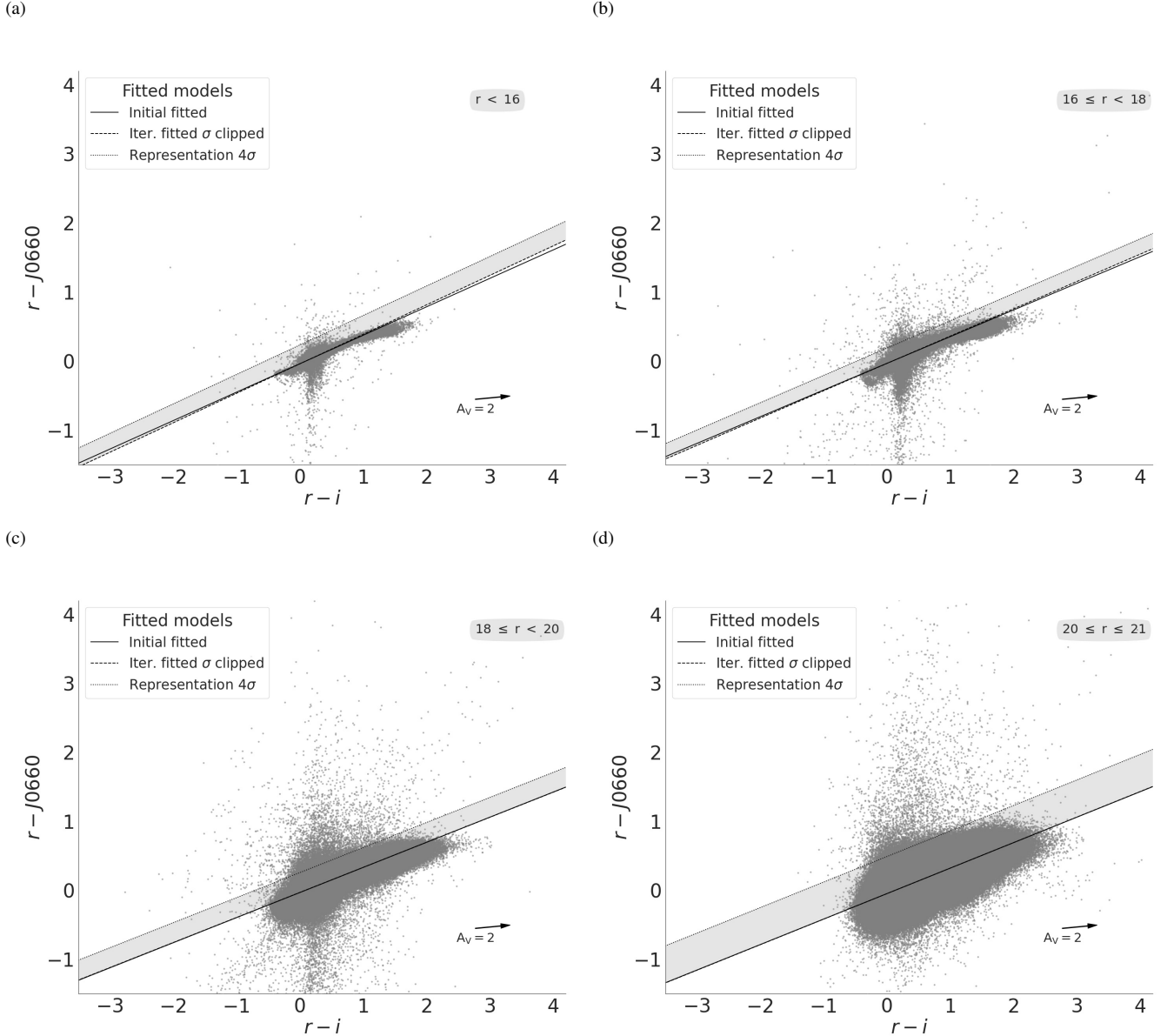


**Figure 2.** An illustration of the selection criteria used to identify strong emission-line objects via colour-colour plots. The data shown here are all from the S-PLUS DR3. The data are split up into four magnitude bins, as shown in the four panels. Objects with H $\alpha$  excess should be located near the top of the colour-colour diagrams. The thin continuous lines illustrate the original linear fit to all the data (grey points). The dashed lines represent the final fits to the stellar locus of points which were obtained by applying an iterative  $\sigma$ -clipping technique to the initial fit. The actual cuts used to select H $\alpha$  emitters are shown by the dotted lines. Objects selected as H $\alpha$  emitters must be located above. Note that the cut lines (selection criteria) shown here are only approximate, as the actual selection criterion also considers the errors on each source. This means that an object could be in the bottom right-hand panel is not selected despite clearly lying above the cut line (EXPLICAR ESTA ÚLTIMA FRASE MEJOR).

resulting in a hierarchical tree structure. The hierarchy of connected components is defined by sorting the edges of the tree by distance in reverse order, describing a dendrogram (this diagram explained in 2.3.1). This is the structure from which the cluster will be identified.

(iv) HDBSCAN allows to extract clusters of variable density, effectively, by cutting the dendrogram at different levels of grouping.

(v) The cluster tree is condensed into a simpler structure (see, for instance, Figure A1 of Appendix A). Considering the single main trunk which contains all the data points, the tree splits into branches. A condensed cluster hierarchy can be described by considering the number of points that are kept in each branch as it splits. It is important

to mention that there is a key parameter called minimum cluster size. If a given branch divides into two, with a branch containing fewer points than the minimum cluster size means, the large branch “persists” and the smaller split branch “falls out” of the cluster. If a branch splits into two with both branches exceeding the minimum cluster size, both new branches are conserved.

(vi) The clusters are extracted on the notion of persistence in the hierarchy. The parameter  $\lambda d_m^{-1}$  is defined, and each cluster has a  $\lambda_{\text{birth}}$  (the point at which the cluster split off) and  $\lambda_{\text{death}}$  (the point when the cluster split into other clusters). In each cluster, we have  $\lambda_p$  describing when each point fell out of the cluster (or was split

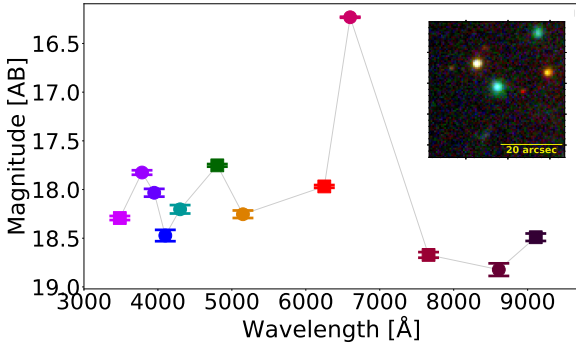


**Figure 3.** S-spectra of a random object with emission lines select with the algorithm explained above. Squares represent the SDSS-like broad-band filters. From left to right they are  $u, g, r, i$  and  $z$ . Circle symbols are the narrow-band filters, which from left to right represent J0378, J0395, J0410, J0515, J0660 and J0861. The inset figure is the coloured image of the object which was produced by combining all twelve bands.

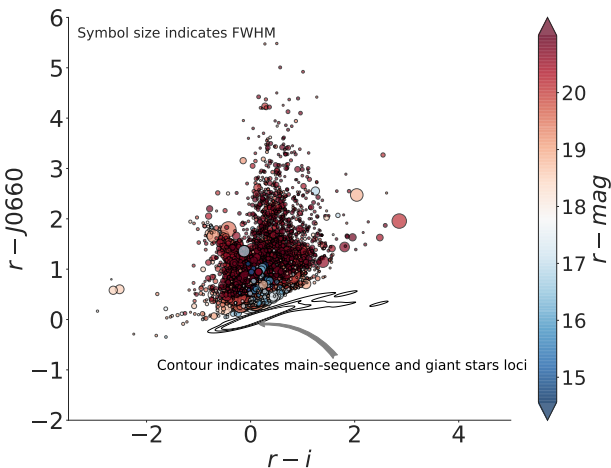


**Figure 4.** Colour-colour diagram with all the emission line objects selected from S-PLUS iDR3. Size of the symbols represent the measured FWHM assuming a Gaussian core (for more detail see Almeida-Fernandes et al. 2021). Coloured bar indicates the magnitude values of the r-band. The contours represent the S-PLUS synthetic photometry of main-sequence and giant stars loci from the library of stellar spectral energy distributions of Pickles (1998).

off into a new cluster), so that  $\lambda_{\text{birth}} \leq \lambda_p \leq \lambda_{\text{death}}$ . Cluster stability  $S$  is defined as the sum of  $\lambda_p - \lambda_{\text{birth}}$  for all points in the cluster. To extract clusters, the following procedure is implemented. First, each leave constitutes a cluster. Then, moving through the hierarchy, it is considered the stability of a parent cluster  $S_p$  and its  $n$  descendants  $S_d^{0,1,2,\dots,n}$ : if  $S_p > \lambda_{\text{birth}}^n S_d^i$ , we unselect all the descendants; otherwise, the cluster stability is set as  $S_p - \lambda_{\text{birth}}^n S_d^i$ . At the root node we have our set of selected cluster. Any point in the sample that does not fall into one of the selected clusters is defined as noise.

(vii) By adopting the soft clustering or fuzzy clustering technique is possible to mitigate the need to establish or define had cluster membership limit. In fact, each source has finite probability of belonging to every selected cluster. In this approach all points (including noises) are not assigned to cluster label, but are instead assigned to

a vector of probabilities, which its length is equal to the number of clusters found. With this can be solved the noise classification.

The HDBSCAN algorithm starts off much the same as DBSCAN: transforming the space according to density, exactly as DBSCAN does, and perform single linkage clustering on the transformed space. Instead of taking an epsilon<sup>4</sup> value as a cut level for the dendrogram, however, a different approach is taken: the dendrogram is condensed by viewing splits that result in a small number of points splitting off as points “falling out of a cluster”. This results in a smaller tree with fewer clusters that “lose points”. That tree can then be used to select the most stable or persistent clusters. This process allows the tree to be cut at varying height, picking our varying density clusters based on cluster stability. The immediate advantage of this is that we can have varying density clusters; the second benefit is that we have eliminated the epsilon parameter as we no longer need it to choose a cut of the dendrogram. Instead we have a new parameter `min_cluster_size` which is used to determine whether points are “falling out of a cluster” or splitting to form two new clusters.

In the last years, HDBSCAN have been used in astronomy for different tasks. Jayasinghe et al. (2019) presented the second data release Milky Way Project (MWP), a citizen science initiative on the Zooniverse platform, presents internet users with infrared (IR) images from Spitzer on which were aggregate  $\sim 3$  million classifications made by volunteers during the years 2012–2017 to produce the DR2 catalogue, which contains 2600 IR bubbles and 599 candidate bow shock driving stars. The reliability of bubble identifications was made by using HDBSCAN. On the other hand, Webb et al. (2020) used HDBSCAN for transient discovery. Recently, Ntwaetsile & Geach (2021) used it to group radio sources into a sequence of morphological classes, illustrating a simple methodology to classify and label new, unseen galaxies in large samples. This approach was also implemented to identify stellar groups in Canis Major OB1 (Santos-Silva et al. 2021).

#### 2.4 Grouping the H $\alpha$ emitters into blue and red colour-types

We adopt the  $g$ ,  $r$ , and  $z$  broad-bands spreading from the blue to the red in the optical to distinguish the blue from the red populations of our sample. In this way, we start by exploiting the  $g - r$  and  $z - g$  colors and the potential of the corresponding diagram to put in evidence different classes of systems.

In order to find the best color-color diagram to separating the final sample of emission line objects into two colour-types, we first attempted to construct color-color diagrams by using the S-PLUS synthetic photometry of several classes of emission line objects.<sup>5</sup> The  $g - r$  versus  $z - g$  color-color diagram is displayed on the Fig. 6. The SySt span a wide range on the  $z - g$  color, from approximately -0.5 to 6.0. This wide range on the color may refer to the different type spectral of the cold stellar component of the binary system. All the YSOs and many SySt are located on the top-left on the diagram indicating a reddening effect of the circumstellar disk for many SySt (for example, for those symbiotic with a Mira star) and YSOs. On the other hand, the PNe, HII regions, CVs, QSOs, and emission line galaxies are located on the lower-right region of the diagram. This

<sup>4</sup> Epsilon parameter in DBSCAN represents the maximum distance between two samples for one to be considered as in the neighborhood of the other. This is the most important DBSCAN parameter to choose appropriately for the data set and distance function.

<sup>5</sup> It is important to note that there are other classes of objects with emission lines that have not been included. Our main objective is to explore different populations and/or types of these objects by using their photometric colors.

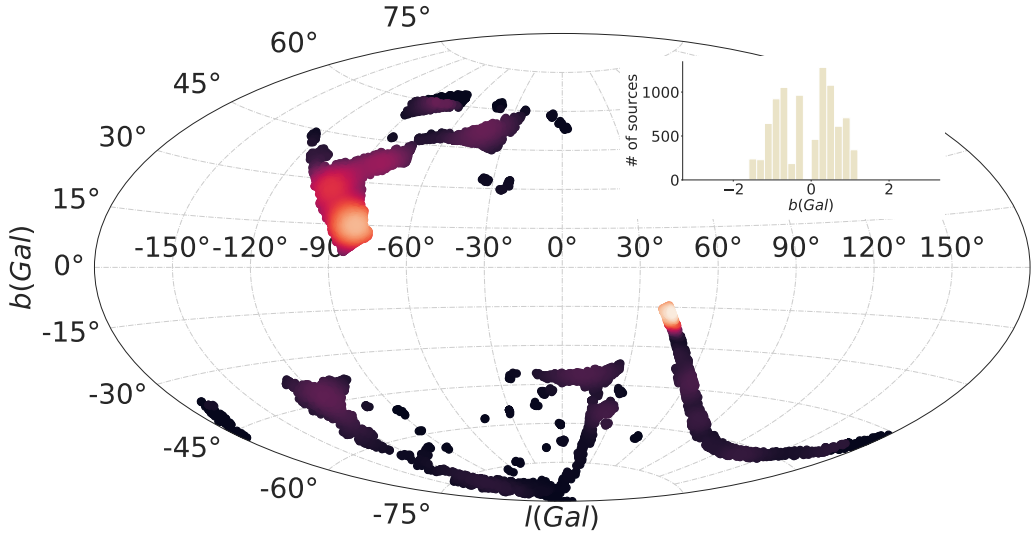


**Figure 5.** Distribution of H $\alpha$  emitters in Galactic longitude and latitude coordinate. Inset figure represents distribution of the objects in Galactic latitude.

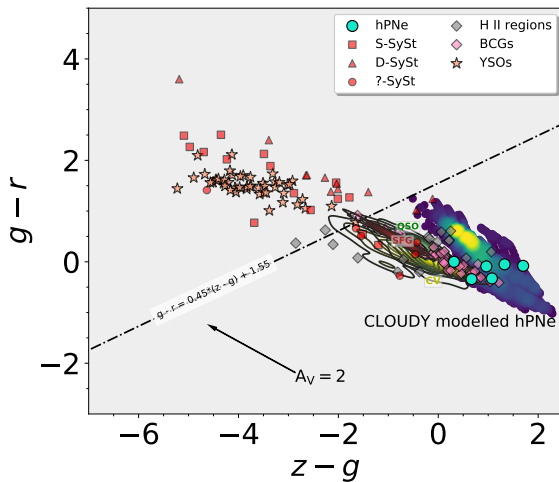


**Figure 6.** The  $g - r$  versus  $z - g$  synthetic color-color diagram of several classes of emission lines objects. Included in the diagrams, there are families of CLOUDY modelled halo PNe spanning a range of properties (density map region). Cyan circles represent S-PLUS photometry from observed spectra. Grey diamonds represent H II regions in NGC 55. Red boxes display symbiotic stars, this group also includes Galactic and external SySt from NGC 205 IC 10 and NGC 185. Yellow circles correspond to cataclysmic variables (CVs) from SDSS. Pink circles indicate blue compact galaxies (BCGs) from SDSS. Orange triangles refer to SDSS star-forming galaxies (SDSS SFGs). SDSS QSOs at different redshift ranges are shown as light blue diamonds, and YSOs from Lupus and Sigma Orionis are represented by salmon stars. The diagonal dashed line represents a subjective criterion to separate the objects into two color types. The arrow indicates the reddening vector with  $AV \approx 2$  mag. MAYBE IS A GOOD IDEA TO PUT THE REDDENED VECTOR OF THIS COLOR-COLOR DIAGRAM.

indicates blue continuum present in each classes of these objects, mainly by the presence of the high excitation component, for instance, white dwarf in planetary nebulae and cataclysm variable systems, and massive young stars in H II regions and starburst galaxies. Although

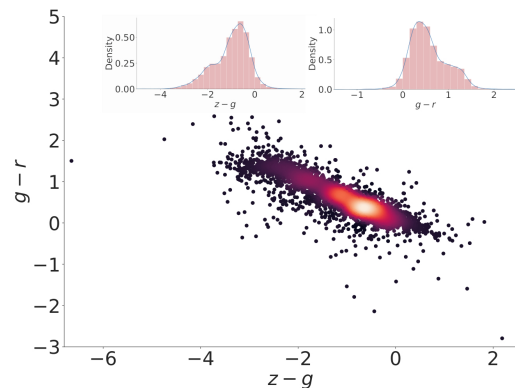


**Figure 7.** The  $g - r$  versus  $z - g$  color-color diagram with all the emission line objects selected in S-PLUS. The inset figures represent the  $g - r$  and  $z - g$  colour distributions.

some SySt are located in the region where appear the blue sources, this color-color diagram seems to separate very well two color types, blue from red sources. The dashed line in Fig. 6 highlights the blue and red zones.

Figure 7 shows the  $g - r$  versus  $z - g$  color-color diagram from our final list of H $\alpha$  emitters. A bimodal, two-color population is suspected by contrast in the CMD and evidenced in the color distributions (see inset plots of the Fig. 7). The two peaks of the  $g - r$  and  $z - g$  distributions have a immediate correspondence with the blue and red zones pointed out from the synthetic color-color diagram (Fig. 6). This histograms also show that the fraction of blue objects is considerable higher than the red ones.

#### 2.4.1 HAC

The ideal way to choose the number of clusters can be done by displaying the **dendrogram diagram**. Firstly, the hierarchical cluster output dendrogram can be implemented to obtain the desired clus-

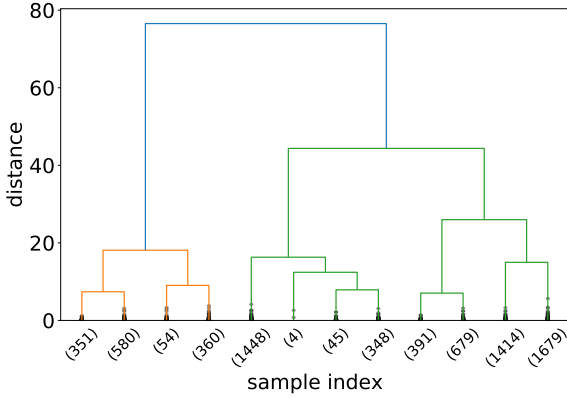


**Figure 8.** Truncated dendrogram of complete-linkage hierarchical clustered based on  $g - r$  and  $z - g$  colours. The cluster sizes are exposed in the brackets for the 12 truncated clusters.

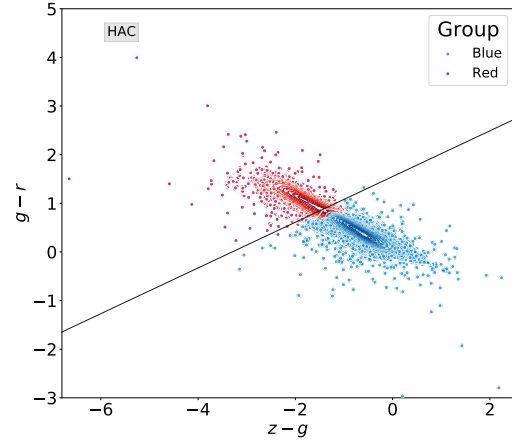
tering. Secondly, the dendrogram schema allows a convenient way to establish the entity-relationship at all levels of granularity.

Figure 8 illustrates the use of a dendrogram based on the  $g - r$  and  $z - g$  colours of H $\alpha$  emitters. It highlights the order and distances of groups in the hierarchical clustering, stopping at 12 nodes:

- The  $x$ -axis specifies the population in the nodes in a given level of grouping – that summed up correspond to the total number of elements under investigation.
- The  $y$ -axis represents the “distance”, which is a measurement of the closeness of the clusters or data points in different levels of clustering.

Reading the diagram from the top to the bottom, we see that all systems are divided after the very first level from the top already into (only) two groups: coincidentally, they correspond to the red and blue populations of H $\alpha$  emitters presented in Fig. 7 as it is showed in Fig. 9. From that point on, the groups were subdivided without evident distinction, and truncation was thus assumed when the 12-node level was reached. The truncation is an usual procedure when dealing with big data.

In this work, we implemented HAC by using the python machine learning library Scikit-learn<sup>6</sup> (Pedregosa et al. 2011). Then we use the `DENDROGRAM()` function, which is include in the Python package `scipy`<sup>7</sup>, and the task *Dendrogram Truncation* to generate the (truncated) dendrogram. There are parameters to be taken into account when the algorithm is applied to the data: `n_clusters`, `Affinity`, and `Linkage`. `n_clusters` defines the number of clusters expected by the user. Given that our goal is to divide our sample in into two groups. we set this parameter to "2". `Affinity` determine the "metric" to compute the linkage. We have found that a simplistic metric, the "Euclidean", is effective for our purpose. **Eu não entendi essa frase:** `Linkage` determines which distance to use between sets of observation. **Linkage criterion determines the distance between sets of observations based on the pairwise distances between observations.** The algorithm merge the pairs of cluster that minimize this criterion. Here was implemented "ward" (**Quais são as outras opções?**) **Na verdade só tem ward method, vou descrever a frase.** which minimizes the variance of the clusters (**Eu não sei o que é variancia de clusters: variância do que?**) **Ward usa error sum**



**Figure 9.** The  $g - r$  versus  $z - g$  color-color diagram with the two population found by implementing HAC algorithm. The blue and red symbols represent the sources with intense blue continuum and those with intense red continuum, respectively. The straight line is the same line of Figure 6.

of squares que a minima varianza dos dados de cada cluster being merged. As it was mentioned, the input variables are the colors; ( $g - r$ ) and ( $z - g$ ).

At this point, we have divided our list into two groups in agreement with the nature of their continuum. We found that the number of blue H $\alpha$  emitters is bigger than the red one.

#### 2.4.2 HDBSCAN

For the sake of comparison with results from HAC, we also used HDBSCAN to separate the blue sources from the red ones. The main difference between these two algorithms is that HDBSCAN is more conservative so that many data points are classified as noise. For this purpose, we used the Python implementation of HDBSCAN<sup>8</sup> (McInnes et al. 2017). Like HAC, in addition to the colors input parameters, there are key parameters that should be considered when the algorithm is applied. Regarding the metric, it is assumed the "Euclidean". The two most critical parameters are the "minimum cluster size" and "minimum number of samples". The former refers to the smallest size grouping that we wish to consider a cluster. We have adopted the value "80". (**Eu não entendi o que você quer dizer com a frase seguinte:**) mudei um pouco a frase. The latter provides a measure of how conservative we want our clustering to be, expressed as the fraction of data classified as noise. The value implemented was "40". With this configuration of our model, we found two clusters. Several small clusters are found when assuming values for the minimum number of samples smaller than 40.

Left panel of Fig. 10 shows the two clusters found with HDBSCAN, one containing XX red and the other with YY blue sources. This result is fully consistent with those from HAC: the two primary clusters from HDBSCAN are located in the same region in the  $(g - r)$ - $(z - g)$  diagram where lie the groups found with the HAC. (**Aqui eu acho que ficaria legal dizer qual é a porcentagem da amostra azul de um método ser**

<sup>6</sup> <https://scikit-learn.org/stable/>

<sup>7</sup> <https://www.scipy.org/>

<sup>8</sup> <https://hdbSCAN.readthedocs.io/en/latest/>

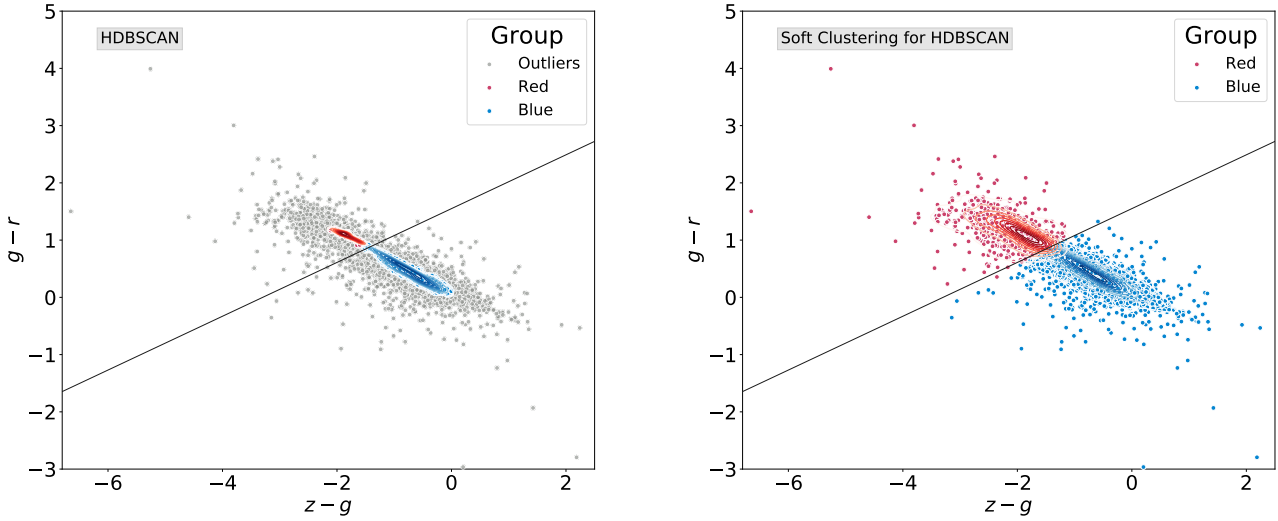


**Figure 10.** As Figure 6 but with the results after to apply HDBSCAN (*left panel*) to the sample of H $\alpha$ . The blue and red symbols correspond to blue and red sources, respectively. Gray symbols are the sources classified as noise by HDBSCAN. And the results after apply a soft clustering to the HDBSCAN results (*right panel*). The straight line is the same line as Figure 6.

identificada no outromodelo; o mesmo para a vermelha.) In fact, by applying the `condensed_tree_` to the data colors two clusters are selected (see Appendix A for more details about `condensed_tree_` attribute.)

#### 2.4.3 Soft clustering for HDBSCAN

Perhaps, the main disadvantage of HDBSCAN is that many of the sources are labelled as “noise” so that they are not assigned to any cluster. As mentioned, this comes from the conservative nature of HDBSCAN and the fact that these data sources (noise) are located far away of the cluster cores. An alternative way to avoid outliers (noises) classifications consists to use the concept of “soft clustering” (see section 2.3.2). We have carried out here soft clustering from HDBSCAN<sup>9</sup> to assign every object to a cluster that they most likely belong to. With this approach, points are not assigned in a deterministic way to clusters but to a vector of probabilities as a measure of belonging to different clusters: the probability value at the  $i$ th entry of the vector is the probability that a data point is a member of the  $i$ th cluster. We can, then, simply assign cluster labels for every point by taking the most likely cluster it belongs to, using probability thresholds. Soft clustering (Já li essa denominação antes mas agora me pergunto: o que é soft clustering? Indicar aqui uma seção do texto na qual já foi explicado isso?) for HDBSCAN is achieved through an outlier score modification to consider how much an outlier is relative to each cluster, which is based on the Global-Local Outlier Score from Hierarchies (GLOSH) algorithm (Campello et al. 2015). This is combined with a measure of distance from a given cluster to produce an estimate of the probability that any given data

point belongs to any of the fixed groups drawn from the condensed tree. (Euachei que essa frase ficou muito grande; estou com receio de mudar e alterar o contexto. Veja plsse você consegue uma versão mais clara, talvez dividindo o conteúdo em duas frases) Mudei um pouco esta frase, dividí em duas.

The right panel of Fig. 10 shows at what most likely cluster belongs the data points classified as the noise by HDBSCAN. We have used blue and red colors for the points that have the highest probability of being in the blue and red groups, respectively. This fills out the clusters nicely. We see that there were many noise points that are most likely to belong to the clusters we would expect, e.g. in agreement with results obtained with HAC. Indeed, we now have improved our classification of our list into blue and red sources because we have estimated the probability of each source to belong to each group (Eu não gostei muito dessa frase. Me pareceu deixar algo solto.) Adicionei a seguinte frase, talvez feche melhor o parágrafo. Instead of forcing the algorithm to make a decision as to which group a data point belongs to, just like HAC does, we have quantified the likelihood of a given observation belonging to any of the two clusters found in our data set, see, for instance, the two last columns of Table B1.

## 3 RESULTS AND DISCUSSION

### 3.1 Matches with other databases

We found a total of 389 emission line sources in all S-PLUS DR3. To understand the nature of the objects and the fractional contribution of different classes of objects with emission lines to the overall sample cross-matching with some catalogs available were carried out.

<sup>9</sup> [https://hdbscan.readthedocs.io/en/latest/soft\\_clustering\\_explanation.html](https://hdbscan.readthedocs.io/en/latest/soft_clustering_explanation.html)

**Table 1.** A summary of the results obtained of the positional cross-match between the S-PLUS list of emission line objects and the SIMBAD database. We used a search radius of 2 arcsec.

Main type	Associated SIMBAD types	Number of S-PLUS objects with SIMBAD match
Nebulae	HII, PN, SN, Candidate_SN*, Nova	37
Cataclysmic variable star	CataclyV*, Candidate_CV*	30
Variable star of RR Lyr type	RRLyr, Candidate_RRLyr	19
X-ray source	HMXB, X	6
Eclipsing binary	EB*	8
Emission object	EmObj	4
Star	star, WD*, Candidate_WD*, Blue, BlueSG*, PM*, low-mass*	57
UV-emission source	UV	2
Cluster of stars	Cl*	3
Far-infrared source	FIR	2
Mid-infrared source	MIR	1
Radio-source	Radio	7
Molecular cloud	MolCld	2
Emission line galaxy	EmG, HII_G, StarburstG, BlueCompG	102
Part of a galaxy	PartofG	9
Interacting galaxies	IG	10
Galaxy in pair of galaxies	GinPair	12
Galaxy in group of galaxies	GinGroup	18
Galaxy in cluster of galaxies	GinCl	23
Low surface brightness galaxy	LSB_G	10
Brightest galaxy in a cluster	BCIG	3
Globular cluster	GiCl	1
QSO	QSO, QSO_Candidate	225
AGN	AGN, AGN_Candidate, Seyfert_1, Seyfert_2, BLLac, RadioG	67
Galaxy	Galaxy	421
Possible gravitationally lensed image	Possible_lensImage	1
Total		10

### 3.1.1 Simbad

We made cross-match between our sample of objects with excesses of emission on the J0660 filter and SIMBAD database. We searched for all objects using a radius of 2 arcsec around the position of the optical source in question. We found 1000 matches that include a great variety of emission line objects. In table 1 is showed the different categories of objects found with SIMBAD coincidence.

**3.1.1.1 Nebulae.** As was mentioned, several classes of objects with nebulosity are listed in our sample. Those include H II region, planetary nebulae and supernova remnants (SNRs). Such sources in our Galaxy and nearby galaxies were identified here. The H II regions are objects with gas that being ionized by amounts of UV light come from massive stars (OB type) on which are formed the emission lines. In theses clouds of ionized gas, new stars are formed. Unlike H II regions, planetary nebulae represent the final stages of low- and intermediate-mass stars where the gas previously ejected in the phase of AGB is ionized by the high energetic radiation come from their central stars.

In our list of H $\alpha$  emission line objects a PN appears cataloged in SIMBAD on which the S-PLUS photometry and SDSS spectrum is displayed on panel (a) of Fig 11. Emission lines like H $\alpha$  and [N II] are clearly perceptible in its spectrum. This objects is a very interesting because is one of the twelves PNe that belong to the Galactic halo. These PNe are low metallizite and present large velocities that can give count of the origin and nucleosynthesis of the early universe. 30 objects cataloged as HII regions on the SIMBAD database are in our list of H $\alpha$  emitters. Panel (b) oh the figure shows the S-

PLUS photometry and SDSS spectrum of the extragalactic HII region GALEX 2417063145906373262.

Supernova and nova are other type of emission lie objects on which shell of gas arise from evolved stars. The physical nature on the gas of them is different to the typical gaseous nebulae (H II regions and planetary nebulae). The general energy-input mechanism is quiet different in each case. However, the emission-line spectra show general similarities, indicating that when the ionized gas is heating tends to produce the same emission-line photons, regardless of the mechanisms by which high temperature and ionization are produced. In agreement with SIMBAD coincidences, supernovas and novas are in our list as show table 1. Panel d of Figure 11 exhibits the SDSS spectrum, S-PLUS photometry and coloured image of an extragalactic SN. The emission lines are clearly perceptively in its spectrum.

**3.1.1.2 Binary systems.** 25 known CVs and 5 candidate CVs (from SIMBAD) were selected with the algorithm. CVs are binary systems of very short orbital period, in which a low-mass and early-type star fills its Roche region and transfers mass to a companion stars, a dwarf white (Patterson 1984). Fig. 11 the S-PLUS photometry overlapped to the SDSS spectrum of the CV FASTT 1560. As expected, this object was classified as blue source by the machine learning approaches. Other binary system in our list are the X-binary sources and eclipsing binary. That type of object is expected to be in our sample because majority of them are known to be H $\alpha$  emitters.

**3.1.1.3 Stars.** Several stars were selected as shows the SIMBAD matches. The SIMBAD types include normal stars, white dwarf stars

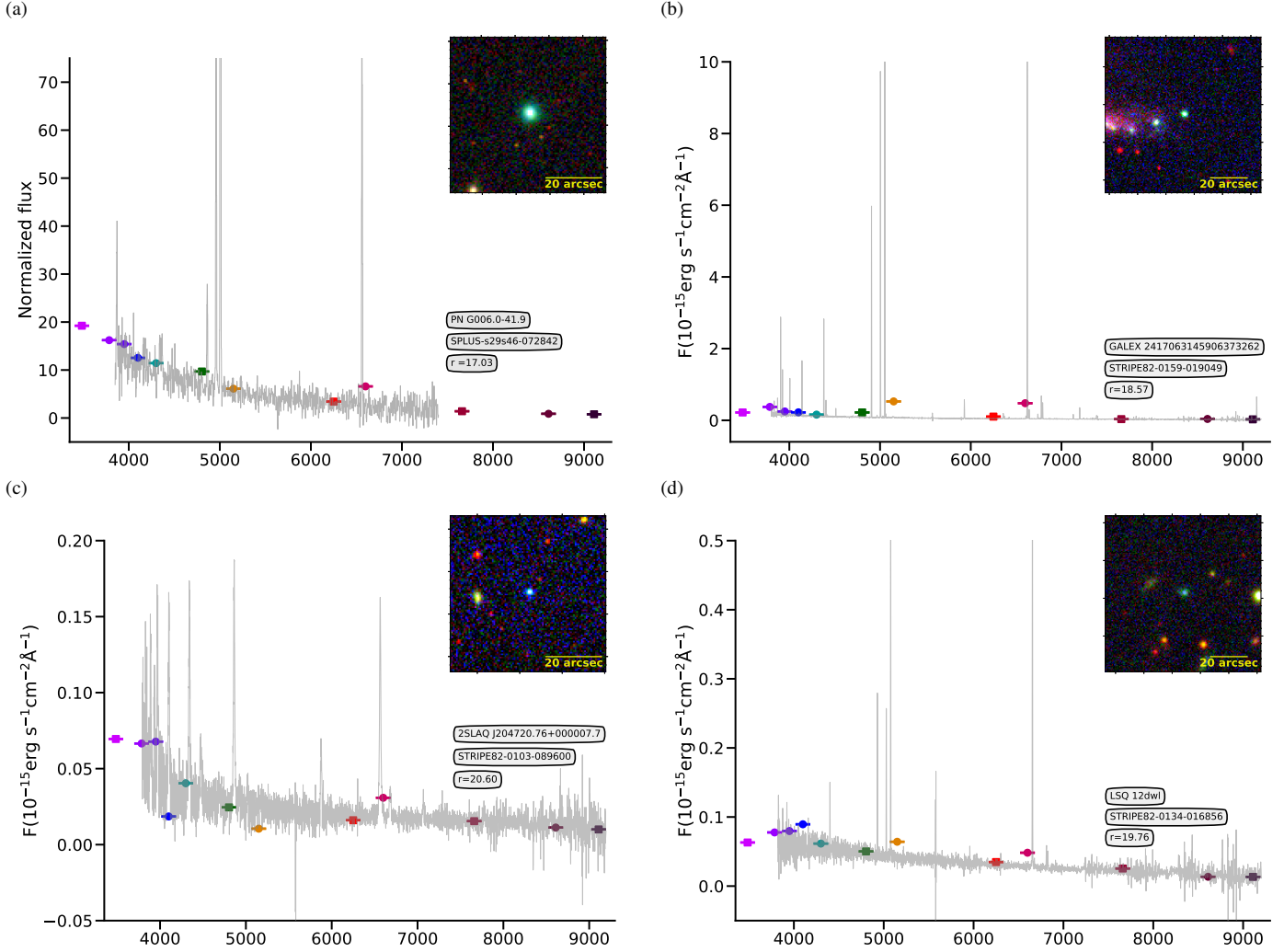


**Figure 11.** Summary of our selection results showing the spectrum (gray line en each panel) of different classes of emission line sources identified in our target list. A spectrum of a PN (a) from REF. The SDSS spectra of an external H II region (b), a cataclysm variable star (c), a super nova (d). As in Figure 3, coloured square and circles symbols represent the S-PLUS photometry. All these objects show a significance excesses on the  $J0660$  filter in comparison with the broad-bands.

(WD\*), white dwarf candidates (Candidate\_WD\*), blue stars, blue super-giant stars (BlueSG\*), high proper-motion stars (PM\*) and low-mass star (low-mass\*;  $M < 1M_{\odot}$ ). All these objects appears in the S-PLUS catalog as  $H\alpha$  emitters. Some of them can be early/late-type emission-line stars and/or different types of stars with the  $H\alpha$  emission lines. Although some of these stars could represent the fraction of contaminants of our sample. There are also matches to variable stars of RR Lyr type as well as candidates of them.

**3.1.1.4 Galaxies.** Emission line galaxies also were selected. This category include several class of galaxies according to SIMBAD types: emission-line galaxy (EmG), blue compact galaxy (Blue-CompG), HII galaxy (HII G), galaxy in cluster of galaxies (GinCl), galaxy in group of galaxies (GinGroup), low surface brightness galaxy (LSB G), interacting galaxies (IG), part of a Galaxy (PartofG), Seyfert 1 and 2 galaxies, AGN and galaxies.

All the emission line galaxies of these category form part of the universe local. This mean that their redshift cover the range on which the  $H\alpha$  emission line still falls into the  $J0660$  filter. Objects with  $z > 0.02$  the  $H\alpha$  is outside of the  $J0660$  filter. Table B1 of

the appendices shows the red-shift of the emission line galaxies of our sample that have SIMBAD matches. Many of the galaxies have small red-shift values probing that mostly of these galaxies are real  $H\alpha$  emitters. In these kind of galaxies such as the blue compact and/or H II galaxies their starburst regions that consist of ensemble of massive ionizing stars and their respective giant H II regions cover the extension of the optical images and the emission lines of their spectra. Fig. 12 shows the SDSS spectra and S-PLUS photometry of the H II galaxy 6dFGS gJ012646.5-003845 (panel a) and of the radio galaxy NVSS J025557+004132 (panel b). The H II galaxy is classified as blue source while the radio galaxy as red by the machine learning algorithm which is obvious from their spectra.

On the other hand, several AGN, Seyfert 1 and Seyfert 2 galaxies have red-shift between 0.31 and 0.37 indicating that the excess on the  $J0660$  filter is not due to the  $H\alpha$  emission but if due to the  $H\beta$  and [O III] 4959, 5007 Å emission lines. These emission lines at the red-shift range  $0.306 < z < 0.376$  are detected in the  $J0660$  band. It is well known that the AGNs have very strong emission lines such as  $H\beta$ , [O III] 4959, 5007 Å and  $H\alpha$ .

One interesting discussion here, is that the SIMBAD type part

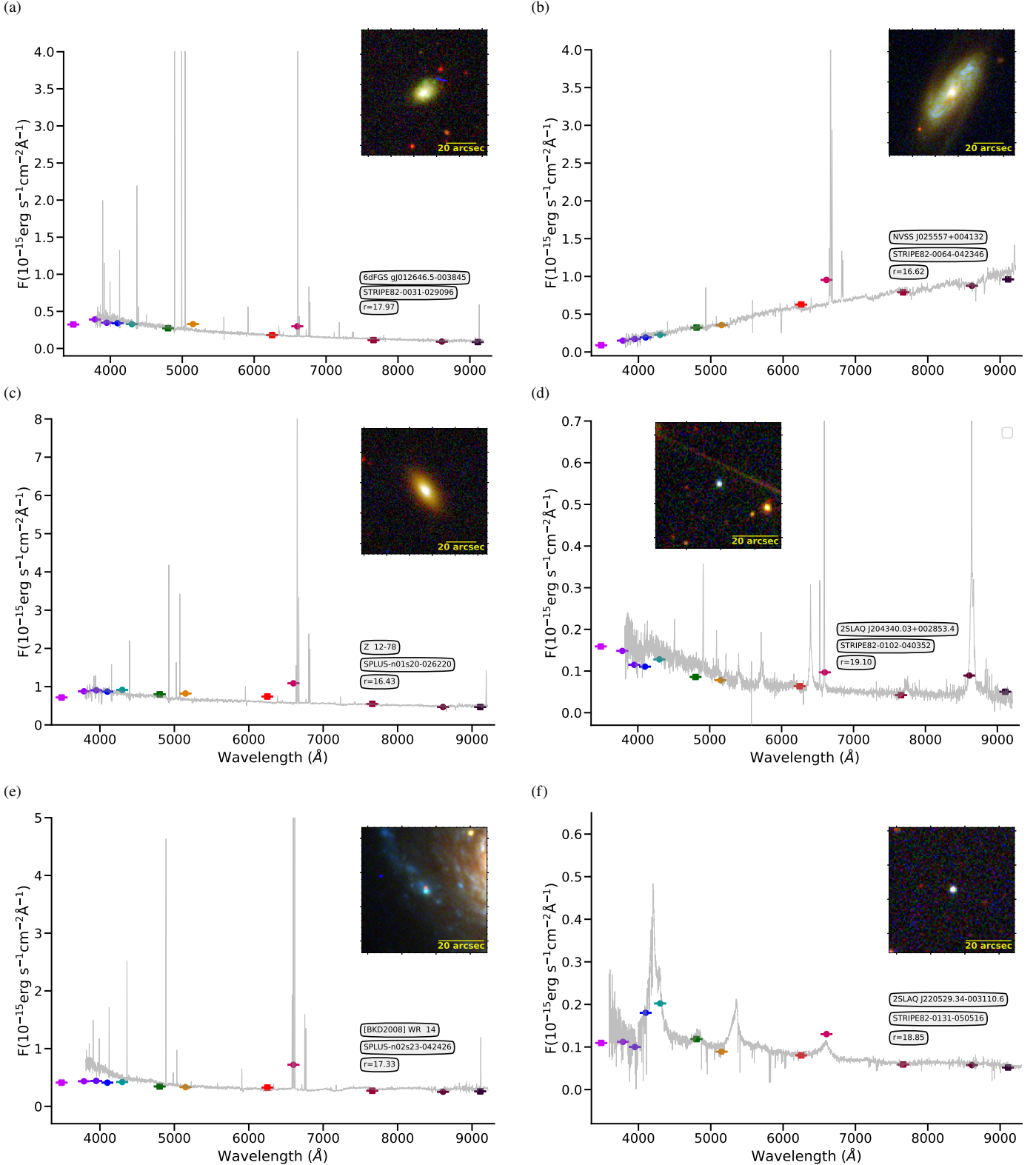


**Figure 12.** SDSS spectra of a H II galaxy with  $z = 0.006$  (a), a radio galaxy with  $z = 0.014$  (b), a star-forming galaxy with  $z = 0.013$  (c). For this object, the H $\alpha$  line is responsible for the  $J0660$  magnitude. And a Seyfert 1 with  $z = 0.317$  (d). For this last object, the excess on the  $J0660$  is due to the [O III] 4959, 5007  $\text{\AA}$  emission lines. A WR in a galaxy (e) and a QSO (f) with red-shift of  $\sim 2.45$ . As in Figure 11 coloured symbols indicate the S-PLUS photometry.

of a Galaxy (PartofG) are actually galaxies with Wolf-Rayet (WR) signature in the low red shift universe also named “WR galaxy” (Osterbrock & Cohen 1982). WR stars in galaxies is perceptible in their spectra with strong emission lines such as H $\alpha$  and [NII]. These spectral features can be of them very similar to extragalactic H II regions present typically of the outskirt of spiral galaxies. Panel (e) of Fig. 11 displays the S-PLUS and SDSS spectra of the galaxy with Wolf-Rayet signature [BKD2008] WR 14.

On the other hand, many of the objects have as main type “galaxy” in SIMBAD. This galaxies could be spiral galaxies on which the star formation is present. It is known that in the spiral arms of the galaxies are present H II regions as well as neutral gas (H I) and molecular gas. Actually some of these galaxies haves for secondary type H I. The reservoir of H I gas in galaxies must ultimately feed their star formation, after cooling and forming molecular clouds (van Driel et al. 2016). Panel c of Figure 12 shows the S-PLUS photometry and the SDSS spectra of star-forming galaxy. The SDSS spectrum clearly exhibits strong emission lines. Note that almost all these galaxies are classified as bluer objects by HAC and HDBSCAN. However, mostly of the Seyfert 2 and radio-galaxies and an handful of galaxies are classified as red sources. These galaxies, belonging to the red sub-sample, are probably nearby, red early-type galaxies with emission lines, mainly, they could be LINERS, AGB or radio galaxies (Capetti & Baldi 2011).

**3.1.1.5 QSOs.** Other extragalactic objects with emission lines that were selected are the QSOs. In the case of the QSOs is not the H $\alpha$  emission line that affects the J0660 filter. This filter is affected by other strong emission lines present in these objects that to specific redshift drop into the J0660 filter. Some of these emission lines are H $\beta$ , C IV 1550 Å, C III] 1909 Å, Mg II 2798 Å (see, also Gutiérrez-Soto et al. 2020; Nakazono et al. 2021). All the objects were classified as blue sources which was expected. Panel f of Figure 12 show the S-PLUS photometry and SDSS spectrum of the QSO 2SLAQ J220529.34-003110.6 which has red-shift of  $\sim 2.45$  indicating that the emission line corresponds to the line C III].

**3.1.1.6 Other type of objects.** Miscellanies the objects were selected as H $\alpha$  emitters that appear classified on SIMBAD as it can see in the table 1. They are included cluster of stars, FIR sources, MIR objects, molecular clouds, UV-emission source, among other.

### 3.1.2 SDSS and LAMOST

We also made cross-match between the sample of H $\alpha$  emission line objects and SDSS DR16 (Ahumada et al. 2020). We have used a  $2\sigma$  error circle as the cross-matching radius. We got 200 spectra from which 195 objects exhibit strong emission lines. 5 objects do not show emission lines, they probably are stars or galaxies.

We also cross-correlate our list with Large Sky Area Multi-Object Fiber Spectroscopic Telescope (LAMOST; Wu et al. 2011) using a radius of 2 arcsec for the match. These spectra also show strong emission lines. These results shows that this technique actually are very effective for selecting sources with strong emission lines.

Comparing with These spectra mainly correspond to HII regions, cataclysm variables, SN, emission-line galaxies (blue compact galaxies, H II galaxies, star-forming galaxies, among others), AGN (Seyfert 1 and 2), and QSOs. However, more detailed analyzes are necessary to see that other possibles types of objects are included in these samples of spectra.

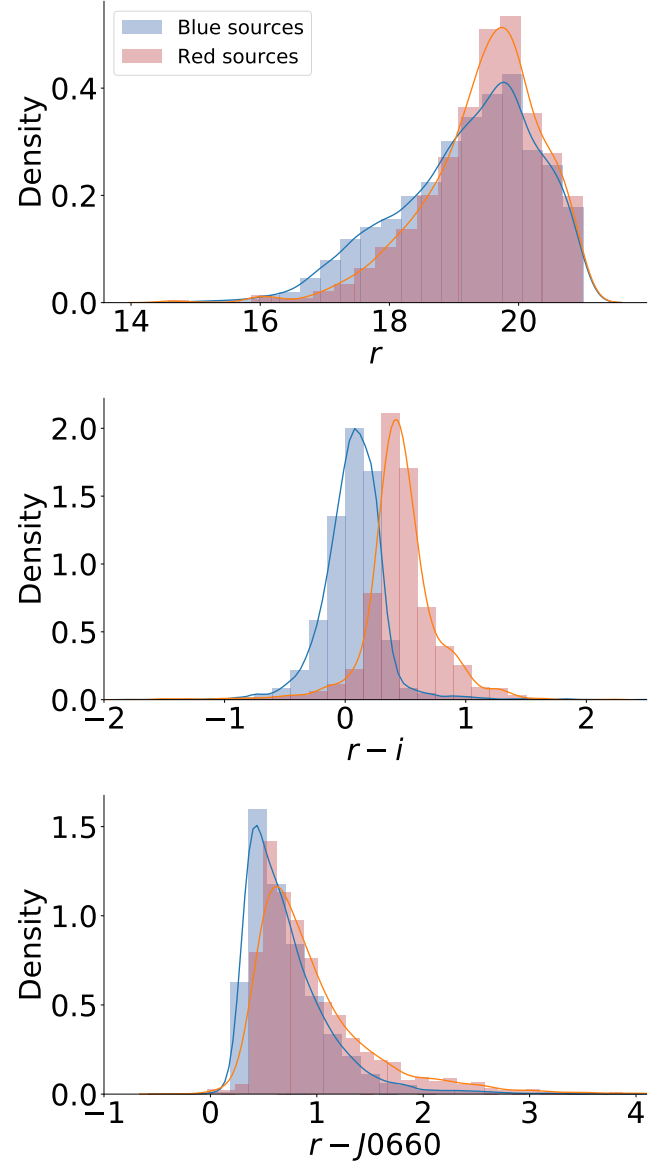


**Figure 13.** Distribution of  $r$  magnitude (top panel),  $r - i$  color (middle panel), and  $r - J0660$  color (bottom panel) for the blue and red sources of the sample of H $\alpha$  emitters. Both sample are normalized to their maximum counts, xx and xx objects for blue and red sources, respectively. The smooth curves represent a Kernel density estimation for both samples.

### 3.2 Magnitudes and color distributions

Figure 13 shows the magnitude and color distribution of the blue and red sources –classification performed with machine learning on Section 2.3–. Upper panel of the figure shows the distribution of the blue and red sources of the  $r$ -magnitude. The peaks of the  $r$  distribution is the same for the blue and red sources, which is around  $r \sim 19.9$ . However, the density at the peak is higher in red sources than the blue ones indicating that the proportion of red objects with  $r$ -value of 19.9 is higher than the blue sources. The fraction of object is very small at  $r < 16$  for each group of objects. The distribution of the objects for both group increase in the range  $16 \geq r \geq 19.9$ . However, the density as indicating the Kernel density estimation curves is higher in the blue sources. This implies that the fraction of sources

with the magnitude range is considerably higher in comparison with the red group. In conclusion much blue sources tends to be brighter than the red ones.

Middle panel of figure displays the ( $r - i$ ) distribution of the blue and red emission line objects. The peaks of the  $r - i$  distributions are distinct for the blue and red sources. The peaks of the red sources at high red continuum,  $r - i \sim 0.5$ , compared to the value of the blue sample,  $r - i \sim 0.9$ . All these results are consistent because the  $r - i$  color is an indicator of reddened sources. It is also consistent with previous works. For instance, Wevers et al. (2017) used different algorithms based on the  $r - i$  color to successfully select blue outliers from the Galactic Bulge Survey (GBS; Jonker et al. 2011).

Bottom panel of Figure 13 shows the  $r - J0660$  color distribution of the blue and red objects. The fraction of objects selected as emitter rises drastically with  $J0660$  excess, until at sufficiently large excesses. The peaks of the  $r - J0660$  color distribution are relatively different for both groups of sources. Having the blue sources the peaks at  $r - J0660 \sim 0.5$  while for the red ones the value peak is  $r - J0660 \sim 0.7$ .

## 4 CONCLUSIONS

We have created and analyzed a sample of emission-line objects in the local universe selected from the S-PLUS catalog. By identifying the locus of main-sequence and giant star on the ( $r - J0660$ ) versus ( $r - i$ ) colour-colour diagram and considering objects with H $\alpha$ -excess, those located above of this locus. The sample contains 9,000 sources that were identified as H $\alpha$  emitters. The big advantage here compared to previous work is that we are providing a significant sample of H $\alpha$  emitters in 12 bands. Seven and five narrow- and broad-band filters, respectively, covering the wavelength range from  $\sim 3000$  to  $\sim 9000\text{\AA}$ . In other words, much more information can be extracted from them in future work only using S-PLUS photometry.

Match with spectroscopic databases (SDSS and LAMOST) evince that mostly of the objects selected are emission line objects, showing that at least the XX% of the objects are genuine H $\alpha$  emitters.

The ( $g - r$ ) and ( $z - g$ ) colour distributions of the H $\alpha$  emitters are bimodal, evidencing two populations. One peak corresponding to blue sources and the another peak to the red sources. Agreement to this results we explore the ( $g - r$ ) versus ( $z - g$ ) color-color diagram to separate the blue sources from the red, finding that it can be used for this task. But there is a zone on the diagram on which the blue and red objects are overlapped. For this reason, we use two types of unsupervised machine learning to group our sample of H $\alpha$  emitters into two groups by color-type. HAC and HDBSCAN clustering algorithms were used to distinguish the blue sources from the red. The two approaches found the same two clusters, but given HDBSCAN is much conservative algorithm than HAC many of the objects were labeled as noise. To solve that we also used a soft clustering approach for HDBSCAN to estimate the probabilities of each data point belongs to (blue or red group). Finding more consistent results between HAC and HDBSCAN. We argue that the ( $g - r$ ) and ( $z - g$ ) colors are useful parameters to classify objects into color-types, with hierarchical soft clustering of the colours features of a given sample providing a convenient means of sorting and classifying sources in the colour parameter space.

The bluer objects corresponds mainly to CV, QSOs, PNe, dwarf compact galaxies, H II regions, among others. The redder sources are early type galaxies with emission lines (for instances, radio-galaxies and Seyfert 2 galaxies), probably young/active late-type stars or even symbiotic stars.

## ACKNOWLEDGEMENTS

RLO acknowledges financial support from the Brazilian institutions CNPq (PQ-312705/2020-4) and FAPESP (#2020/00457-4).

The S-PLUS project, including the T80-South robotic telescope and the S-PLUS scientific survey, was founded as a partnership between the Fundação de Amparo à Pesquisa do Estado de São Paulo (FAPESP), the Observatório Nacional (ON), the Federal University of Sergipe (UFS), and the Federal University of Santa Catarina (UFSC), with important financial and practical contributions from other collaborating institutes in Brazil, Chile (Universidad de La Serena), and Spain (Centro de Estudios de Física del Cosmos de Aragón, CEFCA). We further acknowledge financial support from the São Paulo Research Foundation (FAPESP), the Brazilian National Research Council (CNPq), the Coordination for the Improvement of Higher Education Personnel (CAPES), the Carlos Chagas Filho Rio de Janeiro State Research Foundation (FAPERJ), and the Brazilian Innovation Agency (FINEP).

Funding for the SDSS and SDSS-II has been provided by the Alfred P. Sloan Foundation, the Participating Institutions, the National Science Foundation, the U.S. Department of Energy, the National Aeronautics and Space Administration, the Japanese Monbukagakusho, the Max Planck Society, and the Higher Education Funding Council for England. The SDSS Web Site is <http://www.sdss.org/>.

The SDSS is managed by the Astrophysical Research Consortium for the Participating Institutions. The Participating Institutions are the American Museum of Natural History, Astrophysical Institute Potsdam, University of Basel, University of Cambridge, Case Western Reserve University, University of Chicago, Drexel University, Fermilab, the Institute for Advanced Study, the Japan Participation Group, Johns Hopkins University, the Joint Institute for Nuclear Astrophysics, the Kavli Institute for Particle Astrophysics and Cosmology, the Korean Scientist Group, the Chinese Academy of Sciences (LAMOST), Los Alamos National Laboratory, the Max-Planck-Institute for Astronomy (MPIA), the Max-Planck-Institute for Astrophysics (MPA), New Mexico State University, Ohio State University, University of Pittsburgh, University of Portsmouth, Princeton University, the United States Naval Observatory, and the University of Washington.

Guoshoujing Telescope (the Large Sky Area Multi-Object Fiber Spectroscopic Telescope LAMOST) is a National Major Scientific Project built by the Chinese Academy of Sciences. Funding for the project has been provided by the National Development and Reform Commission. LAMOST is operated and managed by the National Astronomical Observatories, Chinese Academy of Sciences.

Scientific software and databases used in this work include TOPCAT<sup>10</sup> (Taylor 2005), simbad and vizier from Strasbourg Astronomical Data Center (CDS)<sup>11</sup> and the following python packages: numpy, astropy, matplotlib, seaborn, scikit-learn.

## DATA AVAILABILITY

## REFERENCES

- Aggarwal C. C., 2015, Data Mining: The Textbook. Springer, Cham,  
[doi:10.1007/978-3-319-14142-8](https://doi.org/10.1007/978-3-319-14142-8)  
 Ahumada R., et al., 2020, *ApJS*, 249, 3  
 Akras S., Guzman-Ramirez L., Leal-Ferreira M., Ramos-Larios G., 2019a,  
*ApJS*, 240, 21

<sup>10</sup> <http://www.star.bristol.ac.uk/~mbt/topcat/>

<sup>11</sup> <https://cds.u-strasbg.fr/>

- Almeida-Fernandes F., et al., 2021, arXiv e-prints, p. [arXiv:2104.00020](https://arxiv.org/abs/2104.00020)
- Barentsen G., et al., 2014, *MNRAS*, **444**, 3230
- Campello R. J. G. B., Moulavi D., Sander J., 2013, in Pei J., Tseng V. S., Cao L., Motoda H., Xu G., eds, *Advances in Knowledge Discovery and Data Mining*. Springer Berlin Heidelberg, Berlin, Heidelberg, pp 160–172
- Campello R., Moulavi D., Zimek A., Sander J., 2015, *A CM Transactions on Knowledge Discovery from Data*, **10**, 1
- Capetti A., Baldi R. D., 2011, *A&A*, **529**, A126
- Cenarro A. J., et al., 2018, preprint, ([arXiv:1804.02667](https://arxiv.org/abs/1804.02667))
- Corradi R. L. M., Giannanco C., 2010, *A&A*, **520**, A99
- Corradi R. L. M., et al., 2008, *A&A*, **480**, 409
- Corradi R. L. M., Sabin L., Munari U., Cetrulo G., Englano A., Angeloni R., Greimel R., Mampaso A., 2011, *A&A*, **529**, A56
- Davies R. D., Elliott K. H., Meaburn J., 1976, *Mem. RAS*, **81**, 89
- Drew J. E., et al., 2005, *MNRAS*, **362**, 753
- Drew J. E., Greimel R., Irwin M. J., Sale S. E., 2008, *MNRAS*, **386**, 1761
- Drew J. E., et al., 2014, *MNRAS*, **440**, 2036
- Ester M., Kriegel H.-P., Sander J., Xu X., 1996, in Proc. of 2nd International Conference on Knowledge Discovery and Data Mining (KDD-96). pp 226–231
- Fukugita M., Ichikawa T., Gunn J. E., Doi M., Shimasaku K., Schneider D. P., 1996, *AJ*, **111**, 1748
- Gutiérrez-Soto L. A., et al., 2020, *A&A*, **633**, A123
- Horne K., Marsh T. R., 1986, *MNRAS*, **218**, 761
- Jain A. K., Murty M. N., Flynn P. J., 1999, *ACM Comput. Surv.*, **31**, 264
- Jayasinghe T., et al., 2019, *MNRAS*, **488**, 1141
- Jonker P. G., et al., 2011, *ApJS*, **194**, 18
- Malzer C., Baum M., 2021, *Sensors*, **21**
- Mann A., Kaur N., 2013.
- Marín-Franch A., et al., 2012, in Navarro R., Cunningham C. R., Prieto E., eds, Society of Photo-Optical Instrumentation Engineers (SPIE) Conference Series Vol. 8450, Modern Technologies in Space- and Ground-based Telescopes and Instrumentation II. p. 84503S, doi:10.1117/12.925430
- McInnes L., Healy J., Astels S., 2017, *The Journal of Open Source Software*, **2**
- Mendes de Oliveira C., et al., 2019, *MNRAS*, **489**, 241
- Nakazono L., et al., 2021, *MNRAS*,
- Ntwaetsile K., Geach J. E., 2021, *MNRAS*, **502**, 3417
- Oke J. B., Gunn J. E., 1983, *ApJ*, **266**, 713
- Osterbrock D. E., Cohen R. D., 1982, *ApJ*, **261**, 64
- Parker Q. A., et al., 2005, *MNRAS*, **362**, 689
- Parker Q. A., Bojičić I. S., Frew D. J., 2016, in Journal of Physics Conference Series. p. 032008 ([arXiv:1603.07042](https://arxiv.org/abs/1603.07042)), doi:10.1088/1742-6596/728/3/032008
- Patterson J., 1984, *ApJS*, **54**, 443
- Pedregosa F., et al., 2011, *Journal of Machine Learning Research*, **12**, 2825
- Pickles A. J., 1998, *PASP*, **110**, 863
- Ratti E. M., Steeghs D. T. H., Jonker P. G., Torres M. A. P., Bassa C. G., Verbunt F., 2012, *MNRAS*, **420**, 75
- Sabin L., Zijlstra A. A., Wareing C., Corradi R. L. M., Mampaso A., Viironen K., Wright N. J., Parker Q. A., 2010, *Publ. Astron. Soc. Australia*, **27**, 166
- Santos-Silva T., et al., 2021, arXiv e-prints, p. [arXiv:2108.06234](https://arxiv.org/abs/2108.06234)
- Scaringi S., Groot P. J., Verbeek K., Greiss S., Knigge C., Körding E., 2013, *MNRAS*, **428**, 2207
- Schwope A. D., Catalán M. S., Beuermann K., Metzner A., Smith R. C., Steeghs D., 2000, *MNRAS*, **313**, 533
- Taylor M. B., 2005, in Shopbell P., Britton M., Ebert R., eds, *Astronomical Society of the Pacific Conference Series Vol. 347, Astronomical Data Analysis Software and Systems XIV*. p. 29
- Viironen K., et al., 2009, *A&A*, **502**, 113
- Vink J. S., Drew J. E., Steeghs D., Wright N. J., Martin E. L., Gänsicke B. T., Greimel R., Drake J., 2008, *MNRAS*, **387**, 308
- Webb S., et al., 2020, *MNRAS*, **498**, 3077
- Wevers T., et al., 2017, *MNRAS*, **466**, 163
- Witham A. R., et al., 2006, *MNRAS*, **369**, 581
- Witham A. R., et al., 2007, *MNRAS*, **382**, 1158
- Witham A. R., Knigge C., Drew J. E., Greimel R., Steeghs D., Gänsicke B. T., Groot P. J., Mampaso A., 2008, *MNRAS*, **384**, 1277
- Wu Y., et al., 2011, *Research in Astronomy and Astrophysics*, **11**, 924
- van Driel W., et al., 2016, *A&A*, **595**, A118

## APPENDIX A: CONDENSED TREES

The condensed Trees is a diagram for HDBSCAN that allows to see the cluster hierarchy as a dendrogram. It can be displayed via the `condensed_tree_` attribute of the `HDBSCAN` package. Figure A1 shows the condensed trees which was obtained by using the  $(r - g)$  and  $(g - z)$  colours as the the input parameters. It is possible to see that HDBSCAN has found two clusters in agreement with previous results. This means that they represent the blue and red sources.

## APPENDIX B: SIMBAD OBJECTS

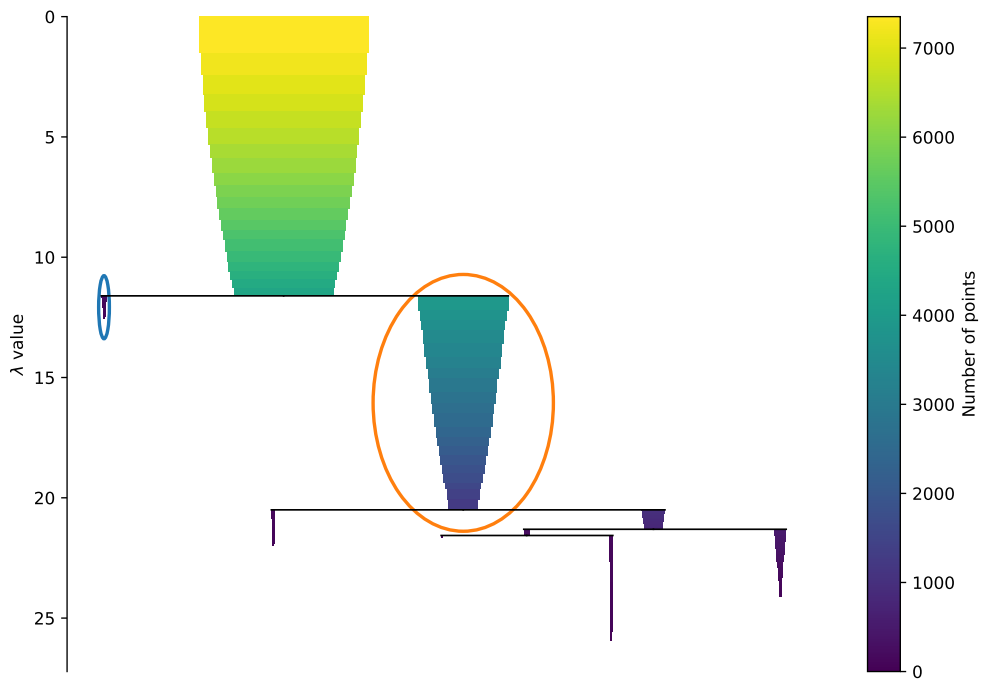


**Figure A1.** The condensed Trees for our sample of H $\alpha$  emitters. The width and color of each branch represent the number of points in the cluster at that level. The orange and blue ellipses represent the branches selected by the HDBSCAN algorithm.

Table B1: Simbad sources.

Id Object	RA	Dec	Type	Redshift	Group	P(Blue)	P(Red)
						HAC	HDBSCAN
CTLGD 9478	00:01:59.25	-29:18:40.4	Star	—	Blue	0.98	0.02
QSO B2359+005	00:02:30.71	00:49:59.2	QSO	1.354	Blue	0.74	0.08
GMB2011 1808	00:02:47.58	-00:22:23.5	CIG	0.351	—	—	—
CTLGD 2037	00:05:08.77	-30:51:04.2	Star	—	Red	0.15	0.73
SDSS J000637.99-003656.2	00:06:37.99	-00:36:56.2	QSO	4.435	—	—	—
LBQS 0004+0036	00:07:10.00	00:53:29.1	QSO	0.316	Blue	0.61	0.11
SDSS J000809.34+004935.5	00:08:09.34	00:49:35.3	QSO	3.293	—	—	—
2SLAQ J000918.74-003907.2	00:09:18.76	-00:39:07.0	Galaxy	—	Blue	0.71	0.07
VV2006 J001040.1-294428	00:10:40.08	-29:44:27.3	QSO	1.361	Blue	0.71	0.14
CTLGD 7291	00:10:48.73	-29:47:28.8	Star	—	Red	0.29	0.35
2QZ J001055.3-304423	00:10:55.37	-30:44:23.5	Galaxy	0.307	Blue	0.58	0.07
VV2006 J001228.8-310241	00:12:28.78	-31:02:40.0	QSO	1.360	Blue	0.49	0.07
LBQS 0010+0035	00:13:27.32	00:52:32.2	Seyfert 1	0.363	Blue	0.77	0.08
GPM2009 J0014-0044 2	00:14:28.79	-00:44:43.8	EmG	0.014	Blue	0.15	0.06
2SLAQ J001455.99+001903.5	00:14:55.99	00:19:03.7	Star	—	Blue	0.79	0.07
2SLAQ J001526.52+001813.2	00:15:26.52	00:18:13.4	QSO	1.362	Blue	0.51	0.09
VV2006 J001535.5+005355	00:15:35.55	00:53:56.1	QSO	1.358	Blue	0.77	0.03
SDSS J001628.25+010801.9	00:16:28.24	01:08:02.0	Galaxy	0.010	Blue	0.70	0.13
VV2006 J001641.9-312657	00:16:41.87	-31:26:56.6	QSO	0.360	Blue	0.74	0.09
2SLAQ J001731.27-004859.3	00:17:31.26	-00:48:59.2	QSO	1.357	Blue	0.76	0.11
LEDA 1156	00:17:39.97	00:30:22.5	StarburstG	0.017	Blue	0.94	0.01
SDSS J001753.82+005057.6	00:17:53.82	00:50:57.7		1.358	—	—	—
2SLAQ J001912.39+000319.6	00:19:12.39	00:03:19.8	QSO	1.372	Blue	0.75	0.07
2SLAQ J001940.23-005435.9	00:19:40.24	-00:54:35.8	QSO	1.374	Blue	0.70	0.05
VV2006 J001950.1-004040	00:19:50.06	-00:40:40.7	QSO	4.340	—	—	—
2SLAQ J002237.90+000519.0	00:22:37.90	00:05:19.2	QSO	1.373	Blue	0.56	0.03
UM 240	00:25:07.40	00:18:45.2	EmObj	0.011	Blue	0.74	0.12
2MASX J00251994+0031312	00:25:19.92	00:31:31.7	Seyfert 1	0.014	Blue	0.82	0.03
LEDA 3107905	00:27:53.84	-00:58:00.2	Galaxy	0.014	Blue	0.96	0.02
SDSS J002916.79-010021.5	00:29:16.81	-01:00:23.1	Galaxy	0.013	Blue	1.00	0.00
SDSS J002940.01+010528.5	00:29:40.02	01:05:28.7	QSO	1.387	Blue	0.55	0.05
VV2010c J002951.5+004159	00:29:51.45	00:42:00.0	AGN	0.315	Red	0.34	0.18
SDSS J003117.70+001705.0	00:31:17.69	00:17:05.1	QSO	4.335	—	—	—
2QZ J003137.5-292815	00:31:37.50	-29:28:15.3	Unknown	—	Blue	0.67	0.03
2dFGRS TGS283Z142	00:31:50.70	-28:55:36.7	Galaxy	0.013	Blue	0.90	0.01
2QZ J003152.5-293534	00:31:52.56	-29:35:33.3	Galaxy	0.313	Blue	0.86	0.07
2SLAQ J003208.53-005303.7	00:32:08.53	-00:53:03.6	QSO	1.344	Blue	0.36	0.06
SDSS J003234.62-001557.1	00:32:34.62	-00:15:57.1	QSO	3.243	Blue	0.41	0.08
LEDA 559945	00:32:34.69	-42:40:10.4	Galaxy	—	Blue	0.70	0.04
VV2006 J003242.7+003111	00:32:42.74	00:31:11.1	QSO	0.360	Blue	0.21	0.07
2dFGRS TGS365Z059	00:33:54.71	-29:56:12.7	Galaxy	0.006	Blue	0.78	0.02
SWIRE J003517.14-420518.6	00:35:17.11	-42:05:19.0	AGN	0.320	Red	0.03	0.66
VV2006 J003545.9+002306	00:35:45.86	00:23:06.0	QSO	3.237	Blue	0.82	0.02
2MASS J00362543-0029075	00:36:25.39	-00:29:07.1	AGN	0.308	Red	0.16	0.75
2dFGRS TGS440Z027	00:36:38.44	-32:34:44.7	Galaxy	0.006	Blue	0.28	0.08
VV2006 J003714.1-005602	00:37:14.11	-00:56:04.0	QSO	4.361	—	—	—
VV2006 J003722.2-001140	00:37:22.17	-00:11:40.6	QSO	1.370	Blue	0.70	0.04
UM 260	00:37:41.13	00:33:20.0	EmObj	0.014	Blue	0.70	0.08
SDSS J003859.34-004252.2	00:38:59.35	-00:42:52.0	QSO	2.502	Blue	0.12	0.04
SDSS J003930.30+012021.6	00:39:30.28	01:20:20.9	BlueCompG	0.015	Blue	0.31	0.06
IRAS 00370+0035	00:39:34.78	00:51:36.9	FIR	—	Blue	0.82	0.04
IRAS 00370+0035	00:39:34.78	00:51:36.9	FIR	—	Blue	0.82	0.04
2QZ J004215.6-321257	00:42:15.62	-32:12:57.2	Galaxy	0.317	Blue	0.91	0.03
GALEX 2673249256393934953	00:42:43.87	01:17:02.2	QSO	1.366	Blue	0.75	0.08
2dFGRS TGS501Z235	00:43:21.88	-33:19:02.9	Galaxy	0.015	Blue	0.58	0.14
2SLAQ J004335.13-003729.7	00:43:35.16	-00:37:29.6	CataclyV*	—	Blue	0.55	0.14
SDSS J004415.83-004303.1	00:44:15.81	-00:43:03.1	QSO	3.248	—	—	—

Table B1: –continued

Id Object	RA	Dec	Type	Redshift	Group	P(Blue)	P(Red)
						HAC	HDBSCAN
VV2006 J004544.4-315729	00:45:44.35	-31:57:29.2	QSO	1.344	Blue	0.78	0.09
2SLAQ J004626.30-011417.0	00:46:26.30	-01:14:16.8	Galaxy	–	Blue	0.86	0.03
VV98 J004826.9-341340	00:48:26.97	-34:13:38.7	QSO	1.910	Blue	0.70	0.11
SDSS J004918.52+011308.9	00:49:18.52	01:13:09.1	QSO	1.339	Blue	0.59	0.09
LEDA 3034	00:51:49.42	00:33:53.8	Seyfert 1	0.015	Blue	0.85	0.02
QSO B0049-272	00:51:55.64	-26:57:43.3	QSO	2.484	Blue	0.21	0.05
BKD2008 WR 353	00:51:59.72	-00:29:20.8	PartofG	0.005	Blue	0.54	0.08
ESO 411-27	00:52:51.61	-27:19:32.8	Galaxy	0.006	Blue	0.98	0.02
SDSS J005343.78+012147.6	00:53:43.76	01:21:47.5	QSO	1.358	Blue	0.60	0.07
RESOLVE rf554	00:54:15.54	-01:04:56.0	Galaxy	0.015	Blue	0.97	0.03
2QZ J005440.1-320042	00:54:40.12	-32:00:42.2	EmG	0.324	Blue	0.56	0.04
QSO B0052-307	00:54:43.95	-30:30:54.1	QSO	2.450	Blue	0.67	0.10
VV2006 J005532.1-311538	00:55:32.08	-31:15:37.8	QSO	1.350	Blue	0.77	0.08
TYZ2012 II 11	00:55:41.32	-00:56:30.6	Galaxy	0.015	Blue	0.80	0.02
CT83 219	00:55:51.35	-30:56:42.8	UV	–	Blue	0.58	0.07
RGO 8439	00:55:53.16	-28:54:57.3	Star	–	Blue	0.99	0.01
2dFGRS TGS502Z028	00:55:53.31	-33:39:01.5	Galaxy	0.325	Blue	0.70	0.14
VV2006 J005609.9-312209	00:56:09.93	-31:22:08.6	QSO	2.460	Blue	0.33	0.07
VV2006 J005639.0-315759	00:56:39.05	-31:57:58.6	QSO	1.350	Blue	1.00	0.00
GPM2009 0057-0022	00:57:12.60	-00:21:57.7	Galaxy	0.010	Blue	0.78	0.13
VV2000 J005840.5-300203	00:58:40.42	-30:02:00.1	QSO	1.361	Blue	0.35	0.06
LEDA 3530	00:59:04.10	01:00:04.2	GinCl	0.018	Blue	0.97	0.03
2dFGRS TGS503Z245	00:59:13.57	-34:19:15.7	Galaxy	0.012	Blue	0.97	0.03
2MASX J00593609-3020390	00:59:36.09	-30:20:39.0	Galaxy	0.155	Red	0.05	0.75
LBQS 0057-0135	00:59:48.81	-01:19:05.2	QSO	0.325	Blue	0.44	0.08
QSO B0057-3948	00:59:53.21	-39:31:57.3	QSO	3.240	Blue	0.85	0.05
CAIRNS J005959.59-005157.2	00:59:59.58	-00:51:57.1	GinCl	0.166	Red	0.00	1.00
SCMS 679	01:00:04.44	-33:39:32.5	Star	–	Blue	0.53	0.05
2QZ J010009.9-320131	01:00:09.94	-32:01:31.1	Unknown	–	Blue	1.00	0.00
2dFGRS TGS561Z059	01:00:16.17	-34:57:40.6	Galaxy	0.113	Blue	0.52	0.06
2SLAQ J010121.76-000301.7	01:01:21.76	-00:03:01.8	Galaxy	–	Blue	0.14	0.05
QSO B0059-304B	01:02:14.65	-30:07:53.8	QSO	3.240	Blue	0.88	0.01
2SLAQ J010230.03-003206.8	01:02:30.02	-00:32:06.8	Seyfert 1	0.343	Blue	0.50	0.08
2MASX J01023175+0120363	01:02:31.78	01:20:36.1	GinCl	0.016	Blue	0.85	0.02
VV2006 J010336.4-005508	01:03:36.39	-00:55:08.8	QSO	2.443	Blue	0.55	0.06
SDSS J010413.86-011552.1	01:04:13.86	-01:15:52.0	QSO	1.366	Blue	0.96	0.04
QSO B0103+00	01:06:19.23	00:48:23.4	QSO	4.435	Red	0.03	0.04
6dFGS gJ010653.4-324342	01:06:53.44	-32:43:41.9	AGN	0.371	Blue	0.64	0.03
LIRAS J010658.95+010438.3	01:06:58.93	01:04:38.2	AGN	0.327	Red	0.12	0.74
VV2006 J010705.6+000609	01:07:05.55	00:06:09.0	QSO	1.357	Blue	0.74	0.08
UGC 695	01:07:46.47	01:03:50.3	LSB G	0.002	Blue	0.88	0.07
SDSS J010748.62+004453.5	01:07:48.62	00:44:53.7	BCIG	0.266	Red	0.14	0.44
MCG+00-04-011	01:09:01.58	01:22:41.5	GinCl	0.018	Blue	0.74	0.07
MCG+00-04-011	01:09:01.58	01:22:41.5	GinCl	0.018	Blue	0.74	0.07
2SLAQ J010907.59+000649.8	01:09:07.59	00:06:50.0	QSO	1.372	Blue	0.55	0.07
LEDA 1185205	01:09:07.95	01:07:15.5	HII G	0.004	Blue	0.75	0.13
SDSS J010918.56+005419.3	01:09:18.56	00:54:19.4	QSO	1.356	Blue	0.64	0.08
2SLAQ J010925.95-003739.0	01:09:25.96	-00:37:39.0	QSO	1.360	Blue	0.69	0.04
2QZ J011014.0-302445	01:10:13.97	-30:24:44.5	EmG	0.313	Blue	0.60	0.05
2QZ J011119.0-300019	01:11:19.02	-30:00:18.2	EmG	0.309	Blue	0.83	0.05
SDSS J011128.38+000143.7	01:11:28.35	00:01:43.3	QSO	0.765	Blue	0.13	0.10
2dFGRS TGS505Z356	01:12:12.64	-33:56:31.1	Galaxy	0.333	Red	0.43	0.13
2SLAQ J011230.55+001441.5	01:12:30.55	00:14:41.7	QSO	3.259	Blue	0.84	0.03
PB 6318	01:12:58.01	00:58:37.0	Star	–	Blue	0.65	0.04
2dFGRS TGS447Z027	01:13:13.03	-32:26:09.9	Galaxy	0.017	Blue	0.86	0.05
UGC 772	01:13:40.42	00:52:39.0	LSB G	0.004	–	–	–
2SLAQ J011402.35-004750.9	01:14:02.35	-00:47:50.8	Seyfert 1	0.350	Blue	0.55	0.07
VV2006 J011405.3-310903	01:14:05.25	-31:09:02.8	QSO	1.333	Blue	0.21	0.05

Table B1: –continued

Id Object	RA	Dec	Type	Redshift	Group	P(Blue)	P(Red)
						HAC	HDBSCAN
2dFGRS TGS505Z120	01:14:36.11	-32:38:41.0	Galaxy	0.020	Blue	0.79	0.09
SDSS J011531.90-005144.5	01:15:31.89	-00:51:44.3	HII G	0.005	Blue	0.89	0.06
2SLAQ J011533.07-005134.9	01:15:33.06	-00:51:34.8	Galaxy	–	Blue	0.56	0.08
BKD2008 WR 354	01:15:33.79	-00:51:31.5	HII G	0.006	Blue	0.22	0.07
BKD2008 WR 354	01:15:33.79	-00:51:31.5	HII G	0.006	Blue	0.22	0.07
2SLAQ J011542.18+002300.2	01:15:42.18	00:23:00.4	QSO	1.373	Blue	0.69	0.04
2dFGRS TGS505Z064	01:16:38.40	-32:55:39.1	Galaxy	0.018	Blue	0.94	0.02
2dFGRS TGS505Z018	01:17:40.21	-33:04:40.7	Galaxy	0.018	Blue	0.67	0.08
2dFGRS TGS377Z137	01:17:56.44	-30:26:25.8	Galaxy	0.018	Blue	0.87	0.08
2dFGRS TGS506Z276	01:18:05.71	-33:03:09.1	Galaxy	0.012	Blue	0.88	0.07
2SLAQ J011818.13+001455.2	01:18:18.12	00:14:55.5	QSO	1.372	Blue	0.62	0.03
2SLAQ J011829.63+004549.4	01:18:29.62	00:45:49.4	Seyfert 1	0.314	Blue	0.67	0.14
2dFGRS TGS506Z243	01:18:49.15	-33:20:13.1	Galaxy	0.012	Blue	0.83	0.07
2MASX J01195427-3414599	01:19:54.23	-34:15:00.0	EmG	0.019	Blue	0.99	0.01
2dFGRS TGS506Z158	01:20:09.99	-33:14:10.7	Galaxy	0.011	Blue	1.00	0.00
2SLAQ J012110.74-005037.2	01:21:10.74	-00:50:37.1	QSO	1.352	Blue	0.71	0.02
HB93 0119-341B	01:21:52.19	-33:56:15.8	Star	–	Red	0.33	0.18
SDSS J012213.85+005731.4	01:22:13.87	00:57:31.6	HII G	0.008	Blue	1.00	0.00
2dFGRS TGS565Z149	01:22:17.09	-34:02:41.6	Galaxy	0.012	Blue	0.87	0.05
2SLAQ J012226.76+000327.5	01:22:26.75	00:03:27.9	QSO	2.480	Blue	0.86	0.04
QSO B0120-002	01:23:01.78	00:03:23.6	QSO	1.356	Blue	0.81	0.08
2dFGRS TGS297Z222	01:23:50.87	-29:11:46.4	Galaxy	0.000	Blue	0.05	0.03
MCG+00-04-113	01:23:54.75	00:16:56.4	GinCl	0.018	Blue	0.70	0.05
SDSS J012356.34+001230.6	01:23:56.35	00:12:31.0	Galaxy	–	Blue	0.99	0.01
ESO 352-67	01:23:57.47	-33:48:07.5	Galaxy	0.005	Blue	0.89	0.06
SDSS J012405.73+005905.0	01:24:05.73	00:59:04.9	Galaxy	0.007	–	–	–
QSO B0121-324	01:24:16.18	-32:12:21.7	QSO	1.358	Blue	0.61	0.08
2dFGRS TGS507Z113	01:24:30.16	-33:38:45.5	Galaxy	0.305	Red	0.45	0.39
QSO B0122-3232	01:25:04.59	-32:17:14.6	QSO	2.450	Blue	0.41	0.09
2QZ J012526.2-304433	01:25:26.24	-30:44:32.8	EmG	0.311	Blue	0.57	0.07
2QZ J012549.3-280944	01:25:49.29	-28:09:43.6	Galaxy	0.324	–	–	–
LEDA 1180903	01:26:27.03	00:58:51.9	Galaxy	0.008	Blue	0.98	0.02
2dFGRS TGS566Z338	01:26:37.73	-34:35:13.8	Galaxy	0.012	Blue	0.89	0.02
6dFGS gJ012646.5-003845	01:26:46.51	-00:38:44.7	HII G	0.006	Blue	0.54	0.08
ESO 413-7	01:27:59.31	-29:05:12.0	GinCl	0.005	Blue	1.00	0.00
6dFGS gJ012926.6-011159	01:29:26.54	-01:11:59.0	GinCl	0.016	Red	0.42	0.24
SDSS J013034.18-002106.6	01:30:34.17	-00:21:06.5	QSO	3.234	Blue	0.64	0.04
2dFGRS TGS509Z295	01:31:21.84	-33:06:06.2	Galaxy	0.017	Blue	0.81	0.07
2dFGRS TGS508Z142	01:31:45.65	-32:56:56.8	Galaxy	0.017	Blue	0.96	0.02
LEDA 679811	01:31:47.24	-33:10:55.1	Galaxy	–	Blue	1.00	0.00
2dFGRS TGS509Z242	01:32:53.43	-33:26:42.7	Galaxy	0.017	Blue	0.62	0.12
2MASS J01330450+0003553	01:33:04.52	00:03:56.1	low-mass*	0.000	Red	0.13	0.47
2SLAQ J013400.41-010358.2	01:34:00.46	-01:03:59.2		–	Blue	0.99	0.01
RESOLVE rf246	01:34:52.04	-00:38:55.2	Galaxy	0.017	Blue	0.66	0.12
VV2006 J013500.8-004054	01:35:00.83	-00:40:54.2	QSO	1.007	Blue	0.17	0.04
FBQS J0135-0019	01:35:17.53	-00:19:39.0	Seyfert 1	0.312	Blue	0.45	0.11
2QZ J013531.1-313651	01:35:31.16	-31:36:51.0	Galaxy	0.320	Blue	0.46	0.07
SDSS J013701.72-012059.3	01:37:01.71	-01:20:59.1	QSO	2.496	Blue	0.85	0.07
VV2006 J013729.4-320715	01:37:29.40	-32:07:15.7	QSO	1.368	Blue	0.56	0.05
VV2006 J013837.3+002818	01:38:37.28	00:28:18.5	QSO	1.348	Blue	0.82	0.08
2SLAQ J013951.07+002537.9	01:39:51.07	00:25:38.0	QSO	1.342	Blue	0.96	0.04
2E 458	01:40:17.06	-00:50:03.0	Seyfert 1	0.334	Blue	0.27	0.05
SDSS J014125.63+000755.6	01:41:25.64	00:07:55.8	QSO	0.322	Red	0.04	0.85
VV2006 J014224.7-320414	01:42:24.73	-32:04:13.7	QSO	2.460	Blue	0.55	0.09
VV2006 J014303.6-295255	01:43:03.49	-29:52:54.8	QSO	2.450	Blue	0.45	0.07
ESO 353-36	01:43:18.29	-34:12:22.4	EmG	0.013	Red	0.06	0.37
SDSS J014721.12-004505.3	01:47:21.12	-00:45:05.3	QSO	1.348	Red	0.33	0.35
VV2006 J014739.2-285259	01:47:39.21	-28:52:59.2	QSO	0.360	Blue	0.75	0.05

Table B1: –continued

Id Object	RA	Dec	Type	Redshift	Group	P(Blue)	P(Red)
						HAC	HDBSCAN
VV2006 J014739.2-285259	01:47:39.21	-28:52:59.3	QSO	0.360	Blue	0.84	0.05
SDSS J014806.25-002841.6	01:48:06.25	-00:28:41.6	Galaxy	0.215	Blue	0.70	0.04
VV2006 J014812.2+000154	01:48:12.24	00:01:53.5	QSO	1.712	Blue	0.07	0.03
2QZ J014844.1-275610	01:48:44.17	-27:56:11.0	Star	–	Blue	0.73	0.07
IC 1734	01:49:17.03	-32:44:33.1	Galaxy	0.017	Blue	0.59	0.06
VV2006 J014921.5-003220	01:49:21.53	-00:32:20.9	QSO	1.379	Blue	0.81	0.08
RGD2013 J015239.744+010557.768	01:52:39.74	01:05:57.9	Galaxy	0.331	Red	0.15	0.63
RGD2013 J015253.854+011215.480	01:52:53.85	01:12:15.5	Galaxy	0.184	Red	0.05	0.87
2QZ J015257.7-284838	01:52:57.76	-28:48:37.8	Seyfert 1	0.326	Blue	0.52	0.08
2SLAQ J015331.85+002252.8	01:53:31.85	00:22:53.0	QSO	1.367	Blue	0.91	0.02
SDSS J015400.48-004509.5	01:54:00.50	-00:45:10.0	HII G	0.016	Blue	0.66	0.04
2SLAQ J015409.27+002645.2	01:54:09.27	00:26:45.3	QSO	1.355	Blue	0.72	0.05
VV2006 J015410.9-285214	01:54:10.94	-28:52:14.6	QSO	1.356	Blue	0.54	0.07
VV2006 J015415.4-285254	01:54:15.48	-28:52:54.9	QSO	1.344	Blue	0.61	0.07
SDSS J015440.44-000643.9	01:54:40.45	-00:06:43.6	EmG	0.019	Blue	0.35	0.08
2SLAQ J015526.89+000615.4	01:55:26.87	00:06:15.8	Galaxy	0.016	Blue	0.79	0.02
2SLAQ J015529.12-003927.3	01:55:29.07	-00:39:27.1	Galaxy	–	Blue	0.70	0.07
SDSS J015813.75+010143.5	01:58:13.75	01:01:43.4	RRLyr	–	Blue	0.94	0.01
VV2006 J015832.1-301703	01:58:32.15	-30:17:02.8	QSO	1.380	Blue	0.76	0.09
VV2006 J015832.1-301703	01:58:32.16	-30:17:02.7	QSO	1.380	Blue	0.61	0.04
VV2006 J015850.2-300438	01:58:50.22	-30:04:38.1	QSO	1.351	–	–	–
VV2006 J015935.4+000401	01:59:35.48	00:04:01.5	QSO	3.277	Blue	0.63	0.08
SDSS J020025.40+002916.5	02:00:25.40	00:29:16.8	QSO	0.313	Red	0.05	0.68
VV2006 J020055.0-293527	02:00:55.02	-29:35:26.5	QSO	1.349	Blue	0.64	0.05
ESO 414-22	02:01:14.49	-31:43:42.9	GinGroup	0.019	Blue	0.66	0.09
VV98 J020115.4+003136	02:01:15.53	00:31:35.1		0.362	Blue	0.34	0.06
2SLAQ J020200.06-000921.2	02:02:00.06	-00:09:21.2	QSO	1.359	Blue	0.59	0.04
VV96 J020435.5-455923	02:04:35.46	-45:59:24.0	QSO	3.240	Blue	0.73	0.05
LEDA 1193771	02:05:00.83	01:24:03.7	Galaxy	–	Blue	0.59	0.06
2dFGRS TGS514Z164	02:07:20.33	-33:01:54.3	Galaxy	0.011	–	–	–
2SLAQ J020804.48-000023.2	02:08:04.49	-00:00:23.0	QSO	1.339	Blue	0.53	0.04
2SLAQ J020827.06-005208.1	02:08:27.07	-00:52:07.9	QSO	1.341	Blue	0.77	0.06
SDSS J020921.99-005455.5	02:09:22.00	-00:54:55.4	QSO	1.367	Blue	0.97	0.03
2dFGRS TGS515Z070	02:12:25.05	-33:04:59.0	Galaxy	0.106	–	–	–
2dFGRS TGS515Z311	02:14:24.22	-33:14:52.0	Galaxy	0.012	Blue	0.86	0.09
2dFGRS TGS461Z092	02:14:47.63	-32:42:35.2	Galaxy	0.012	Blue	0.82	0.06
2SLAQ J021529.02-005314.8	02:15:29.02	-00:53:14.9	QSO	1.369	Blue	0.63	0.05
2dFGRS TGS460Z130	02:16:01.62	-31:36:51.8	Galaxy	0.012	Blue	0.92	0.02
2dFGRS TGS387Z025	02:16:13.75	-30:50:56.8	Galaxy	0.012	Blue	1.00	0.00
SDSS J021617.19-011046.9	02:16:17.19	-01:10:46.7	QSO	3.264	Blue	0.96	0.01
2SLAQ J021810.52-010147.4	02:18:10.52	-01:01:47.2	QSO	1.353	Blue	0.68	0.06
V* AX For	02:19:28.00	-30:45:46.0	CataclyV*	–	Blue	0.45	0.07
2QZ J022112.5-302559	02:21:12.54	-30:25:59.0		0.315	Blue	0.80	0.08
2SLAQ J022316.91-010049.7	02:23:16.93	-01:00:49.6	Galaxy	–	Blue	0.85	0.06
SHOC 120	02:24:17.14	00:06:26.1	Seyfert 1	0.060	–	–	–
LEDA 667000	02:24:52.74	-34:06:34.3	Galaxy	–	Blue	0.78	0.06
SDSS J022530.93-005007.0	02:25:30.92	-00:50:07.1	Galaxy	0.059	Blue	0.61	0.07
BKD2008 WR 346	02:26:28.28	01:09:37.6	PartofG	0.005	Blue	1.00	0.00
BKD2008 WR 346	02:26:28.28	01:09:37.6	PartofG	0.005	Blue	1.00	0.00
LEDA 546974	02:26:46.27	-43:35:29.6	Galaxy	–	Blue	0.65	0.07
SDSS J022714.48+010536.1	02:27:14.47	01:05:36.3	EmG	0.349	Blue	0.66	0.07
RESOLVE rf668	02:27:19.29	01:01:32.2	Galaxy	0.015	Blue	0.98	0.02
VV2006 J022738.3-313627	02:27:38.28	-31:36:26.4	QSO	1.350	Blue	0.46	0.06
VV2006 J022758.2+000226	02:27:58.20	00:02:25.6	QSO	1.066	–	–	–
LCRS B022613.7-392927	02:28:14.52	-39:16:04.0	Galaxy	–	Blue	0.68	0.05
BKD2008 WR 315	02:28:28.73	-01:08:58.6	PartofG	0.005	Blue	0.91	0.01
2SLAQ J022945.34+000856.2	02:29:45.34	00:08:56.4	Star	–	Blue	0.54	0.09
2QZ J022954.6-303558	02:29:54.69	-30:35:58.4	Seyfert 1	0.372	Blue	0.34	0.06

Table B1: –continued

Id Object	RA	Dec	Type	Redshift	Group	P(Blue)	P(Red)
						HAC	HDBSCAN
Pul -3 180355	02:29:57.00	-01:00:32.3	Star	–	Red	0.04	0.06
2dFGRS TGS463Z130	02:30:09.77	-31:36:18.2	Galaxy	0.015	Blue	1.00	0.00
SDSS J023020.93+001355.5	02:30:20.93	00:13:55.8	Seyfert 1	0.335	Blue	0.20	0.06
UGC 2009	02:32:09.34	-01:23:10.3	Galaxy	0.015	Red	0.03	0.88
2dFGRS TGS518Z089	02:32:18.08	-33:50:43.0	Galaxy	0.016	Blue	0.59	0.14
SDSS J023230.63-011654.5	02:32:30.63	-01:16:54.5	QSO	1.364	Blue	0.61	0.05
6dFGS gJ023241.8-391744	02:32:41.88	-39:17:42.8	Galaxy	0.005	Blue	0.51	0.08
SDSS J023248.71+005138.8	02:32:48.71	00:51:38.8	Galaxy	0.344	Blue	0.57	0.06
V* HP Cet	02:33:22.62	00:50:59.4	Nova	-0.000	Blue	0.54	0.09
NGC 986	02:33:34.29	-39:02:40.9	EmG	0.007	Blue	0.93	0.07
VV2006 J023335.4-010744	02:33:35.37	-01:07:44.6	QSO	0.367	Blue	0.50	0.06
SDSS J023628.77-005829.7	02:36:28.75	-00:58:30.0	Galaxy	0.008	Blue	0.78	0.08
VV2006 J023635.7-003203	02:36:35.69	-00:32:03.4	QSO	1.362	–	–	–
SDSS J024059.15+004545.8	02:40:59.14	00:45:45.9	QSO	3.233	Blue	0.99	0.01
VV2006 J024235.0-010351	02:42:34.91	-01:03:51.9	QSO	1.373	Blue	0.56	0.03
EKS96 NGC 1068 91	02:42:46.94	00:01:26.2	HII	–	Blue	0.14	0.06
ZBF2015 NGC1073 1	02:43:35.61	01:22:37.9	HII	–	Blue	0.27	0.06
ZBF2015 NGC1073 16	02:43:37.69	01:22:22.5	HII	–	Blue	0.94	0.06
ZBF2015 NGC1073 21	02:43:42.74	01:21:34.4	HII	–	Blue	0.50	0.07
ZBF2015 NGC1073 10	02:43:44.03	01:22:40.5	HII	–	Blue	0.80	0.05
6dFGS gJ024605.3-330500	02:46:05.28	-33:04:59.4	Galaxy	0.017	Blue	0.83	0.01
2MASS J02462415-0029539	02:46:24.14	-00:29:52.9	Star	–	Blue	0.76	0.03
Gaia DR2 2497764348684940160	02:46:24.75	-00:30:16.3	QSO	–	Blue	0.53	0.07
BKD2008 WR 316	02:46:25.42	-00:30:09.8	PartofG	0.005	Blue	0.57	0.04
2SLAQ J024626.59-003000.2	02:46:26.57	-00:30:00.4	Star	–	Blue	1.00	0.00
2SLAQ J025100.64+001707.2	02:51:00.64	00:17:07.3	QSO	2.466	Blue	0.70	0.07
2SLAQ J025216.75+001741.2	02:52:16.73	00:17:41.2	Galaxy	0.005	Blue	0.89	0.06
2SLAQ J025252.02-002211.7	02:52:52.00	-00:22:11.6	QSO	1.370	Blue	0.85	0.05
SHOC 143	02:54:26.13	-00:41:22.7	Seyfert 1	0.015	Blue	0.88	0.08
NVSS J025557+004132	02:55:57.24	00:41:33.5	RadioG	0.014	Red	0.12	0.32
QSO B0253+0058	02:56:07.25	01:10:38.8	QSO	1.349	Blue	0.66	0.08
HBQS 0253+0022	02:56:25.32	00:34:29.4	HII	0.013	Blue	0.99	0.01
LEDA 1170514	02:56:28.43	00:36:28.2	Galaxy	0.009	Blue	0.64	0.05
2dFGRS TGS522Z138	02:57:45.54	-33:28:55.5	Galaxy	0.335	Red	0.43	0.28
2MASSI J0259103-002239	02:59:10.38	-00:22:39.8	Seyfert 1	0.360	Blue	0.54	0.09
2SLAQ J030309.82+001337.5	03:03:09.83	00:13:37.8	Galaxy	–	–	–	–
UGC 2517	03:04:12.47	-01:11:33.8	Galaxy	0.013	Red	0.53	0.20
2SLAQ J030417.77-004931.7	03:04:17.77	-00:49:31.5	Galaxy	–	Blue	0.62	0.11
LEDA 1142424	03:04:34.76	-00:28:30.7	Seyfert 1	0.006	Blue	0.98	0.02
LBQS 0302-0019	03:04:49.85	-00:08:13.4	QSO	3.295	Blue	0.95	0.02
2MASS J03045799+0057131	03:04:57.98	00:57:14.0	Blue	0.012	Blue	0.99	0.01
MCG+00-08-089	03:05:18.24	-00:09:34.1	Galaxy	0.009	Blue	0.72	0.04
LBQS 0303+0110	03:06:12.72	01:21:57.3	QSO	1.335	Blue	0.70	0.07
WISE J030629.21-335332.3	03:06:29.22	-33:53:32.3	AGN	0.780	Blue	0.67	0.11
SDSS J030630.33-000622.9	03:06:30.33	-00:06:22.9	Galaxy	0.106	Red	0.12	0.72
SDSS J030715.63+004352.1	03:07:15.60	00:43:52.6	Galaxy	0.010	Blue	1.00	0.00
2SLAQ J030757.55+000712.0	03:07:57.55	00:07:12.1	QSO	1.343	Blue	0.74	0.04
2SLAQ J031129.69-001701.4	03:11:29.70	-00:17:01.5	QSO	1.357	Blue	0.72	0.05
2QZ J031130.9-315250	03:11:30.92	-31:52:51.1	WD*	–	Blue	0.58	0.13
ESO 417-20	03:12:48.61	-31:29:10.7	GinGroup	0.013	Blue	0.96	0.03
SDSS J031258.36-000453.6	03:12:58.36	-00:04:53.6	Galaxy	0.117	Blue	0.76	0.02
2dFGRS TGS398Z109	03:13:56.08	-31:28:12.6	Galaxy	0.014	Blue	0.32	0.09
2SLAQ J031428.25+004506.6	03:14:28.25	00:45:07.0	Galaxy	–	Blue	1.00	0.00
2dFGRS TGS471Z114	03:16:15.31	-31:12:33.3	Galaxy	0.004	Blue	0.81	0.04
2SLAQ J031618.00-003025.2	03:16:18.01	-00:30:24.9	Galaxy	–	Blue	1.00	0.00
2dFGRS TGS524Z054	03:16:50.65	-33:18:03.8	Galaxy	0.006	Blue	0.94	0.02
2dFGRS TGS524Z054	03:16:50.66	-33:18:04.0	Galaxy	0.006	Blue	0.96	0.04
2SLAQ J031829.06-000040.3	03:18:29.06	-00:00:40.5	Galaxy	–	Blue	0.65	0.04

Table B1: –continued

Id Object	RA	Dec	Type	Redshift	Group	P(Blue)	P(Red)
						HAC	HDBSCAN
VV2006 J031845.2-001844	03:18:45.17	-00:18:45.3	QSO	3.224	Blue	0.97	0.03
2SLAQ J031937.30-002641.1	03:19:37.29	-00:26:41.0	QSO	1.371	Blue	0.37	0.08
SDSS J032244.90+004442.4	03:22:44.90	00:44:42.3	QSO Candidate	0.304	Blue	0.94	0.03
6dFGS gJ032504.2-365540	03:25:04.15	-36:55:39.9	GinPair	0.006	Blue	0.64	0.08
6dFGS gJ032512.9-362210	03:25:13.07	-36:22:09.7	Galaxy	0.004	Blue	0.75	0.12
JPB2015 051.4803133-32.8829964	03:25:55.27	-32:52:58.9	GlCl	–	Blue	0.83	0.08
SDSS J033226.29-011126.2	03:32:26.29	-01:11:26.0	QSO	1.361	Blue	0.52	0.07
SDSS J033226.29-011126.2	03:32:26.30	-01:11:26.3	QSO	1.361	Blue	0.53	0.05
SDSS J033310.10+000849.1	03:33:10.08	00:08:49.2	Seyfert 2	0.327	Red	0.13	0.37
VV2006 J033458.5-000744	03:34:58.48	-00:07:43.9	QSO	1.357	Blue	0.77	0.02
VV2006 J033821.6+003106	03:38:21.51	00:31:06.6	QSO	1.349	Blue	0.64	0.04
2XMM J033841.3-353134	03:38:41.36	-35:31:34.4	BLLac	0.360	Blue	0.26	0.06
2XMM J033841.3-353134	03:38:41.37	-35:31:34.2	BLLac	0.360	Blue	0.25	0.05
VV2006 J033927.5-344707	03:39:27.45	-34:37:07.0	QSO	1.364	Blue	0.55	0.04
CXO J034012.4-353740	03:40:12.39	-35:37:40.1	HMXB	–	Blue	0.18	0.05
SDSS J034019.89+010330.7	03:40:19.89	01:03:30.7	EmG	0.322	Blue	0.72	0.11
VV2006 J034023.0-351606	03:40:22.99	-35:16:07.0	QSO	1.372	Blue	0.55	0.08
2XMM J034050.4-352620	03:40:50.48	-35:26:21.7	AGN	1.366	Blue	0.59	0.08
ESO 358-51	03:41:32.55	-34:53:19.0	GinGroup	0.006	Blue	0.88	0.07
2MASS J03424773+0109331	03:42:47.72	01:09:33.0	Seyfert 1	0.360	Blue	0.16	0.07
2SLAQ J034304.64+002512.1	03:43:04.65	00:25:12.3	Star	–	Blue	0.43	0.09
LCRS B034214.4-381736	03:44:04.68	-38:08:11.9	Galaxy	–	Red	0.00	1.00
VV2006 J034408.3-003106	03:44:08.25	-00:31:05.8	QSO	1.646	Blue	0.93	0.03
SDSS J034427.73-002740.4	03:44:27.73	-00:27:40.2	Galaxy	0.041	Red	0.53	0.25
SDSS J034517.02-001549.8	03:45:17.01	-00:15:49.7	QSO	1.335	Blue	1.00	0.00
6dFGS gJ034545.4-362046	03:45:45.38	-36:20:46.1	GinCl	0.004	Blue	0.84	0.02
SDSS J034602.53-000058.7	03:46:02.53	-00:00:58.6	Seyfert 2	0.308	Red	0.18	0.50
2MASX J03472195-3251054	03:47:21.94	-32:51:05.2	GinCl	0.116	Red	0.29	0.56
SDSS J034907.92+010943.3	03:49:07.93	01:09:43.2	LSB G	0.014	Blue	0.96	0.04
MCG+00-10-021	03:49:08.87	01:09:46.3	LSB G	0.014	Blue	0.85	0.05
FASTT 83	03:51:19.36	00:32:16.6	EB*	–	Red	0.12	0.54
LEDA 607287	03:55:02.55	-38:35:40.2	Galaxy	–	Red	0.17	0.75
Gaia DR2 4857261601188886016	03:55:16.01	-37:29:44.7	Candidate WD*	–	–	–	–
ZJM2003 SA 95-2230	03:55:38.45	00:28:34.9	Star	–	Blue	0.98	0.02
2dFGRS TGS817Z154	03:56:05.58	-49:28:40.7	Galaxy	0.003	Blue	0.98	0.01
SDSSCGB 74387.1	03:56:50.79	-00:14:34.9	Galaxy	–	Red	0.37	0.27
2dFGRS TGS848Z501	03:57:22.10	-37:01:54.1	Galaxy	0.016	Blue	0.97	0.03
6dFGS gJ035732.5-000047	03:57:32.27	-00:00:47.6	Galaxy	0.017	Blue	0.69	0.06
UGC 2913	03:59:03.91	01:21:33.6	Galaxy	0.013	Blue	0.55	0.09
UGC 2913	03:59:03.91	01:21:33.6	Galaxy	0.013	Blue	0.55	0.09
ESO 201-14	04:00:29.38	-49:01:48.4	EmG	0.004	Blue	0.78	0.05
2MASS J04004608-3424277	04:00:46.07	-34:24:27.7	AGN Candidate	–	Blue	0.53	0.11
6dFGS gJ040053.2-351416	04:00:53.13	-35:14:16.2	Galaxy	0.015	Blue	0.80	0.04
QSO B0401-3505	04:03:10.56	-34:56:56.8	QSO	3.251	Blue	0.67	0.04
LCRS B040209.0-382209	04:03:56.75	-38:13:58.5	Galaxy	–	Blue	0.54	0.14
6dFGS gJ040441.2-345756	04:04:41.14	-34:57:55.8	Galaxy	0.008	Blue	0.80	0.07
6dFGS gJ040520.4-364859	04:05:20.40	-36:48:59.0	Galaxy	0.003	Blue	0.39	0.11
6dFGS gJ040520.4-364859	04:05:20.40	-36:48:58.8	Galaxy	0.003	Blue	0.40	0.12
Gaia DR2 4845009910624639232	04:05:27.97	-38:11:22.1	Star	–	Blue	0.99	0.01
VV96 J041130.5-335331	04:11:30.51	-33:53:31.1	QSO	1.350	Blue	0.76	0.04
2dFGRS TGS894Z351	04:11:58.37	-37:58:44.0	Galaxy	0.013	Blue	0.96	0.04
ESO 420-11	04:12:53.30	-31:18:30.2	GinGroup	0.005	Blue	0.97	0.03
2dFGRS TGS894Z291	04:13:00.00	-38:19:42.5	Galaxy	0.012	Blue	0.98	0.02
Gaia DR2 4872129059981617536	04:20:06.78	-32:51:20.0	Candidate WD*	–	–	–	–
LEDA 685147	04:20:56.84	-32:50:42.8	Galaxy	–	–	–	–
2MASX J04255940-4316225	04:25:59.40	-43:16:22.6	Galaxy	0.078	Blue	0.98	0.02
LEDA 579779	04:26:32.58	-41:01:56.6	Galaxy	–	Blue	1.00	0.00
LEDA 125483	04:26:44.34	-42:15:41.2	Galaxy	0.015	Blue	1.00	0.00

Table B1: –continued

Id Object	RA	Dec	Type	Redshift	Group	P(Blue)	P(Red)
						HAC	HDBSCAN
LEDA 568379	04:26:44.87	-42:05:40.5	Galaxy	–	Blue	0.98	0.01
LEDA 554934	04:26:44.91	-42:58:38.4	Galaxy	–	Blue	0.90	0.03
MCG-07-10-009	04:27:42.24	-42:38:20.4	Galaxy	0.016	Blue	0.83	0.06
2MASX J04282877-4314283	04:28:28.71	-43:14:29.1	Galaxy	0.015	Blue	0.70	0.04
6dFGS gJ043139.6-301514	04:31:39.57	-30:15:14.1	CataclyV*	-0.000	Blue	0.27	0.08
LEDA 697927	04:32:44.32	-32:01:20.1	Galaxy	–	Red	0.10	0.85
ESO 251-12	04:33:09.79	-43:46:13.6	Galaxy	0.010	Blue	0.82	0.05
ESO 304-2	04:35:19.80	-42:12:11.8	Galaxy	0.007	Blue	1.00	0.00
LEDA 494343	04:35:41.79	-47:52:43.9	Galaxy	–	Blue	0.89	0.05
HM2015b 236 3	04:37:11.17	-46:41:06.8	Galaxy	–	Blue	0.38	0.06
LEDA 692923	04:37:18.21	-32:22:10.3	Galaxy	–	Blue	1.00	0.00
Gaia DR2 4790561549357871744	04:37:35.04	-44:20:28.8	Candidate RRLyr	–	Blue	0.99	0.01
LEDA 681270	04:38:23.53	-33:05:08.6	Galaxy	–	Blue	0.83	0.02
6dFGS gJ043927.4-425912	04:39:27.45	-42:59:11.8	Galaxy	0.362	Blue	0.41	0.06
LEDA 606705	04:45:44.98	-38:38:48.7	Galaxy	–	Blue	1.00	0.00
LEDA 88363	04:48:23.05	-44:52:57.7	Galaxy	–	Blue	0.97	0.03
2dFGRS TGS880Z325	04:50:02.35	-47:28:39.0	Galaxy	0.010	Blue	0.68	0.10
LEDA 512705	04:51:48.86	-46:37:36.8	Galaxy	–	Blue	1.00	0.00
Gaia DR2 4811451372635865984	04:52:31.12	-44:11:04.3	Star	–	Blue	0.48	0.11
LEDA 686311	04:53:19.46	-32:46:32.8	Galaxy	–	Blue	0.85	0.04
VV98 J045444.5-481300	04:54:43.04	-48:13:20.2	Seyfert 1	0.363	Blue	0.68	0.06
SN 2012at	04:54:52.74	-37:19:15.5	SN	–	Blue	0.56	0.13
2MASX J04550020-3715351	04:55:00.19	-37:15:35.4	GinPair	0.008	Blue	0.88	0.05
LEDA 715392	04:55:26.51	-30:35:28.6	Galaxy	–	Blue	0.20	0.07
ESO 499-24	09:57:01.69	-26:29:28.5	Galaxy	0.015	Blue	0.89	0.03
LEDA 859547	09:57:06.62	-19:07:06.1	Galaxy	–	Blue	0.84	0.08
LEDA 1022680	09:57:23.46	-07:12:51.4	Galaxy	–	Blue	0.18	0.06
2MASX J09583711-4704597	09:58:37.10	-47:05:00.4	Galaxy	0.012	Blue	0.63	0.07
CMI2006b H42-f02-1939	09:59:46.82	-19:28:00.0	Galaxy	0.265	Blue	0.99	0.01
CRTS J095950.7-383024	09:59:50.88	-38:30:22.9	RRLyr	–	Blue	0.97	0.03
LEDA 605183	10:00:05.44	-38:47:28.7	Galaxy	–	Blue	0.57	0.08
NGC 3095	10:00:05.83	-31:33:10.8	GinGroup	0.009	Red	0.08	0.49
LEDA 154528	10:00:49.12	-30:32:41.9	Galaxy	–	Blue	0.75	0.07
SDSS J100059.08+032751.4	10:00:59.07	03:27:51.5	Galaxy	0.007	Blue	0.74	0.08
ESO 567-3	10:01:09.07	-19:26:29.7	LSB G	0.012	Blue	0.99	0.01
LEDA 1011555	10:01:34.08	-07:52:55.7	Galaxy	–	Blue	0.90	0.08
Gaia DR2 5670829935783719936	10:02:11.73	-19:25:37.1	Star	–	Blue	0.32	0.06
2QZ J100215.7-001056	10:02:15.83	-00:10:55.8	QSO	0.353	Blue	0.63	0.09
VVDS 100108471	10:02:25.38	01:19:36.8	Galaxy	0.123	Blue	1.00	0.00
ESO 262-15	10:02:38.71	-45:29:53.9	GinGroup	0.012	Red	0.17	0.48
BCP93 F2 H6	10:02:51.82	-26:09:23.9	HII	–	Blue	1.00	0.00
EBU2007 7	10:02:54.69	-26:08:59.6	BlueSG*	0.001	Blue	0.24	0.09
H69 NGC 3109 12	10:02:56.31	-26:08:58.5	HII	–	Blue	0.26	0.09
PRS2007 HII 44	10:02:59.47	-26:08:46.4	HII	–	Blue	0.43	0.11
PRS2007 HII 44	10:02:59.48	-26:08:46.4	HII	–	Blue	0.48	0.10
PSO J150.7588-26.1494	10:03:02.10	-26:08:58.7	AGN Candidate	–	Blue	0.67	0.08
2MASX J10030450-1949377	10:03:04.51	-19:49:38.1	Galaxy	0.012	Blue	0.84	0.04
2dFGRS TGN094Z280	10:03:15.05	-05:54:32.8	Galaxy	0.013	Blue	0.96	0.04
EBU2007 3	10:03:17.64	-26:10:01.7	BlueSG*	0.001	Blue	0.26	0.08
VV96 J100342.1-150808	10:03:41.93	-15:08:08.9	QSO	0.342	Blue	0.43	0.07
2MASX J10035230-3124480	10:03:52.32	-31:24:48.5	Galaxy	0.009	Blue	0.99	0.01
2MASX J10041992-4425311	10:04:19.86	-44:25:32.6	Galaxy	0.012	Blue	0.90	0.07
2MASX J10050765-1951299	10:05:07.68	-19:51:30.2	Galaxy	–	Blue	0.64	0.06
2dFGRS TGN421Z115	10:05:17.31	01:38:21.7	Galaxy	0.004	Blue	0.88	0.05
2MFGC 7816	10:05:28.51	-38:07:30.1	Galaxy	–	Blue	1.00	0.00
VV2006 J100539.9+040914	10:05:39.88	04:09:14.7	QSO	1.355	Blue	0.59	0.07
CRTS J100548.9-254146	10:05:48.99	-25:41:47.1	RRLyr	–	Blue	0.99	0.01
2MASX J10061715-0634276	10:06:17.20	-06:34:27.7	Galaxy	0.011	Blue	0.95	0.05

Table B1: –continued

Id Object	RA	Dec	Type	Redshift	Group	P(Blue)	P(Red)
						HAC	HDBSCAN
6dFGS gJ100622.2-264958	10:06:22.20	-26:49:57.2	Galaxy	0.015	Blue	0.99	0.01
6dFGS gJ100631.4-320236	10:06:31.39	-32:02:35.9	GinGroup	0.008	Red	0.42	0.24
NGC 3125	10:06:33.37	-29:56:07.8	HII G	0.004	Blue	0.53	0.10
1RXH J100633.9-295612	10:06:33.90	-29:56:11.6	X	–	Blue	0.73	0.07
2MASX J10071106-1904039	10:07:11.07	-19:04:04.6	Galaxy	0.012	Blue	0.87	0.05
LEDA 699275	10:07:27.24	-31:55:26.9	Galaxy	–	Blue	0.94	0.06
CRTS J100733.7-301921	10:07:33.84	-30:19:19.4	EB*	–	Blue	0.80	0.03
RX J1007.5-2017	10:07:34.65	-20:17:32.4	CataclyV*	–	Blue	0.48	0.11
RX J1007.5-2017	10:07:34.66	-20:17:32.5	CataclyV*	–	Blue	0.18	0.08
2MASX J10081071-3331017	10:08:10.76	-33:31:02.2	Galaxy	0.010	Red	0.54	0.20
2MASX J10082199-1448362	10:08:22.01	-14:48:36.1	Galaxy	0.008	Blue	0.75	0.06
LEDA 768685	10:08:30.09	-26:21:33.0	Galaxy	–	Blue	0.97	0.03
2MASX J10091380-4300089	10:09:13.81	-43:00:09.0	GinGroup	0.015	Red	0.21	0.33
LEDA 648630	10:09:50.26	-35:27:43.3	Galaxy	–	Blue	0.97	0.03
LEDA 3094360	10:09:58.73	-20:30:59.5	Galaxy	–	Blue	0.84	0.06
ESO 435-50	10:10:50.41	-30:25:24.4	Galaxy	0.009	Blue	0.73	0.06
LEDA 654529	10:10:51.81	-35:00:28.1	Galaxy	–	Blue	1.00	0.00
NGC 3146	10:11:09.90	-20:52:14.0	EmG	0.013	Blue	0.75	0.06
LEDA 729120	10:11:13.49	-29:27:27.9	Galaxy	–	Blue	0.65	0.13
CRTS J101200.8-365725	10:12:00.81	-36:57:25.2	EB*	–	Red	0.32	0.28
LEDA 691325	10:12:03.36	-32:28:06.8	Galaxy	–	Blue	1.00	0.00
Gaia DR2 5407412036686860672	10:12:47.58	-47:33:51.1	Star	–	Blue	0.63	0.10
LEDA 655538	10:12:59.65	-34:56:06.6	Galaxy	–	Blue	0.99	0.01
2MASX J10134201-3451194	10:13:41.91	-34:51:18.3	EmG	0.015	Blue	0.72	0.08
LEDA 658182	10:13:54.08	-34:44:23.0	Galaxy	–	Blue	0.85	0.04
LEDA 713928	10:14:25.56	-30:42:30.1	Galaxy	–	Blue	0.67	0.03
2MASX J10142679-2329036	10:14:26.81	-23:29:04.9	Galaxy	0.012	Blue	0.99	0.01
ESO 263-21	10:14:41.74	-44:51:14.1	EmG	0.004	Blue	0.80	0.03
IC 2559	10:14:45.36	-34:03:33.0	EmG	0.010	Red	0.29	0.36
ESO 263-22	10:14:48.13	-43:31:49.5	Galaxy	0.010	Blue	0.69	0.06
ESO 263-23	10:14:57.32	-43:37:09.2	Galaxy	0.010	Red	0.35	0.23
ESO 567-32	10:15:44.54	-20:17:44.0	EmG	0.012	Red	0.06	0.34
Gaia DR2 5407327747940309248	10:15:58.31	-47:58:09.1	Star	–	Blue	0.32	0.08
IC 2560	10:16:18.68	-33:33:49.8	Seyfert 2	0.010	Red	0.33	0.28
ESO 567-39	10:17:13.15	-21:04:00.3	EmG	0.012	Blue	0.72	0.04
LEDA 702814	10:18:05.73	-31:38:49.0	Galaxy	–	Blue	0.64	0.07
VV96 J101821.7-214008	10:18:21.76	-21:40:07.7	QSO	2.470	Blue	0.48	0.08
CRTS SSS120320 J101854-400644	10:18:53.51	-40:06:43.7	Candidate CV*	–	Blue	0.29	0.10
ESO 375-7	10:19:01.23	-37:40:19.2	Galaxy	0.016	Blue	1.00	0.00
CTS 1011	10:19:21.17	-22:08:33.4	HII G	0.012	Blue	0.43	0.12
CTS 1011	10:19:21.28	-22:08:35.9	HII G	0.012	Blue	0.58	0.14
NGC 3208	10:19:41.31	-25:48:52.9	EmG	0.010	Blue	0.62	0.06
6dFGS gJ102028.5-232845	10:20:28.52	-23:28:45.3	Galaxy	0.012	Blue	1.00	0.00
LEDA 800754	10:20:32.72	-23:26:54.0	Galaxy	–	Blue	0.48	0.09
CRTS SSS120215 J102042-335002	10:20:42.16	-33:50:02.4	Candidate CV*	–	Blue	0.61	0.08
Gaia DR2 5668001579559758720	10:20:43.31	-20:47:54.6	Star	–	Blue	0.54	0.07
ESO 500-30	10:20:48.90	-23:27:57.1	EmG	0.012	Red	0.63	0.18
6dFGS gJ102109.3-325140	10:21:09.27	-32:51:39.9	Galaxy	0.010	Blue	0.96	0.04
6dFGS gJ102121.0-213628	10:21:21.03	-21:36:27.7	Galaxy	0.011	Blue	0.99	0.01
LEDA 592969	10:22:02.22	-39:52:45.9	Galaxy	–	Blue	0.89	0.06
6dFGS gJ102239.9-302931	10:22:39.94	-30:29:30.6	AGN Candidate	0.317	Blue	0.45	0.08
ESO 263-30	10:22:59.54	-42:49:38.9	Galaxy	0.009	Blue	0.83	0.03
ESO 317-19	10:23:02.34	-39:09:59.8	GinGroup	0.010	Blue	0.84	0.06
ESO 375-18	10:23:40.27	-35:49:33.5	EmG	0.015	Red	0.40	0.39
ESO 375-18	10:23:40.27	-35:49:33.5	EmG	0.015	Red	0.29	0.45
ESO 263-32	10:24:21.47	-43:55:01.6	Galaxy	–	Blue	0.85	0.02
ESO 500-34	10:24:31.43	-23:33:09.6	Seyfert 2	0.012	Red	0.05	0.52
CRTS J102513.4-354014	10:25:13.46	-35:40:16.7	EB*	–	Blue	0.99	0.01

Table B1: –continued

Id Object	RA	Dec	Type	Redshift	Group	P(Blue)	P(Red)
						HAC	HDBSCAN
6dFGS gJ102607.5-243321	10:26:07.41	-24:33:20.2	Galaxy	0.013	Blue	0.75	0.08
ESO 436-21	10:26:21.70	-29:11:57.8	GinCl	–	Blue	0.96	0.01
NAME OT J102706-434341	10:27:05.83	-43:43:41.3	CataclyV*	–	Blue	0.75	0.05
ESO 500-42	10:27:20.27	-23:48:19.6	Galaxy	0.012	Blue	0.97	0.01
SN 2001db	10:27:50.35	-43:54:20.8	SN	–	Red	0.57	0.34
SN 2001db	10:27:50.37	-43:54:20.8	SN	–	Red	0.40	0.30
LWZ2002 5	10:27:51.28	-43:53:58.5	X	–	Blue	0.70	0.11
NGC 3256	10:27:51.29	-43:54:14.0	IG	0.009	Red	0.35	0.40
NGC 3256	10:27:51.30	-43:54:13.7	IG	0.009	Red	0.37	0.38
LDT2000 R02	10:27:51.73	-43:54:13.6	X	–	Blue	0.94	0.06
LDT2000 R02	10:27:51.73	-43:54:13.3	X	–	Blue	0.94	0.06
EF2003 B3	10:27:52.88	-43:54:11.5	HII	0.010	Blue	0.45	0.07
EF2003 B3	10:27:52.89	-43:54:11.2	HII	0.010	Blue	0.46	0.07
EF2003 B3	10:27:52.89	-43:54:11.2	HII	0.010	Blue	0.46	0.07
ESO 436-26	10:28:42.96	-31:02:17.7	AGN	0.014	Red	0.33	0.27
CRTS CSS140309 J102844-161303	10:28:43.86	-16:13:03.3	CataclyV*	–	Blue	0.13	0.07
SHM2017 J157.24190-30.14112	10:28:58.05	-30:08:27.7	RRLyr	–	Blue	0.19	0.04
ESO 317-34	10:29:00.71	-40:04:57.9	GinGroup	0.009	Blue	0.97	0.03
IC 2582	10:29:11.07	-30:20:32.7	EmG	0.014	Blue	0.79	0.05
LEDA 636268	10:30:30.59	-36:28:47.1	Galaxy	–	Blue	0.76	0.08
LEDA 636268	10:30:30.59	-36:28:47.1	Galaxy	–	Blue	0.65	0.05
LEDA 83158	10:30:57.69	-34:42:28.5	GinGroup	–	Blue	0.74	0.05
ESO 317-39	10:31:00.18	-40:10:42.5	Galaxy	0.015	Red	0.13	0.29
ESO 436-32	10:31:29.90	-32:42:47.1	EmG	0.013	Blue	0.51	0.11
NGC 3281	10:31:52.11	-34:51:13.0	Seyfert 2	0.011	Red	0.05	0.36
LEDA 571751	10:31:57.37	-41:48:41.1	Galaxy	–	Blue	0.62	0.02
BM98 2	10:32:59.22	-27:32:36.9	GinCl	0.016	Blue	0.95	0.02
6dFGS gJ103317.5-430444	10:33:17.40	-43:04:43.1	Galaxy	0.010	Blue	0.64	0.07
ESO 375-64	10:34:00.75	-35:16:57.6	GinGroup	0.009	Blue	0.62	0.07
ESO 375-64	10:34:00.75	-35:16:57.3	GinGroup	0.009	Blue	0.64	0.07
LEDA 754029	10:34:26.74	-27:30:04.0	GinCl	0.012	Blue	0.98	0.02
ESO 436-42	10:34:38.75	-28:35:00.1	EmG	0.012	Blue	0.76	0.04
ESO 568-18	10:34:54.59	-20:32:55.6	EmG	0.012	Blue	0.98	0.01
2MASX J10345852-4054438	10:34:58.52	-40:54:43.3	Galaxy	0.016	Blue	0.73	0.06
6dFGS gJ103502.9-293024	10:35:02.88	-29:30:23.8	GinCl	0.012	Blue	0.97	0.03
ESO 437-3	10:35:07.72	-27:59:28.7	EmG	0.008	Blue	0.70	0.04
ESO 375-69	10:35:18.72	-36:52:42.5	EmG	0.011	Blue	0.95	0.05
ESO 501-22	10:35:21.68	-27:41:44.5	GinCl	0.010	Blue	0.96	0.04
LEDA 712419	10:35:31.70	-30:50:00.0	Galaxy	–	Blue	0.62	0.03
LEDA 535830	10:35:34.16	-44:34:41.1	Galaxy	–	Blue	0.77	0.08
LEDA 784823	10:36:02.66	-24:54:24.1	Galaxy	–	Blue	0.81	0.03
LEDA 743415	10:36:06.94	-28:17:45.0	Galaxy	–	Blue	0.87	0.06
ESO 501-32	10:36:22.11	-25:22:35.4	EmG	0.013	Blue	0.81	0.05
CZ2003 1060C-393 25	10:36:30.34	-27:54:04.0	GinCl	0.008	Blue	0.82	0.06
6dFGS gJ103645.4-281005	10:36:45.48	-28:10:02.7	GinCl	0.012	Blue	0.90	0.03
LEDA 769967	10:36:54.86	-26:14:26.0	HII G	0.012	Blue	0.14	0.05
6dFGS gJ103656.1-265414	10:36:56.08	-26:54:13.6	Galaxy	0.096	Blue	0.99	0.01
LEDA 742546	10:37:01.84	-28:22:01.7	GinCl	–	Blue	0.87	0.05
6dFGS gJ103704.4-312157	10:37:04.45	-31:21:57.3	Galaxy	0.010	Blue	0.81	0.03
NGC 3314	10:37:12.87	-27:41:02.2	EmG	0.009	Blue	0.64	0.11
6dFGS gJ103719.9-281420	10:37:19.89	-28:14:19.9	GinCl	0.012	Blue	1.00	0.00
LEDA 753354	10:37:22.21	-27:32:41.9	Galaxy	–	Blue	0.70	0.08
WISE J103754.92-242544.5	10:37:54.92	-24:25:44.6	MIR	–	Red	0.14	0.47
ESO 501-61	10:38:05.84	-25:05:40.1	IG	0.012	Blue	0.94	0.02
WLH83 1036-378A	10:38:14.37	-38:05:25.5	HII	–	Blue	0.93	0.03
LEDA 740766	10:38:28.68	-28:30:55.0	GinCl	–	Blue	0.97	0.03
2MASX J10383034-2332546	10:38:30.34	-23:32:54.7	Galaxy	–	Blue	0.91	0.05
ESO 501-65	10:38:33.42	-27:44:13.8	EmG	0.015	Blue	0.86	0.06

Table B1: –continued

Id Object	RA	Dec	Type	Redshift	Group	P(Blue)	P(Red)
						HAC	HDBSCAN
WPVS 78	10:38:41.50	−25:35:32.2	EmG	0.010	Blue	0.49	0.12
6dFGS gJ103857.2-200242	10:38:57.24	−20:02:41.8	Galaxy	0.007	Blue	0.91	0.02
LEDA 838980	10:39:13.02	−20:38:12.5	Galaxy	—	Blue	0.64	0.04
MCG-04-25-054	10:39:26.01	−23:45:16.8	EmG	0.013	Blue	0.60	0.06
2MASS J10395999-4701261	10:39:59.97	−47:01:26.3	CataclyV*	—	Blue	0.55	0.12
2MASS J10395999-4701261	10:39:59.97	−47:01:26.3	CataclyV*	—	Blue	0.55	0.12
ESO 437-37	10:40:31.01	−29:16:10.5	IG	0.012	Blue	0.90	0.03
ESO 568-20	10:40:58.70	−21:47:04.3	EmG	0.012	Red	0.22	0.50
6dFGS gJ104102.1-304740	10:41:02.12	−30:47:40.1	Galaxy	0.011	Blue	0.82	0.05
CRTS J104104.0-341120	10:41:03.86	−34:11:23.4	RRLyr	—	Blue	1.00	0.00
ESO 568-21	10:41:15.17	−21:01:22.9	Seyfert 1	0.012	Blue	0.95	0.03
ESO 437-42	10:41:27.71	−31:46:49.1	Galaxy	0.009	Blue	0.82	0.05
ESO 437-42	10:41:27.71	−31:46:49.1	Galaxy	0.009	Blue	0.82	0.05
LEDA 3081775	10:41:35.15	−37:28:09.5	Galaxy	—	Blue	0.81	0.05
6dFGS gJ104139.4-274638	10:41:39.43	−27:46:38.2	Galaxy	0.014	Blue	0.66	0.07
ESO 568-22	10:42:06.62	−22:06:20.1	IG	0.007	Blue	0.74	0.05
LEDA 31904	10:42:19.50	−36:19:13.7	Galaxy	—	Blue	0.97	0.03
6dFGS gJ104238.0-235609	10:42:37.99	−23:56:08.4	Galaxy	0.003	Blue	0.90	0.02
ESO 437-50	10:43:31.00	−30:46:20.0	EmG	0.013	Blue	0.76	0.03
ESO 437-50	10:43:31.00	−30:46:20.0	EmG	0.013	Blue	0.76	0.03
6dFGS gJ104409.7-204909	10:44:09.71	−20:49:09.5	Galaxy	0.013	Blue	0.82	0.04
ESO 569-2	10:45:00.21	−22:09:08.2	IG	0.010	Blue	1.00	0.00
6dFGS gJ104534.8-241702	10:45:34.75	−24:17:01.3	Galaxy	0.012	Blue	0.80	0.07
6dFGS gJ104617.1-282524	10:46:17.11	−28:25:23.6	EmG	0.012	Blue	0.73	0.04
LEDA 718607	10:46:30.26	−30:19:17.8	Galaxy	—	Blue	0.83	0.04
ESO 376-20	10:46:38.45	−36:21:11.9	EmG	0.014	Blue	0.69	0.07
ESO 501-96	10:46:47.54	−23:19:39.8	Galaxy	0.011	Blue	0.94	0.06
Gaia DR2 5391507429181636352	10:47:23.91	−41:59:49.3	Star	—	Blue	0.56	0.07
EC 10453-2041	10:47:44.36	−20:57:48.8	EmG	0.012	Blue	0.53	0.09
2MASX J10475221-2004542	10:47:52.11	−20:04:53.3	HII G	0.013	Blue	0.87	0.02
2MASX J10475221-2004542	10:47:52.13	−20:04:53.5	HII G	0.013	Blue	1.00	0.00
KRB2015 A	10:48:23.47	−25:09:43.6	Radio	—	Red	0.62	0.19
2MASX J10482527-2151000	10:48:25.30	−21:51:00.5	Galaxy	0.015	Blue	0.73	0.04
SN 2018aqi	10:48:25.45	−25:09:36.1	SN	0.012	Red	0.20	0.07
LEDA 688498	10:48:42.32	−32:38:37.4	Galaxy	—	Blue	1.00	0.00
LEDA 738826	10:49:46.88	−28:40:37.1	Galaxy	—	Blue	0.50	0.08
2MASX J10503963-1832342	10:50:39.64	−18:32:34.4	Galaxy	0.014	Red	0.43	0.22
LEDA 844461	10:51:00.37	−20:14:21.3	Galaxy	—	Blue	1.00	0.00
6dFGS gJ105101.9-282017	10:51:01.81	−28:20:16.5	Galaxy	0.011	Blue	0.85	0.03
LEDA 851789	10:51:27.40	−19:41:37.0	Galaxy	—	Blue	0.99	0.01
6dFGS gJ105149.2-215323	10:51:49.07	−21:53:17.5	Galaxy	0.010	Blue	0.67	0.05
6dFGS gJ105233.0-230900	10:52:33.04	−23:08:59.6	Galaxy	0.318	Blue	0.29	0.08
MASTER OT J105440.86-391319.0	10:54:40.84	−39:13:19.0	Candidate SN*	—	Blue	0.76	0.08
6dFGS gJ105521.6-232527	10:55:21.62	−23:25:27.3	Galaxy	0.012	Blue	0.87	0.06
6dFGS gJ105521.6-232527	10:55:21.63	−23:25:27.3	Galaxy	0.012	Blue	0.90	0.04
2MASX J10563839-2047119	10:56:38.39	−20:47:12.2	Galaxy	0.012	Blue	0.87	0.03
LEDA 849870	10:56:48.51	−19:50:00.4	Galaxy	—	Blue	0.85	0.08
ESO 376-28	10:57:04.32	−33:09:20.3	Galaxy	0.013	Red	0.45	0.30
ESO 264-52	10:57:13.91	−47:40:11.3	Galaxy	0.016	Red	0.63	0.14
LEDA 648093	10:57:36.52	−35:30:15.8	Galaxy	—	Blue	1.00	0.00
2MASX J10584423-1909304	10:58:44.25	−19:09:31.1	Galaxy	0.012	Blue	1.00	0.00
EC 10566-3120	10:58:59.03	−31:36:34.1	CataclyV*	—	Blue	0.52	0.08
2MASX J10590982-2759589	10:59:09.86	−27:59:59.3	Galaxy	0.005	Blue	0.91	0.04
Gaia DR2 5386613537284200960	11:01:51.26	−46:53:04.5	Candidate RRLyr	—	Blue	1.00	0.00
Gaia DR2 3537117430403448320	11:01:57.97	−23:47:27.3	PM*	—	Blue	0.53	0.10
V* TU Crt	11:03:36.57	−21:37:45.9	CataclyV*	—	Blue	0.58	0.09
NGC 3513	11:03:46.16	−23:14:42.1	GinPair	0.004	Blue	0.76	0.04
FAUST 2807	11:03:59.06	−18:46:36.1	UV	—	Blue	1.00	0.00

Table B1: –continued

Id Object	RA	Dec	Type	Redshift	Group	P(Blue)	P(Red)
						HAC	HDBSCAN
ESO 570-5	11:07:13.10	-19:49:07.2	IG	0.012	Blue	0.89	0.05
NGC 3529	11:07:19.13	-19:33:20.0	EmG	0.013	Blue	0.96	0.03
NGC 3529	11:07:19.14	-19:33:19.5	EmG	0.013	Blue	0.96	0.02
NGC 3565	11:07:47.84	-20:01:20.2	IG	0.013	Blue	0.89	0.04
ESO 570-10	11:10:50.57	-21:58:28.3	Galaxy	0.012	Blue	0.86	0.08
LEDA 821419	11:10:57.23	-21:56:53.3	Galaxy	–	Blue	0.89	0.03
6dFGS gJ111351.0-212655	11:13:50.97	-21:26:54.8	Galaxy	0.012	Blue	0.88	0.07
NGC 3597	11:14:42.00	-23:43:39.9	EmG	0.012	Blue	0.67	0.08
VV96 J111644.8-171127	11:16:43.58	-17:11:41.5	QSO	0.375	Blue	0.41	0.07
LEDA 861413	11:17:15.01	-18:58:24.4	Galaxy	–	–	–	–
LEDA 809402	11:17:35.06	-22:45:06.2	Galaxy	–	Red	0.29	0.49
CRTS J112256.0-242841	11:22:56.09	-24:28:40.0	EB*	–	Blue	1.00	0.00
LEDA 786212	11:29:34.18	-24:46:39.1	Galaxy	–	Blue	0.50	0.08
VV2010c J113128.4-195903	11:31:28.46	-19:59:02.8	AGN	0.363	Blue	0.58	0.07
CRTS SSS110509 J113219-213943	11:32:19.01	-21:39:42.9	Candidate CV*	–	–	–	–
2dFGRS TGN444Z198	11:34:24.52	01:09:15.7	Galaxy	0.017	Blue	0.88	0.04
MGC 22410	11:36:12.70	00:04:54.9	Star	–	Blue	1.00	0.00
UGC 6578	11:36:36.73	00:49:02.1	EmG	0.004	Blue	0.58	0.13
GAMA 6821	11:36:36.79	00:48:55.8	Galaxy	0.004	Blue	0.08	0.04
V* RZ Leo	11:37:22.18	01:48:58.9	CataclyV*	-0.000	Blue	0.17	0.05
Gaia DR2 3541998025080414336	11:37:49.97	-20:07:37.1	Candidate WD*	–	Blue	0.37	0.10
2dFGRS TGN238Z266	11:38:54.33	-01:38:34.1	Galaxy	0.006	Blue	0.49	0.08
CRTS J113855.5-211148	11:38:55.60	-21:11:47.7	RRLyr	–	Blue	0.97	0.03
SDSS J113901.39+012017.8	11:39:01.39	01:20:17.7	Galaxy	0.005	Blue	0.37	0.11
LBQS 1136-0109	11:39:04.35	-01:26:25.0	QSO	1.375	Blue	0.81	0.03
6dFGS gJ114135.0-181141	11:41:35.04	-18:11:40.5	Galaxy	0.012	Blue	0.95	0.02
2dFGRS TGN238Z191	11:41:45.67	-01:54:04.8	HII G	0.006	Blue	0.86	0.06
ESO 571-16	11:42:09.14	-18:10:08.7	Galaxy	0.012	Red	0.05	0.40
SDSS J114212.38+002002.5	11:42:12.33	00:20:03.4	PartofG	0.019	Blue	0.98	0.02
2QZ J114214.5-023154	11:42:14.64	-02:31:53.3	Galaxy	0.319	Blue	0.90	0.02
CRTS J114238.0-202722	11:42:37.96	-20:27:21.8	RRLyr	–	Blue	0.99	0.01
2QZ J114250.9+013057	11:42:50.95	01:30:58.2	Seyfert 1	0.361	Blue	0.80	0.08
SDSS J114329.34-020319.7	11:43:29.34	-02:03:19.5	QSO	3.304	–	–	–
SDSS J114329.34-020319.7	11:43:29.35	-02:03:19.9	QSO	3.304	–	–	–
SDSSCGB 59619.2	11:43:46.11	-01:16:34.0	Galaxy	–	–	–	–
GAMA 396970	11:43:47.41	01:30:53.9	Galaxy	0.102	Blue	0.59	0.06
LINEAR 2118419	11:44:08.82	01:24:20.7	RRLyr	0.001	Blue	0.98	0.02
2QZ J114450.8+014324	11:44:50.95	01:43:24.8	EmG	0.333	Blue	0.58	0.07
Gaia DR2 3544179185567992320	11:44:55.76	-17:56:39.4	Candidate WD*	–	Blue	0.46	0.11
2dFGRS TGN310Z256	11:45:08.04	-00:59:18.2	Galaxy	0.004	Blue	0.48	0.09
SDSS J114511.70-005402.6	11:45:11.72	-00:54:02.5	Galaxy	0.204	Red	0.15	0.75
2MASX J11451524-2044471	11:45:15.26	-20:44:47.5	Galaxy	0.012	Blue	0.70	0.08
Z 12-78	11:45:26.30	00:00:14.8	Galaxy	0.013	Blue	0.95	0.05
SDSS J114600.44+001037.4	11:46:00.45	00:10:37.0	Galaxy	0.311	Red	0.29	0.55
2dFGRS TGN310Z211	11:46:07.72	-00:27:28.7	Galaxy	0.013	Blue	0.97	0.03
SDSS J114643.10+011118.6	11:46:43.12	01:11:18.8	QSO	3.220	Blue	0.80	0.05
2QZ J114711.4-002706	11:47:11.47	-00:27:05.8	EmG	0.312	Blue	0.98	0.02
2MASX J11481815-0138230	11:48:18.21	-01:38:23.8	Seyfert 1	0.013	Blue	0.81	0.06
SDSS J114818.33-013830.8	11:48:18.35	-01:38:30.5	Galaxy	0.013	Blue	0.52	0.08
VV2006 J114939.6+014624	11:49:39.60	01:46:25.5	QSO	1.362	Blue	0.56	0.06
2dFGRS TGN378Z115	11:50:23.78	-00:31:41.9	HII G	0.013	Blue	0.54	0.11
P78 ACO 1392 C	11:50:36.30	-00:34:06.6	GinCl	0.006	Blue	0.58	0.13
SDSS J115036.42-003402.0	11:50:36.39	-00:34:02.6	Galaxy	0.006	Blue	0.57	0.13
VV2006 J115049.2-005149	11:50:49.29	-00:51:49.1	QSO	1.354	Blue	0.34	0.08
LEDA 807513	11:51:13.02	-22:53:25.2	Galaxy	–	Red	0.34	0.44
SDSS J115129.42-000333.8	11:51:29.45	-00:03:33.6	Galaxy	0.326	Red	0.20	0.34
2dFGRS TGN242Z154	11:51:32.96	-02:22:21.9	Galaxy	0.004	Blue	0.26	0.09
LEDA 37102	11:51:33.35	-02:22:21.7	Seyfert 1	0.003	Blue	0.06	0.03

Table B1: –continued

Id Object	RA	Dec	Type	Redshift	Group	P(Blue)	P(Red)
						HAC	HDBSCAN
SDSS J115216.86+012327.2	11:52:16.88	01:23:27.5	Galaxy	0.304	Red	0.11	0.59
2QZ J115217.3-025303	11:52:17.34	-02:53:02.7	EmG	0.320	Blue	0.97	0.02
ESO 572-7	11:52:27.62	-20:06:14.1	GinGroup	0.005	Blue	0.80	0.03
Mrk 1307	11:52:37.30	-02:28:09.4	Seyfert 1	0.004	Blue	0.24	0.08
SDSS J115237.67-022806.3	11:52:37.67	-02:28:06.8	HII G	0.004	Blue	0.27	0.09
2dFGRS TGN311Z206	11:52:47.52	-00:40:07.7	Seyfert 1	0.005	Blue	0.25	0.09
2dFGRS TGN311Z206	11:52:47.53	-00:40:07.8	Seyfert 1	0.005	Blue	0.26	0.09
2dFGRS TGN176Z274	11:53:14.07	-03:24:32.6	Galaxy	0.004	Blue	0.66	0.07
2dFGRS TGN243Z103	11:53:28.66	-03:13:48.9	Galaxy	0.005	Blue	1.00	0.00
VV2006 J115345.5-024320	11:53:45.44	-02:43:20.4	QSO	1.347	Blue	0.84	0.04
UM 465B	11:54:12.31	00:08:12.4	GinPair	–	Blue	0.88	0.07
SDSS J115456.54+001106.0	11:54:56.59	00:11:05.5	Galaxy	0.004	–	–	–
SDSS J115511.13+002905.1	11:55:11.19	00:29:05.5	Galaxy	0.011	Blue	0.30	0.09
SDSS J115511.67+002925.0	11:55:11.70	00:29:25.0	Galaxy	0.011	Blue	0.39	0.09
2dFGRS TGN243Z202	11:57:11.86	-02:41:12.9	Galaxy	0.005	Blue	0.57	0.13
SDSS J115712.38-024111.2	11:57:12.29	-02:41:11.3	Galaxy	0.005	Blue	0.58	0.14
ESO 572-25	11:57:28.04	-19:37:26.5	Galaxy	0.006	Blue	0.52	0.08
2QZ J115737.0-020138	11:57:37.08	-02:01:37.3	Galaxy	0.328	Blue	0.80	0.07
2QZ J115737.0-020138	11:57:37.09	-02:01:37.2	Galaxy	0.328	Blue	0.84	0.04
VV2006 J115748.0+014320	11:57:48.02	01:43:20.9	QSO	1.364	Blue	0.56	0.05
VV2006 J115754.2-013815	11:57:54.26	-01:38:16.0	QSO	4.380	–	–	–
LEDA 839904	11:57:56.69	-20:33:56.4	Galaxy	–	Blue	0.39	0.11
2MASX J11580803-1753363	11:58:08.00	-17:53:36.2	Galaxy	0.008	Blue	0.83	0.04
6dFGS gJ115823.8-193103	11:58:23.80	-19:31:03.2	Galaxy	0.005	Blue	0.54	0.07
ESO 572-34	11:58:58.18	-19:01:47.7	EmG	0.004	Blue	0.55	0.13
GAMA 137854	11:59:23.49	-01:43:22.3	Galaxy	0.304	Blue	0.59	0.16
SN 1996W	11:59:28.93	-19:15:22.8	SN	–	Blue	0.85	0.04
LEDA 836770	12:00:19.81	-20:48:07.5	Galaxy	–	Blue	0.78	0.05
2MASX J12002013-0106229	12:00:20.20	-01:06:23.8	Galaxy	0.005	Blue	0.89	0.04
SDSS J120021.76-024331.0	12:00:21.77	-02:43:30.9	QSO	3.248	Blue	0.81	0.03
BKD2008 WR 14	12:00:26.30	-01:06:07.0	PartofG	0.005	Blue	0.51	0.08
VV2006 J120038.3+011246	12:00:38.29	01:12:46.5	QSO	1.358	Blue	0.68	0.08
QSO B1158-1842	12:00:44.95	-18:59:44.5	QSO	2.453	Blue	0.53	0.07
2dFGRS TGN244Z048	12:00:47.47	-03:25:12.1	Galaxy	0.005	Blue	0.99	0.01
RDS2004 MGS sure 22	12:00:47.72	-00:01:24.3	HI	0.006	Blue	0.97	0.03
UGC 7000	12:01:10.85	-01:17:50.2	GinPair	0.005	Blue	1.00	0.00
QSO B1158+007	12:01:23.26	00:28:28.5	QSO	1.369	Blue	0.78	0.08
LEDA 802182	12:01:30.48	-23:19:06.8	Galaxy	–	Blue	0.71	0.02
CEB2007 Cluster 2	12:01:50.41	-18:52:12.4	Cl*	–	Blue	0.54	0.08
CXOU J120150.4-185221	12:01:50.41	-18:52:19.8	HMXB	–	Blue	0.56	0.07
ZBF2015 Arp244 82	12:01:50.49	-18:52:02.5	HII	–	Blue	0.94	0.06
NU2000 9 3	12:01:51.13	-18:52:28.8	Radio	–	Blue	0.85	0.03
NU2000 13 5	12:01:51.24	-18:51:45.3	Radio	–	Blue	0.60	0.04
MLT2008 S2-2	12:01:51.90	-18:52:28.2	Cl*	–	Blue	0.78	0.03
ZBF2015 Arp244 123	12:01:52.28	-18:52:19.4	HII	–	Blue	0.99	0.01
ZBF2015 Arp244 80	12:01:52.96	-18:52:03.5	HII	–	Red	0.31	0.60
ZBF2015 Arp244 5	12:01:52.98	-18:52:08.7	HII	–	Blue	0.98	0.02
ZBF2015 Arp244 14	12:01:53.52	-18:51:44.2	HII	–	Blue	0.92	0.03
WZ2002 1	12:01:53.57	-18:53:09.0	Radio	–	Red	0.29	0.29
BEK2006 Complex 6	12:01:54.54	-18:52:07.5	Cl*	–	Blue	0.56	0.03
WS95 89	12:01:54.54	-18:53:03.8	PartofG	–	Blue	0.57	0.07
WBC2014 180.48062-18.88025	12:01:55.35	-18:52:48.7	MolCld	0.005	Blue	0.34	0.06
ZBF2015 Arp244 6	12:01:55.54	-18:52:22.9	HII	–	Blue	0.85	0.02
ZFB2014 GMC 98	12:01:55.68	-18:52:14.0	MolCld	–	Blue	0.67	0.02
WZ2002 9	12:01:55.70	-18:52:42.8	Radio	–	Blue	0.35	0.06
ZBF2015 Arp244 10	12:01:56.29	-18:52:38.8	HII	–	Blue	1.00	0.00
CRTS J120206.7-230305	12:02:06.75	-23:03:06.0	EB*	–	Blue	0.95	0.02
SDSS J120250.38+001931.6	12:02:50.39	00:19:31.5	Galaxy	0.333	Red	0.05	0.39

Table B1: –continued

Id Object	RA	Dec	Type	Redshift	Group	P(Blue)	P(Red)
						HAC	HDBSCAN
SDSS J120515.80-024222.6	12:05:15.80	-02:42:22.6	WD*	0.000	Blue	0.38	0.08
LEDA 913203	12:06:37.73	-15:17:17.2	Galaxy	–	Blue	0.97	0.03
6dFGS gJ120650.7-141256	12:06:50.66	-14:12:55.9	Galaxy	0.013	Blue	0.79	0.04
VV2006 J120700.4+011155	12:07:00.41	01:11:56.4	QSO	1.520	Blue	0.75	0.07
SDSS J120920.53-002855.3	12:09:20.55	-00:28:55.3	QSO	3.237	Blue	0.83	0.05
VV2006 J121010.8-003909	12:10:10.82	-00:39:09.7	QSO	1.008	Blue	0.07	0.06
SDSS J121026.38-000513.2	12:10:26.41	-00:05:13.2	Galaxy	0.310	Blue	0.70	0.04
SDSS J121043.55-003907.2	12:10:43.59	-00:39:08.5	Seyfert 1	0.331	Red	0.03	0.06
2QZ J121101.0+012024	12:11:01.05	01:20:25.0	EmG	0.333	Blue	0.96	0.04
Mrk 1313	12:12:14.73	00:04:20.6	Seyfert 1	0.008	Blue	0.77	0.08
2dFGRS TGN246Z007	12:12:15.90	-00:33:53.2	Galaxy	0.008	Blue	0.54	0.07
2MASS J12125978+0149231	12:12:59.78	01:49:23.2	EB*	–	Red	0.63	0.21
SDSS J121304.91-003901.2	12:13:04.93	-00:39:01.2	Galaxy	0.189	Red	0.06	0.64
2dFGRS TGN247Z167	12:13:38.79	-01:17:36.3	Galaxy	0.008	Blue	0.86	0.03
6dFGS gJ121348.2-143140	12:13:48.16	-14:31:39.8	Galaxy	0.330	Blue	0.62	0.06
SDSS J121435.24-015924.4	12:14:35.26	-01:59:24.4	QSO	3.233	Blue	0.86	0.09
VV2006 J121515.2-013542	12:15:15.23	-01:35:40.8	QSO	1.350	Blue	0.57	0.04
2QZ J121539.4-022149	12:15:39.47	-02:21:47.2	Galaxy	0.319	Blue	0.78	0.05
2QZ J121607.5-022559	12:16:07.54	-02:25:57.6	Galaxy	0.324	Blue	1.00	0.00
SDSS J121759.99+002558.1	12:18:00.05	00:25:57.7	Galaxy	0.003	–	–	–
2dFGRS TGN181Z079	12:18:07.07	-03:06:28.8	Galaxy	0.001	Red	0.12	0.71
LEDA 927634	12:18:19.06	-14:12:19.9	Galaxy	–	Blue	0.97	0.03
LEDA 927634	12:18:19.06	-14:12:20.0	Galaxy	–	Blue	0.96	0.04
QSO B1216+0216	12:18:55.80	02:00:02.1	QSO	0.327	Blue	0.31	0.09
VV2006 J121942.5-001821	12:19:42.47	-00:18:21.4	QSO	1.337	Blue	0.79	0.07
2dFGRS TGN385Z034	12:19:53.13	01:46:24.0	HII G	0.007	Blue	0.88	0.05
SDSS J122003.72+010632.0	12:20:03.73	01:06:32.4	Galaxy	0.315	Red	0.07	0.21
2dFGRS TGN385Z025	12:20:11.53	01:57:31.1	LSB G	0.007	Blue	0.54	0.13
2dFGRS TGN181Z173	12:20:28.80	-01:50:21.0	Galaxy	0.008	Blue	0.82	0.06
LEDA 1143004	12:20:30.39	-00:27:03.0	Galaxy	0.007	–	–	–
VV2006 J122130.9+010727	12:21:30.97	01:07:28.1	QSO	1.370	Blue	0.66	0.04
Gaia DR2 3521773745637847552	12:21:34.41	-14:57:50.5	Star	–	Blue	0.09	0.04
LEDA 3294456	12:21:55.83	-01:35:36.0	Galaxy	0.006	Blue	0.54	0.08
Gaia DR2 3521681421020417408	12:22:39.34	-15:29:12.1	Star	–	Blue	0.43	0.09
SDSS J122322.39-000801.6	12:23:22.39	-00:08:01.7	Galaxy	0.318	Blue	0.69	0.03
MCG+00-32-004	12:24:12.47	00:34:01.0	Galaxy	0.007	Blue	0.96	0.04
2SLAQ J122421.12+002354.1	12:24:21.13	00:23:54.4	QSO	0.334	Blue	0.55	0.11
NGC 4385	12:25:42.74	00:34:21.9	AGN	0.007	Blue	0.60	0.04
2QZ J122547.3-012007	12:25:47.38	-01:20:05.7	Galaxy	0.317	Blue	0.72	0.03
SHOC 373a	12:26:22.64	-01:15:17.3	HII G	0.007	Blue	0.34	0.09
SHOC 373b	12:26:22.73	-01:15:12.3	HII G	0.007	Blue	0.21	0.07
VV2006 J122625.7+011604	12:26:25.67	01:16:04.6	QSO	2.478	Blue	0.57	0.09
2SLAQ J122641.43-002005.1	12:26:41.45	-00:20:05.1	Seyfert 1	0.353	Blue	0.60	0.06
MCG+00-32-013	12:27:04.54	-00:54:21.5	GinPair	0.007	Blue	0.84	0.07
MCG+00-32-013	12:27:04.56	-00:54:22.0	GinPair	0.007	Blue	0.87	0.03
VV2006 J122707.1+010811	12:27:07.13	01:08:11.3	QSO	2.189	Blue	0.16	0.04
MIO2012 R1	12:27:46.07	01:36:01.5	Cl*	–	Blue	0.57	0.12
2dFGRS TGN387Z059	12:28:15.92	01:49:43.7	Galaxy	0.003	Blue	1.00	0.00
2QZ J122851.2-022630	12:28:51.34	-02:26:29.2	EmG	0.331	Blue	0.93	0.07
2dFGRS TGN250Z094	12:29:14.65	-01:21:55.2	Galaxy	0.007	Blue	0.51	0.08
2dFGRS TGN250Z087	12:29:46.33	-01:17:42.0	LSB G	0.008	Blue	0.76	0.15
2dFGRS TGN321Z099	12:29:58.88	00:01:37.9	RadioG	0.008	Red	0.08	0.68
2dFGRS TGN388Z078	12:30:54.31	00:57:50.5	Galaxy	0.008	Blue	0.66	0.08
BKD2008 WR 29	12:31:48.01	-02:58:13.0	PartofG	0.008	Blue	0.80	0.03
2QZ J123202.6+003124	12:32:02.70	00:31:24.7	EmG	0.329	Blue	0.79	0.07
2dFGRS TGN251Z016	12:32:23.64	-01:44:24.3	HII G	0.007	Blue	0.77	0.03
GALEX 2414740977348515009	12:32:36.17	-03:18:39.4	Blue	–	Blue	0.57	0.05
MGC 34804	12:32:41.58	00:03:26.4	Star	–	Blue	0.74	0.11

Table B1: –continued

Id Object	RA	Dec	Type	Redshift	Group	P(Blue)	P(Red)
						HAC	HDBSCAN
DCD2013 CSS J123702.3-151643	12:37:02.41	-15:16:43.5	RRLyr	–	Blue	0.90	0.01
Gaia DR2 3527007524064861312	12:39:19.45	-14:47:31.1	Star	–	–	–	–
2MASX J12442692-1252359	12:44:26.92	-12:52:35.9	Galaxy	0.018	Blue	1.00	0.00
LEDA 924051	12:50:47.04	-14:29:01.5	Galaxy	–	Blue	1.00	0.00
LEDA 932206	12:58:59.15	-13:51:42.3	Galaxy	–	Blue	0.52	0.08
CRTS SSS120721 J125901-133442	12:59:00.82	-13:34:42.0	Candidate CV*	–	Blue	0.48	0.09
6dFGS gJ125904.7-144623	12:59:04.67	-14:46:23.5	Galaxy	0.016	Blue	0.73	0.04
2MASX J12593269-1514196	12:59:32.75	-15:14:19.3	Galaxy	–	Blue	0.31	0.10
LEDA 914340	13:00:03.04	-15:12:17.2	Galaxy	–	Blue	0.98	0.02
NGC 4887	13:00:39.30	-14:39:59.3	GinPair	0.009	Blue	0.98	0.02
LEDA 936912	13:01:07.09	-13:31:02.4	Galaxy	0.004	Blue	0.33	0.09
VV96 J130243.5-135553	13:02:43.59	-13:55:52.8	QSO	1.391	Blue	0.54	0.07
LEDA 45114	13:03:33.44	-14:19:23.1	EmObj	0.008	Blue	0.76	0.08
2MASX J13044961-1311288	13:04:49.65	-13:11:28.2	Galaxy	0.010	Blue	0.72	0.06
LCRS B130214.7-120615	13:04:52.39	-12:22:18.7	Galaxy	–	Blue	1.00	0.00
LEDA 949391	13:05:58.52	-12:40:08.5	Galaxy	–	Blue	0.62	0.07
LEDA 105081	13:10:08.77	-12:12:20.4	Galaxy	0.013	Blue	0.90	0.02
UGCA 332	13:11:58.29	-12:03:51.4	EmG	0.007	Blue	0.90	0.04
LEDA 976320	13:12:28.41	-10:35:24.4	Galaxy	–	Blue	0.86	0.07
LCRS B131057.8-121222	13:13:36.14	-12:28:15.2	EmObj	0.013	Blue	0.49	0.12
LEDA 126038	13:15:07.97	-12:31:05.1	Galaxy	0.013	Blue	1.00	0.00
LEDA 981336	13:17:40.89	-10:10:59.5	Galaxy	–	Blue	1.00	0.00
SDSS J131742.35-002015.8	13:17:42.37	-00:20:15.7	Galaxy	0.356	–	–	–
6dFGS gJ131743.9-010002	13:17:43.96	-01:00:01.1	AGN	0.004	Blue	0.08	0.04
2MASX J13192221-1509232	13:19:22.29	-15:09:23.6	Galaxy	0.009	Blue	0.96	0.04
MCG-02-34-029	13:19:42.72	-11:28:28.5	GinGroup	0.009	Blue	0.98	0.02
2SLAQ J131957.59-003446.7	13:19:57.60	-00:34:46.6	Star	–	Blue	0.97	0.03
QSO B1317-122	13:19:59.20	-12:29:16.8	QSO	0.329	Blue	0.46	0.09
NGC 5088	13:20:20.33	-12:34:18.1	Galaxy	0.005	Blue	0.89	0.03
SDSS J132023.46-004730.9	13:20:23.47	-00:47:30.8	QSO	3.255	–	–	–
6dFGS gJ132134.7-151056	13:21:34.68	-15:10:55.5	Galaxy	0.009	Blue	1.00	0.00
6dFGS gJ132137.8-145120	13:21:37.83	-14:51:19.7	Galaxy	0.009	Blue	0.97	0.01
2dFGRS TGN263Z056	13:22:17.11	-00:32:54.4	EmG	0.018	–	–	–
SHM2017 J200.93368-12.05326	13:23:44.09	-12:03:11.8	RRLyr	–	Blue	0.96	0.03
LEDA 46982	13:25:48.67	-11:36:37.8	BlueCompG	0.004	Blue	0.06	0.03
LEDA 46982	13:25:48.68	-11:36:38.0		0.004	Blue	0.06	0.03
LEDA 991902	13:26:05.10	-09:22:12.6	Galaxy	–	Blue	0.54	0.09
BPS CS 22889-0007	13:31:59.47	-09:53:02.6	RRLyr	0.001	Blue	0.99	0.01
NVSS J133618-072251	13:36:18.64	-07:22:51.8	Radio	–	Blue	0.73	0.08
LCRS B133356.3-061328	13:36:33.05	-06:28:45.2	Galaxy	–	Red	0.07	0.85
GALEX 2697385722761974216	13:39:09.19	-08:19:40.8	Blue	–	Blue	0.65	0.03
LEDA 1025584	13:41:04.99	-07:01:05.8	Galaxy	–	Blue	0.65	0.02
DCD2013 CSS J134330.9-151858	13:43:31.01	-15:18:58.9	RRLyr	–	Blue	1.00	0.00
V* HS Vir	13:43:38.44	-08:14:03.7	CataclyV*	–	Blue	0.86	0.06
SN 2018evt	13:46:39.20	-09:38:36.0		SN	0.029	Blue	0.83
GALEX 2697315366902694354	13:47:49.82	-04:10:10.6	Blue	–	Blue	0.61	0.05
2dFGRS TGN202Z201	13:49:42.20	-02:11:59.1	Galaxy	0.011	Blue	0.74	0.03
GALEX 2699039396840082228	13:50:33.33	-12:16:42.9	Blue	–	Blue	0.55	0.07
6dFGS gJ135123.7-060412	13:51:23.70	-06:04:11.7	Galaxy	0.010	Blue	0.98	0.02
2dFGRS TGN202Z136	13:51:35.65	-02:33:15.0	Galaxy	0.015	Blue	0.99	0.01
SDSSCGB 287.4	13:52:03.90	-02:07:22.3	Galaxy	–	Blue	0.79	0.09
SDSSCGB 287.2	13:52:04.24	-02:07:48.9	Galaxy	0.015	Blue	0.65	0.07
LEDA 126156	13:54:11.29	-03:26:27.2	Galaxy	0.014	Blue	0.80	0.08
LEDA 126156	13:54:11.40	-03:26:27.0	Galaxy	0.014	Blue	0.90	0.04
QSO B1352-104	13:54:46.53	-10:41:02.6	QSO	0.330	Blue	0.41	0.06
VV 99b	13:55:33.98	-05:58:17.0	GinPair	–	Blue	0.87	0.07
2dFGRS TGN141Z158	13:55:37.68	-04:11:43.8	Galaxy	0.012	Blue	0.33	0.10
VV 100a	13:55:45.46	-06:00:15.9	Galaxy	–	Blue	0.74	0.07

Table B1: –continued

Id Object	RA	Dec	Type	Redshift	Group	P(Blue)	P(Red)
						HAC	HDBSCAN
VV 100d	13:55:46.68	-06:00:40.8	Galaxy	–	Blue	0.56	0.14
VV2006 J135602.8-022624	13:56:02.79	-02:26:23.3	QSO	1.373	–	–	–
2dFGRS TGN203Z232	13:56:53.48	-02:38:52.2	Galaxy	0.013	Blue	0.62	0.05
2dFGRS TGN142Z266	13:58:08.62	-04:08:43.6	Galaxy	0.015	Blue	0.75	0.02
SDSSCGB 16922.1	13:58:41.49	-01:31:15.7	Galaxy	–	Red	0.28	0.36
LEDA 1020082	14:02:45.08	-07:22:25.8	Galaxy	–	Blue	0.52	0.08
2MASS J14265388+0525172	14:26:53.89	05:25:17.4	QSO	0.323	Blue	0.45	0.10
UGC 9252	14:27:10.82	05:07:59.3	Galaxy	0.005	Blue	1.00	0.00
LAM2019 J1428+0500 B	14:28:55.39	05:00:21.9	Possible lensImage	–	Blue	0.62	0.10
GALEX 2429518413625830432	14:28:55.46	05:00:19.9	Blue	–	Blue	0.81	0.07
DES J142943.42+052122.7	14:29:43.44	05:21:22.9	GinCl	–	Red	0.37	0.42
SDSS J142958.66+044611.0	14:29:58.65	04:46:11.3	BCIG	0.456	Red	0.08	0.18
LEDA 1290447	14:41:28.04	05:51:52.3	Galaxy	0.027	Blue	1.00	0.00
SDSS J145344.51+045645.8	14:53:44.52	04:56:46.0	QSO	3.328	Blue	0.71	0.03
SDSSCGB 43444.3	14:55:33.70	04:46:43.2	AGN	0.334	Red	0.38	0.38
SDSS J200143.74+004918.4	20:01:43.73	00:49:18.4	QSO	–	Blue	0.36	0.07
SDSS J200432.38+001041.3	20:04:32.39	00:10:41.4	low-mass*	–	–	–	–
SHM2017 J302.70083-00.21773	20:10:48.20	-00:13:03.9	RRLyr	–	Blue	1.00	0.00
SHM2017 J302.70083-00.21773	20:10:48.20	-00:13:03.9	RRLyr	–	Blue	1.00	0.00
SSV2012 4869177	20:22:35.51	-00:40:09.9	RRLyr	–	Blue	0.92	0.02
SSV2012 4472518	20:22:37.80	-00:02:50.5	RRLyr	–	Blue	0.99	0.01
UGC 11566	20:28:12.02	00:17:18.2	Galaxy	0.006	Blue	0.88	0.05
SDSS J202906.80+005453.5	20:29:06.81	00:54:53.6	QSO	–	Blue	0.97	0.03
2SLAQ J204340.03+002853.4	20:43:40.04	00:28:53.6	Seyfert 1	0.317	Blue	0.53	0.08
SDSS J204626.10+002337.7	20:46:26.11	00:23:37.8	QSO	0.332	Red	0.24	0.39
2SLAQ J204720.76+000007.7	20:47:20.76	00:00:07.8	CataclyV*	0.001	Blue	1.00	0.00
2SLAQ J204720.76+000007.7	20:47:20.76	00:00:07.7	CataclyV*	0.001	Blue	0.70	0.07
2SLAQ J204910.96+001557.2	20:49:10.95	00:15:57.5	Seyfert 1	0.363	Blue	0.41	0.07
VV2006 J204956.6-001201	20:49:56.62	-00:12:01.7	QSO	0.369	Blue	0.46	0.09
VV2006 J204956.6-001201	20:49:56.62	-00:12:01.7	QSO	0.369	Blue	0.53	0.08
VV2006 J205316.7+005920	20:53:16.77	00:59:21.1	QSO	4.299	–	–	–
2SLAQ J205352.03-001601.5	20:53:52.04	-00:16:01.5	QSO	0.363	Blue	0.68	0.11
2SLAQ J205614.55-004050.9	20:56:14.55	-00:40:50.6	Star	–	–	–	–
2SLAQ J205712.69+001211.3	20:57:12.69	00:12:11.4	QSO	0.335	Blue	0.50	0.11
SDSS J205740.76+005418.5	20:57:40.75	00:54:19.0	QSO	0.332	Red	0.13	0.68
Gaia DR2 6794425304909258752	20:58:06.45	-30:08:18.1	Candidate WD*	–	Blue	0.40	0.07
LEDA 687146	20:58:24.54	-32:43:22.5	Galaxy	–	Blue	1.00	0.00
2MASX J20584976-4420243	20:58:49.69	-44:20:24.7	Galaxy	0.018	Blue	0.98	0.02
6dFGS gJ205957.5-213935	20:59:57.53	-21:39:34.9	Galaxy	-0.001	Blue	0.72	0.06
SDSS J210014.12+004446.0	21:00:14.11	00:44:45.9	CataclyV*	0.000	Blue	0.57	0.10
SDSSCGB 52599.6	21:01:55.95	-00:31:24.9	Galaxy	–	Red	0.15	0.64
LEDA 598660	21:01:56.43	-39:23:40.3	Galaxy	–	Blue	0.70	0.03
QSO B2059-330	21:02:41.71	-32:52:44.1	QSO	3.280	Blue	0.76	0.07
QSO B2059-330	21:02:41.72	-32:52:44.4	QSO	3.280	Blue	0.98	0.02
LEDA 528866	21:03:02.23	-45:14:41.1	Galaxy	–	Blue	0.88	0.04
Gaia DR2 6808104805812408064	21:03:56.66	-21:47:27.1	Star	–	Blue	0.89	0.03
ESO 286-33	21:04:08.52	-43:32:03.2	IG	0.017	Blue	0.68	0.05
ESO 286-35	21:04:11.17	-43:35:33.8	GinGroup	0.017	Blue	0.58	0.15
LEDA 720203	21:04:21.46	-30:11:50.0	Galaxy	–	Red	0.06	0.19
GPM2009 J2104-0035 1	21:04:55.31	-00:35:21.8	EmG	0.005	Blue	0.75	0.15
LEDA 520361	21:05:20.69	-45:59:19.3	Galaxy	–	Blue	0.63	0.06
ESO 286-44	21:05:38.68	-42:46:52.4	Galaxy	0.008	Blue	0.71	0.13
PN G006.0-41.9	21:05:53.57	-37:08:40.4	PN	–	Blue	0.04	0.02
EC 21035-4032	21:06:48.02	-40:20:03.7	Star	–	Blue	0.38	0.11
2MASX J21071198-4733258	21:07:11.98	-47:33:25.2	GinPair	–	Blue	0.94	0.01
2MASX J21071385-4733258	21:07:13.86	-47:33:25.3	GinPair	0.015	Blue	1.00	0.00
GPM2009 J2112-0016 2	21:12:00.92	-00:16:49.2	EmG	0.012	Blue	0.97	0.03
6dFGS gJ211224.6-412854	21:12:24.59	-41:28:53.3	AGN	0.349	Blue	0.66	0.05

Table B1: –continued

Id Object	RA	Dec	Type	Redshift	Group	P(Blue)	P(Red)
						HAC	HDBSCAN
CRTS J211328.1+000332	21:13:28.17	00:03:32.6	EB*	–	Blue	1.00	0.00
ESO 402-20	21:15:19.13	−33:13:34.6	Galaxy	0.018	Blue	0.93	0.07
CTCV J2118-3412	21:18:04.28	−34:13:43.5	CataclyV*	–	Blue	0.53	0.06
AT20G J212302-291504	21:23:02.82	−29:15:04.0	Radio(cm)	–	Blue	0.52	0.08
CRTS CSS120613 J212655-012054	21:26:54.54	−01:20:54.1	Candidate CV*	–	Blue	0.32	0.06
LEDA 710984	21:27:08.26	−30:57:08.4	Galaxy	–	Blue	1.00	0.00
2SLAQ J212954.20-010323.3	21:29:54.22	−01:03:23.3	EmG	0.335	Blue	0.70	0.03
LBQS 2128-4555	21:31:29.53	−45:41:50.5	QSO	0.623	Blue	0.63	0.07
2SLAQ J213242.28-010309.0	21:32:42.29	−01:03:09.2	Galaxy	–	Blue	0.87	0.05
2SLAQ J213245.24+000146.4	21:32:45.26	00:01:46.8	Seyfert 1	0.234	Blue	0.28	0.07
2MASS J21333817+0126291	21:33:38.14	01:26:29.0	QSO	1.004	Blue	0.97	0.03
SDSS J213455.08+001056.9	21:34:55.09	00:10:56.8	QSO	3.289	Blue	0.76	0.03
WISEA J213649.75-012852.2	21:36:49.75	−01:28:52.2	QSO	3.280	Blue	1.00	0.00
QSO B2134-453	21:38:07.49	−45:08:18.0	QSO	4.360	–	–	–
2MASS J21381896+0112224	21:38:18.96	01:12:22.5	Seyfert 1	0.344	Blue	0.44	0.10
CRTS J213937.6-023913	21:39:37.58	−02:39:13.0	Candidate CV*	–	Blue	0.36	0.08
2SLAQ J214106.46+004733.3	21:41:06.44	00:47:33.5	QSO	2.452	Blue	0.45	0.08
SDSSCGB 15831.2	21:41:42.73	00:45:34.9	Galaxy	–	Blue	0.91	0.02
SDSS J214155.04-011734.3	21:41:55.04	−01:17:34.2	QSO	3.286	Blue	1.00	0.00
SDSS J214155.04-011734.3	21:41:55.04	−01:17:34.3	QSO	3.286	Blue	0.47	0.06
SN 2017hxv	21:44:22.94	−29:54:59.0	SN	0.019	Red	0.12	0.19
2SLAQ J214455.94+002305.8	21:44:55.92	00:23:06.1	EmG	0.330	Blue	0.86	0.05
6dFGS gJ214540.0-291937	21:45:40.01	−29:19:36.9	Galaxy	0.341	Red	0.17	0.22
2SLAQ J214830.60-004752.6	21:48:30.61	−00:47:52.6	EmG	0.332	Blue	0.90	0.03
2SLAQ J214830.60-004752.6	21:48:30.61	−00:47:52.5	EmG	0.332	–	–	–
SDSS J215002.69+011343.8	21:50:02.70	01:13:43.8	QSO	3.267	Blue	0.98	0.02
2SLAQ J215010.52-001000.6	21:50:10.53	−00:10:00.6	QSO	0.335	Blue	0.48	0.10
2dFGRS TGS406Z223	21:53:05.55	−31:28:17.9	Galaxy	0.019	Blue	0.54	0.09
2dFGRS TGS406Z223	21:53:05.55	−31:28:17.9	Galaxy	0.019	Blue	0.54	0.09
2dFGRS TGS406Z223	21:53:05.55	−31:28:17.9	Galaxy	0.019	Blue	0.54	0.09
2dFGRS TGS406Z223	21:53:05.55	−31:28:17.9	Galaxy	0.019	Blue	0.54	0.09
2MASX J21541799+0056318	21:54:18.00	00:56:31.9	Galaxy	0.010	Blue	1.00	0.00
LEDA 214792	21:56:13.83	−01:09:42.8	Galaxy	–	Blue	0.85	0.03
LEDA 214792	21:56:13.85	−01:09:43.2	Galaxy	–	Blue	0.97	0.03
SDSSCGB 16345.1	21:56:19.79	−01:10:03.6	Galaxy	0.016	Blue	0.78	0.12
SDSSCGB 16345.1	21:56:19.81	−01:10:03.7	Galaxy	0.016	Blue	0.79	0.12
2dFGRS TGS059Z257	21:57:20.89	−25:08:02.4	Galaxy	0.009	Blue	0.96	0.04
SDSS J215824.23-004413.7	21:58:24.28	−00:44:13.7	HII G	0.016	Blue	0.94	0.03
SDSS J215902.90-003318.4	21:59:02.89	−00:33:18.0	Galaxy	–	Blue	0.73	0.08
LEDA 214793	21:59:03.11	−01:57:18.3	Galaxy	–	Blue	0.66	0.05
LEDA 1136721	22:01:50.08	−00:42:26.7	Galaxy	0.018	Blue	0.96	0.04
2dFGRS TGS114Z230	22:02:07.08	−26:26:38.0	Galaxy	0.309	Blue	0.59	0.11
PB 5049	22:03:15.14	01:17:21.0	Star	–	Blue	0.06	0.03
2dFGRS TGS115Z105	22:04:53.68	−25:03:05.2	Galaxy	0.009	Blue	0.97	0.03
2SLAQ J220529.34-003110.6	22:05:29.34	−00:31:10.7	QSO	2.454	Blue	0.66	0.05
NGC 7204	22:06:55.31	−31:03:10.6	IG	0.009	Red	0.25	0.29
2dFGRS TGS251Z159	22:07:34.55	−28:39:29.3	Galaxy	0.018	Blue	0.58	0.14
NGC 7208	22:08:24.43	−29:03:03.6	GinGroup	0.009	Blue	0.96	0.04
2dFGRS TGS333Z140	22:08:51.96	−30:38:58.8	Galaxy	0.008	–	–	–
VV2006 J220852.0-010603	22:08:51.97	−01:06:03.7	QSO	0.351	Blue	0.46	0.09
VV2006 J220852.0-010603	22:08:51.97	−01:06:03.7	QSO	0.351	Blue	0.48	0.08
MCG-05-52-033a	22:08:55.90	−27:13:22.0	GinPair	0.009	Blue	0.78	0.06
2dFGRS TGS061Z180	22:09:19.05	−24:07:12.4	QSO	0.320	Red	0.16	0.17
2dFGRS TGS116Z088	22:09:22.91	−25:25:04.6	Galaxy	0.008	Blue	0.58	0.08
2QZ J220948.6-301357	22:09:48.63	−30:13:55.8	WD*	–	Blue	0.21	0.08
SDSSCGB 41857.2	22:09:51.35	01:09:00.0	Galaxy	0.149	Red	0.38	0.38
SDSS J220954.57-012717.6	22:09:54.57	−01:27:17.6	QSO	3.296	Blue	0.57	0.03
2QZ J221000.7-311400	22:10:00.75	−31:14:00.0	EmG	0.328	Blue	0.63	0.05

Table B1: –continued

Id Object	RA	Dec	Type	Redshift	Group	P(Blue)	P(Red)
						HAC	HDBSCAN
2dFGRS TGS116Z082	22:10:03.74	-25:20:07.3	Galaxy	0.009	Blue	0.99	0.01
2QZ J221005.7-275439	22:10:05.76	-27:54:38.7	Galaxy	0.330	Blue	0.95	0.03
6dFGS gJ221058.1-250431	22:10:58.01	-25:04:31.1	Galaxy	0.017	Blue	0.78	0.03
2QZ J221058.3-273930	22:10:58.33	-27:39:29.4	Galaxy	0.313	Blue	0.81	0.07
LSQ 12dwl	22:12:41.57	00:30:43.1	SN	0.014	Blue	0.51	0.10
VV2006 J221335.7-282542	22:13:35.65	-28:25:41.7	QSO	2.469	Blue	0.41	0.08
2dFGRS TGS175Z009	22:14:02.86	-27:32:21.4	Galaxy	0.014	Blue	1.00	0.00
2dFGRS TGS175Z009	22:14:02.88	-27:32:21.5	Galaxy	0.014	Blue	0.96	0.04
NGC 7229	22:14:03.23	-29:22:57.8	EmG	0.014	Blue	0.77	0.05
2dFGRS TGS254Z244	22:14:05.10	-29:22:52.9	Galaxy	0.015	Blue	0.97	0.03
ESO 467-25	22:14:24.23	-29:58:51.5	EmG	0.015	Blue	0.74	0.03
2dFGRS TGS254Z138	22:14:41.93	-28:26:39.6	Galaxy	0.012	Blue	1.00	0.00
2dFGRS TGS334Z074	22:14:47.16	-29:41:12.4	Galaxy	0.006	Blue	0.76	0.02
2QZ J221517.1-285358	22:15:17.10	-28:53:57.5	EmG	0.312	Blue	0.74	0.07
VV2006 J221532.6-281805	22:15:32.58	-28:18:03.9	QSO	1.330	Blue	0.67	0.04
2QZ J221630.0-290054	22:16:30.07	-29:00:53.3	EmG	0.330	Red	0.18	0.09
6dFGS gJ221706.5-303447	22:17:06.52	-30:34:46.1	Galaxy	0.337	Red	0.34	0.24
VV2006 J221722.5+010436	22:17:22.44	01:04:36.3	QSO	1.403	Blue	0.10	0.05
2dFGRS TGS176Z011	22:17:41.15	-27:21:54.6	Galaxy	0.009	Blue	0.76	0.03
SDSS J221813.90+001625.1	22:18:13.91	00:16:25.3	Galaxy	0.333	–	–	–
2MASX J22181503+0115169	22:18:15.03	01:15:16.9	Galaxy	0.049	Blue	0.80	0.04
SDSS J221817.26+003623.6	22:18:17.26	00:36:23.7	AGN	0.331	Red	0.08	0.20
2QZ J221819.4-271544	22:18:19.39	-27:15:44.2	Seyfert 1	0.355	Blue	0.44	0.09
2SLAQ J221846.76-011119.0	22:18:46.74	-01:11:18.8	Galaxy	–	Blue	0.77	0.03
2SLAQ J221846.76-011119.0	22:18:46.74	-01:11:18.8	Galaxy	–	Blue	0.84	0.03
SDSS J221852.63-010310.1	22:18:52.65	-01:03:10.5	Galaxy	0.016	Blue	0.69	0.11
2QZ J221925.9-305108	22:19:25.92	-30:51:07.7	EmG	0.307	Blue	0.66	0.04
SDSSCGB 28259.2	22:19:44.75	-00:14:40.0	Galaxy	–	Red	0.21	0.38
2QZ J221945.1-293414	22:19:45.08	-29:34:13.4	EmG	0.343	Blue	0.97	0.03
DD2013 W4+2-1 115196	22:19:53.86	00:29:04.8	Galaxy	0.087	Blue	0.61	0.11
2SLAQ J222021.37+004040.2	22:20:21.36	00:40:40.5	Star	–	Blue	0.57	0.06
2QZ J222113.6-280421	22:21:13.62	-28:04:20.9	Seyfert 1	0.332	Red	0.27	0.18
2dFGRS TGS337Z130	22:22:54.92	-30:42:28.4	Galaxy	0.014	Blue	0.94	0.02
6dFGS gJ222313.7-285844	22:23:13.70	-28:58:44.6	Galaxy	0.006	Blue	0.45	0.11
2SLAQ J222332.83-010614.8	22:23:32.84	-01:06:14.8	QSO	2.460	Blue	0.52	0.06
2QZ J222336.0-283140	22:23:36.03	-28:31:39.6	EmG	0.333	Blue	0.82	0.07
2SLAQ J222403.36-005724.2	22:24:03.35	-00:57:24.2	QSO	0.313	Blue	0.56	0.11
2SLAQ J222403.36-005724.2	22:24:03.36	-00:57:24.1	QSO	0.313	Blue	0.48	0.11
2QZ J222416.2-292421	22:24:16.26	-29:24:21.7	Candidate CV*	–	Blue	0.59	0.11
2dFGRS TGS338Z083	22:27:38.90	-31:08:10.3	Galaxy	0.015	Blue	0.80	0.06
2SLAQ J222825.11-002217.4	22:28:25.12	-00:22:17.2	Galaxy	–	Red	0.51	0.18
LEDA 711478	22:28:47.80	-30:54:43.2	Galaxy	–	Blue	0.41	0.12
LEDA 711478	22:28:47.82	-30:54:43.2	Galaxy	–	Blue	0.43	0.11
2dFGRS TGS337Z266	22:28:53.67	-30:58:51.4	Galaxy	0.013	Blue	0.85	0.05
2dFGRS TGS337Z266	22:28:53.67	-30:58:51.4	Galaxy	0.013	Blue	0.80	0.03
SDSS J222923.00-020042.7	22:29:23.00	-02:00:42.4	QSO	3.294	–	–	–
2SLAQ J222956.53+003126.5	22:29:56.54	00:31:26.5	QSO	1.340	Blue	0.45	0.07
2dFGRS TGS338Z165	22:30:01.84	-29:35:52.7	Galaxy	0.010	Blue	0.83	0.02
2dFGRS TGS338Z165	22:30:01.85	-29:35:52.6	Galaxy	0.010	Blue	0.80	0.05
NAME Kinman Dwarf	22:30:36.83	-00:06:35.8	BlueCompG	0.006	Blue	0.58	0.14
LEDA 1149494	22:31:06.00	-00:11:43.9	Galaxy	–	Blue	1.00	0.00
2QZ J223114.0-312005	22:31:13.95	-31:20:04.4	Star	–	Blue	0.77	0.08
VV2006 J223251.7-303250	22:32:51.74	-30:32:49.6	QSO	0.350	Blue	0.31	0.07
2QZ J223342.5-301936	22:33:42.56	-30:19:35.4	Galaxy	0.324	Blue	0.80	0.06
2MASS J22340663+0001199	22:34:06.67	00:01:20.8	Star	–	Red	0.06	0.20
FASTT 1560	22:34:39.93	00:41:27.5	CataclyV*	0.001	Blue	0.54	0.07
2dFGRS TGS414Z208	22:34:56.56	-31:08:44.1	Galaxy	0.009	Blue	1.00	0.00
2dFGRS TGS414Z208	22:34:56.57	-31:08:44.1	Galaxy	0.009	Blue	1.00	0.00

Table B1: –continued

Id Object	RA	Dec	Type	Redshift	Group	P(Blue)	P(Red)
						HAC	HDBSCAN
SDSS J223508.41-005359.3	22:35:08.42	-00:53:59.4	Seyfert 2	0.328	Red	0.26	0.32
SDSS J223508.41-005359.3	22:35:08.43	-00:53:59.4	Seyfert 2	0.328	Red	0.33	0.61
2QZ J223532.2-294634	22:35:32.24	-29:46:33.0	EmG	0.325	Blue	0.82	0.03
2SLAQ J223543.05-005436.5	22:35:43.04	-00:54:36.6	Galaxy	–	Blue	0.81	0.11
2SLAQ J223543.05-005436.5	22:35:43.05	-00:54:36.6	Galaxy	–	Blue	0.67	0.02
2SLAQ J223543.05-005436.5	22:35:43.06	-00:54:36.4	Galaxy	–	Blue	0.50	0.07
SDSS J223543.94-003931.4	22:35:43.93	-00:39:32.1	low-mass*	0.000	Red	0.15	0.18
EKS96 NGC 7314 28	22:35:44.87	-26:02:27.4			HII	–	Blue
EKS96 NGC 7314 43	22:35:45.40	-26:02:10.8	HII	–	Blue	0.68	0.02
EKS96 NGC 7314 71	22:35:46.29	-26:04:29.1	HII	–	Blue	0.80	0.09
EKS96 NGC 7314 130	22:35:48.23	-26:01:24.0	HII	–	Blue	0.91	0.07
VV2006 J223633.5+002652	22:36:33.54	00:26:52.8	QSO	1.354	Blue	0.69	0.07
SDSS J223649.60+005413.5	22:36:49.60	00:54:13.8	QSO	3.313	–	–	–
2SLAQ J223723.84-010120.3	22:37:23.88	-01:01:19.2	Galaxy	–	Blue	0.97	0.03
SDSS J223729.86-010549.1	22:37:29.86	-01:05:49.3	HB*	-0.001	–	–	–
PHL 354	22:38:23.25	-00:57:08.2	QSO	0.361	Blue	0.34	0.06
PHL 354	22:38:23.26	-00:57:08.1	QSO	0.361	Blue	0.43	0.08
2SLAQ J223844.30-005655.3	22:38:44.29	-00:56:55.3	QSO	1.357	Blue	0.53	0.08
LEDA 131686	22:41:19.49	-39:58:23.3	Galaxy	–	Blue	0.72	0.05
2QZ J224149.5-301945	22:41:49.50	-30:19:44.5	Galaxy	0.322	Blue	0.66	0.08
GDB2008 503	22:43:16.38	-39:51:39.9	Galaxy	0.007	Blue	0.80	0.05
GDB2008 504	22:43:19.40	-39:52:44.4	Galaxy	0.007	Blue	0.49	0.13
GDB2008 509	22:43:25.11	-39:55:20.0	Galaxy	0.327	Red	0.11	0.88
SDSS J224352.11-002259.7	22:43:52.21	-00:22:59.9	Galaxy	0.010	Blue	0.97	0.03
2SLAQ J224531.20-004509.4	22:45:31.20	-00:45:09.4	QSO	1.368	Blue	0.58	0.05
2SLAQ J224531.20-004509.4	22:45:31.20	-00:45:09.3	QSO	1.368	Blue	0.31	0.06
SDSS J224539.94-002419.7	22:45:39.94	-00:24:19.6	QSO	3.280	Blue	0.98	0.02
2MASS J22495608+0002182	22:49:56.08	00:02:18.4	QSO	3.307	Blue	0.88	0.07
2SLAQ J225012.91-003959.0	22:50:12.92	-00:39:58.9	Galaxy	–	Blue	0.78	0.08
SDSS J225149.74-002811.7	22:51:49.75	-00:28:11.4	QSO	3.228	Blue	0.97	0.03
2QZ J225157.1-292451	22:51:57.10	-29:24:50.8	EmG	0.318	Blue	0.39	0.06
2SLAQ J225257.45+002731.5	22:52:57.44	00:27:31.6	Star	–	Blue	0.59	0.12
2QZ J225352.9-300944	22:53:52.96	-30:09:43.7	Seyfert 1	0.326	Blue	0.26	0.09
VV2006 J225411.2-312712	22:54:11.15	-31:27:11.3	QSO	1.360	Blue	0.71	0.04
SDSS J225411.96-004949.5	22:54:11.96	-00:49:49.4	QSO	3.297	Blue	0.50	0.06
SDSS J225411.96-004949.5	22:54:11.96	-00:49:49.3	QSO	3.297	Blue	0.99	0.01
2QZ J225503.9-301914	22:55:03.89	-30:19:13.3	EmG	0.326	Blue	0.99	0.01
2QZ J225908.1-312717	22:59:08.12	-31:27:16.7	Star	–	Blue	0.30	0.07
2SLAQ J230030.09-003005.9	23:00:30.09	-00:30:05.8	Galaxy	–	Blue	0.61	0.07
2SLAQ J230201.20+003047.2	23:02:01.20	00:30:47.3	QSO	1.344	Blue	0.63	0.05
VV2006 J230235.5-285630	23:02:35.44	-28:56:29.7	QSO	0.368	Blue	0.60	0.07
2SLAQ J230316.40-001211.5	23:03:16.41	-00:12:11.4	QSO	1.516	Blue	0.60	0.08
V* HY Psc	23:03:51.63	01:06:51.4	CataclyV*	-0.000	Blue	0.67	0.07
SDSS J230428.31+005701.2	23:04:28.34	00:57:01.2			Blue	0.56	0.11
2SLAQ J230444.16-010251.7	23:04:44.16	-01:02:51.5	QSO	1.377	Blue	0.44	0.08
LEDA 1122038	23:08:10.78	-01:17:58.5	Galaxy	–	Blue	0.74	0.06
SDSS J230855.49+003705.6	23:08:55.49	00:37:05.7	QSO	1.784	Blue	1.00	0.00
ESO 469-15	23:08:55.60	-30:51:28.2	GinGroup	0.005	Blue	0.73	0.14
VV2006 J230914.4-305913	23:09:14.31	-30:59:12.5			Blue	0.61	0.05
2MASS J23094616+0000496	23:09:46.15	00:00:49.1	Seyfert 1	0.352	Blue	0.61	0.10
2MASS J23094616+0000496	23:09:46.16	00:00:49.0	Seyfert 1	0.352	Blue	0.65	0.11
GPM2009 J2310-0109 2	23:10:41.99	-01:09:48.0	EmG	0.012	Blue	0.78	0.07
VV2006 J231135.1-312644	23:11:35.12	-31:26:44.1	QSO	1.350	Blue	0.58	0.04
2dFGRS TGS422Z155	23:12:08.96	-31:04:13.3	Galaxy	0.165	Red	0.43	0.21
2SLAQ J231231.36-011137.5	23:12:31.36	-01:11:37.3	QSO	1.360	Blue	0.71	0.05
SDSS J231259.07+010805.6	23:12:59.06	01:08:05.9	QSO	3.295	Blue	0.84	0.04
VV2006 J231311.9-004538	23:13:11.91	-00:45:38.0	QSO	1.364	Blue	0.54	0.04
SDSS J231351.87-011031.9	23:13:51.86	-01:10:30.8	HII G	0.012	Blue	0.84	0.08

Table B1: –continued

Id Object	RA	Dec	Type	Redshift	Group	P(Blue)	P(Red)
						HAC	HDBSCAN
2MASX J23145046+0123280	23:14:50.52	01:23:26.7	LSB G	0.016	Blue	1.00	0.00
VV2006 J231519.4-303857	23:15:19.39	-30:38:57.2	QSO	1.356	Blue	0.81	0.05
V* CC Scl	23:15:31.78	-30:48:48.7	CataclyV*	–	Blue	0.70	0.10
VV2006 J231652.0+005125	23:16:52.04	00:51:25.9	QSO	3.229	Blue	0.80	0.03
3XMM J231742.5+000535	23:17:42.61	00:05:35.3	Seyfert 1	0.321	Blue	0.56	0.06
VV2006 J231942.8-302629	23:19:42.76	-30:26:29.5	QSO	2.473	Blue	0.83	0.08
LEDA 71137	23:20:35.21	-00:52:50.9	Galaxy	0.015	Blue	0.64	0.08
LEDA 71137	23:20:35.22	-00:52:50.8	Galaxy	0.015	Blue	0.56	0.08
2QZ J232126.5-310730	23:21:26.51	-31:07:29.5	Galaxy	0.309	Blue	1.00	0.00
SIG2010 389821	23:23:31.32	01:08:06.0	RRLyr	–	Blue	0.86	0.02
GALEX 2417063145906373262	23:24:20.34	-00:06:25.0	HII	–	Blue	0.10	0.04
GPM2009 J2324-0006	23:24:21.37	-00:06:29.4	HII G	0.009	Blue	0.24	0.08
2SLAQ J232457.75+002153.2	23:24:57.75	00:21:53.4	QSO	0.345	Blue	0.20	0.07
2SLAQ J232524.40+004612.0	23:25:24.43	00:46:12.2	Galaxy	0.016	Blue	0.87	0.06
2MASS J23255145-0140232	23:25:51.48	-01:40:23.8	CataclyV*	–	Blue	0.33	0.10
VV2006c J232555.5-003710	23:25:55.51	-00:37:10.7	Seyfert 1	0.332	–	–	–
SDSS J232743.68-020055.8	23:27:43.70	-02:00:55.7	BlueCompG	0.018	Blue	0.13	0.05
6dFGS gJ232744.4-020047	23:27:44.38	-02:00:46.8	Galaxy	0.018	Blue	0.10	0.04
LEDA 1127711	23:28:12.30	-01:03:44.8	HII G	0.009	Blue	0.79	0.06
GD 1662	23:29:00.44	-29:46:46.0	CataclyV*	0.000	Blue	0.55	0.08
SDSS J233104.38-004237.2	23:31:04.40	-00:42:37.1	QSO	1.353	Red	0.53	0.09
2MASS J23315973-0048192	23:31:59.77	-00:48:18.5	Galaxy	0.017	Blue	0.99	0.01
2QZ J233254.8-305844	23:32:54.78	-30:58:43.8	EmG	0.329	Blue	0.58	0.07
SDSS J233256.68+011122.9	23:32:56.68	01:11:23.1	BCIG	0.382	–	–	–
SDSS J233300.21-002030.5	23:33:00.22	-00:20:30.5	QSO	3.328	Blue	0.95	0.05
VV2006 J233438.5+002341	23:34:38.55	00:23:41.9	QSO	1.385	Blue	0.46	0.07
2MASX J23352102+0110271	23:35:20.98	01:10:27.4	Galaxy	0.085	Red	0.45	0.31
2SLAQ J233522.69-000635.2	23:35:22.69	-00:06:35.2	QSO	1.373	Blue	0.53	0.07
LEDA 135900	23:36:46.97	00:37:23.8	LSB G	0.009	Blue	0.99	0.01
VV2006 J233722.0+002239	23:37:22.02	00:22:39.2	QSO	1.377	Blue	0.46	0.06
2XMM J233731.7+002559	23:37:31.79	00:25:59.9	AGN	0.314	Blue	0.72	0.13
DES J233747.57+001742.6	23:37:47.57	00:17:42.8	GinCl	–	–	–	–
RESOLVE rf772	23:40:38.43	-00:53:30.6	Galaxy	0.019	Blue	0.66	0.07
VV2006 J234329.1-300200	23:43:29.16	-30:02:00.1	QSO	1.358	Blue	0.53	0.07
2SLAQ J234440.53-001205.8	23:44:40.53	-00:12:06.1	CataclyV*	–	Blue	0.40	0.06
LEDA 1109937	23:48:23.99	-01:47:31.1	Galaxy	–	Blue	1.00	0.00
2dFGRS TGS356Z227	23:50:01.55	-30:11:07.1	Galaxy	0.010	Blue	0.63	0.07
2SLAQ J235115.66-000000.0	23:51:15.66	-00:00:00.0	Galaxy	–	Blue	0.23	0.05
2SLAQ J235115.66-000000.0	23:51:15.68	-00:00:00.2	Galaxy	–	Blue	0.55	0.08
VV2006 J235546.2-002342	23:55:46.14	-00:23:42.8	QSO	3.245	Blue	0.99	0.01
VV2006 J235718.4+004350	23:57:18.37	00:43:50.5	QSO	4.366	Red	0.04	0.10
SDSS J235805.25-012153.9	23:58:05.25	-01:21:53.9	QSO	1.368	Blue	0.63	0.04

Table B2: Espectra from SDSS DR16

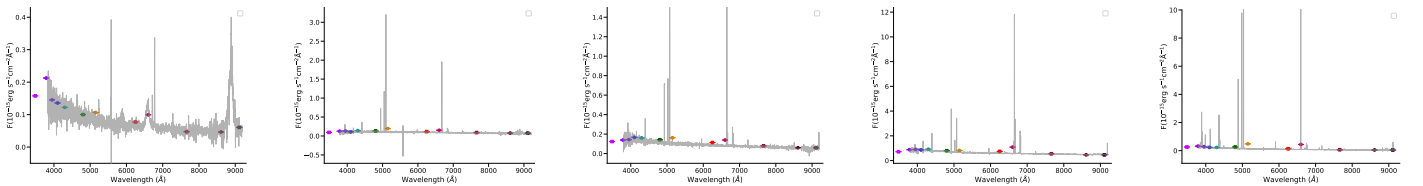


Table B2: –continued

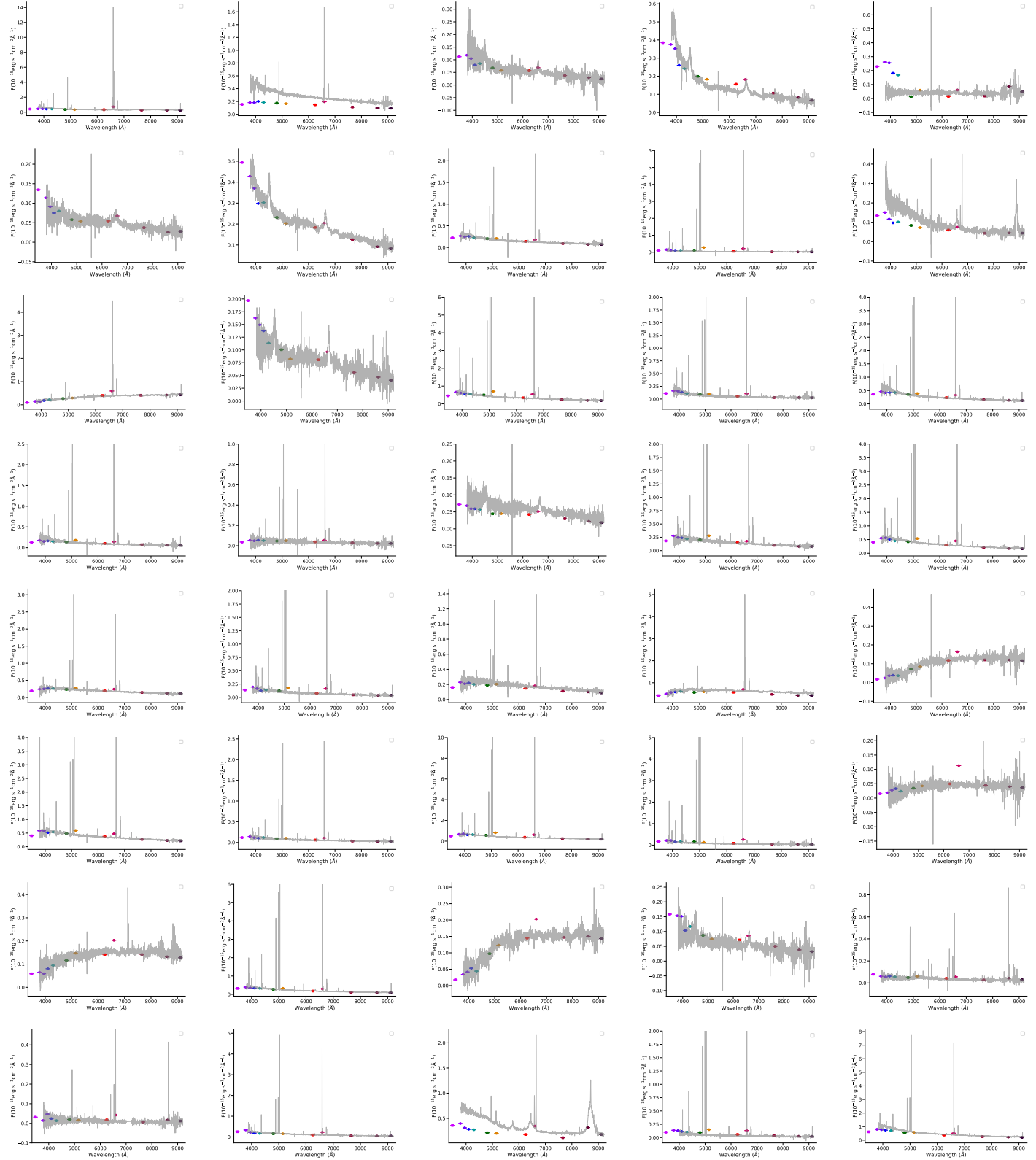


Table B2: –continued

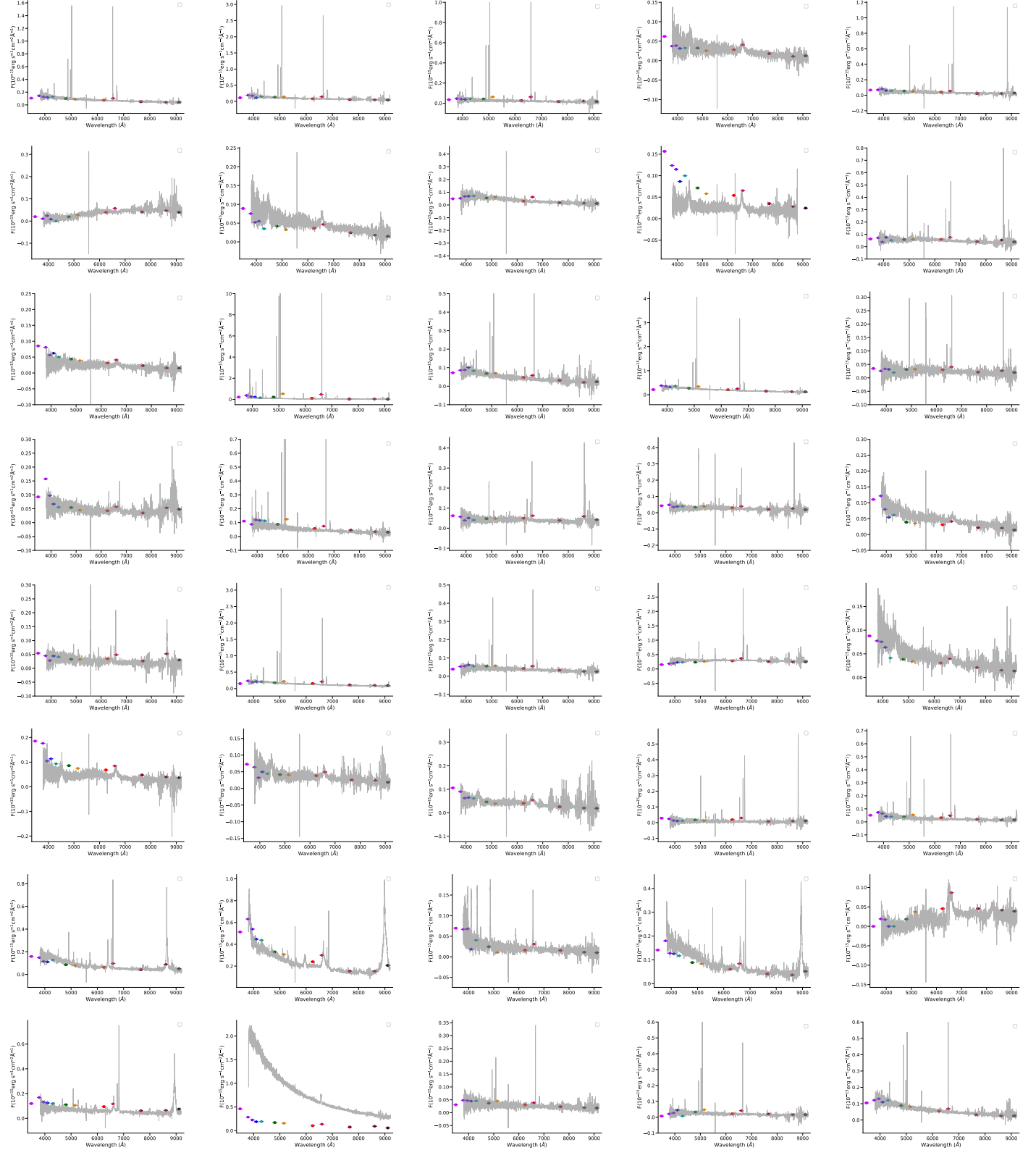


Table B2: –continued

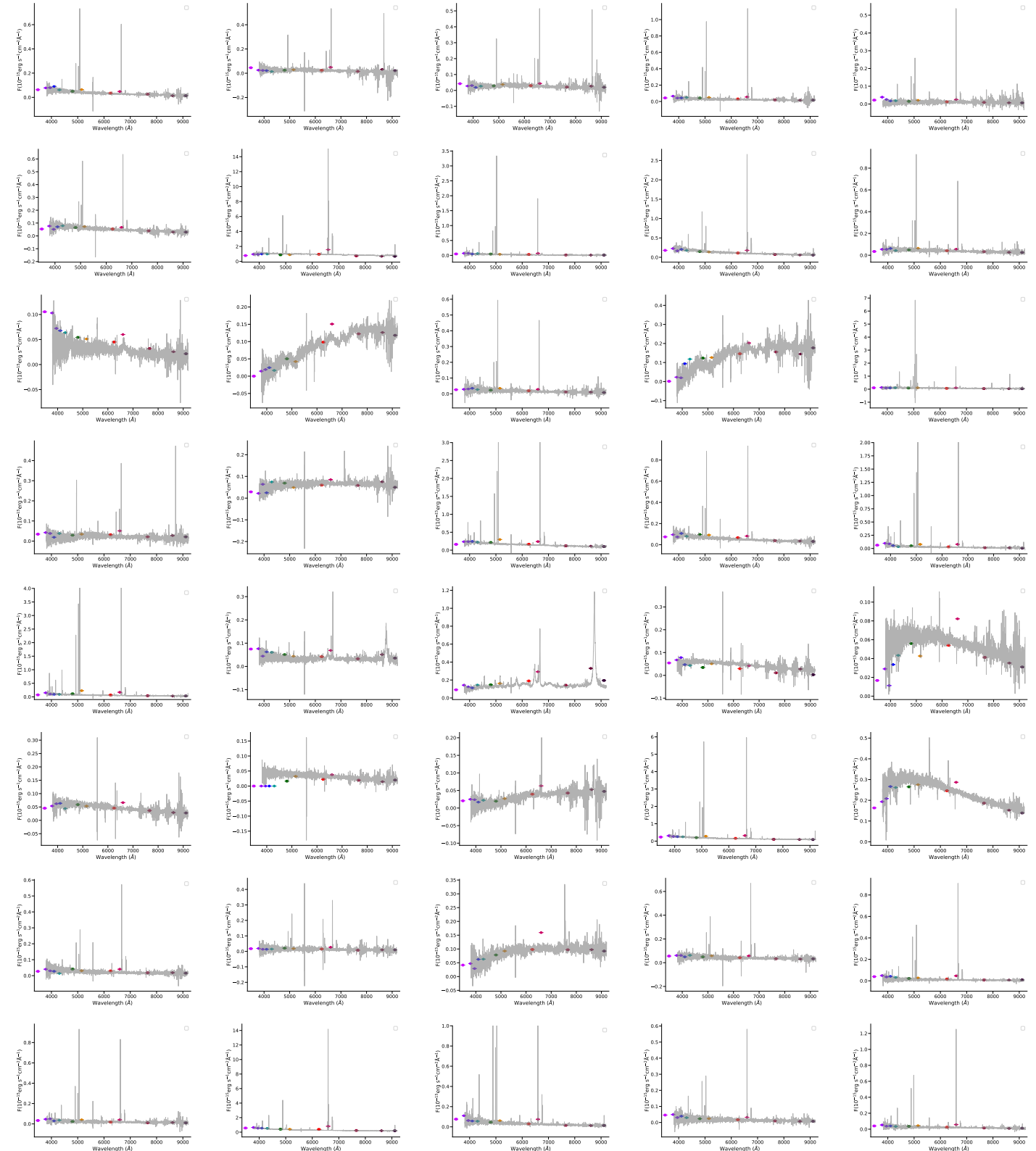


Table B2: –continued

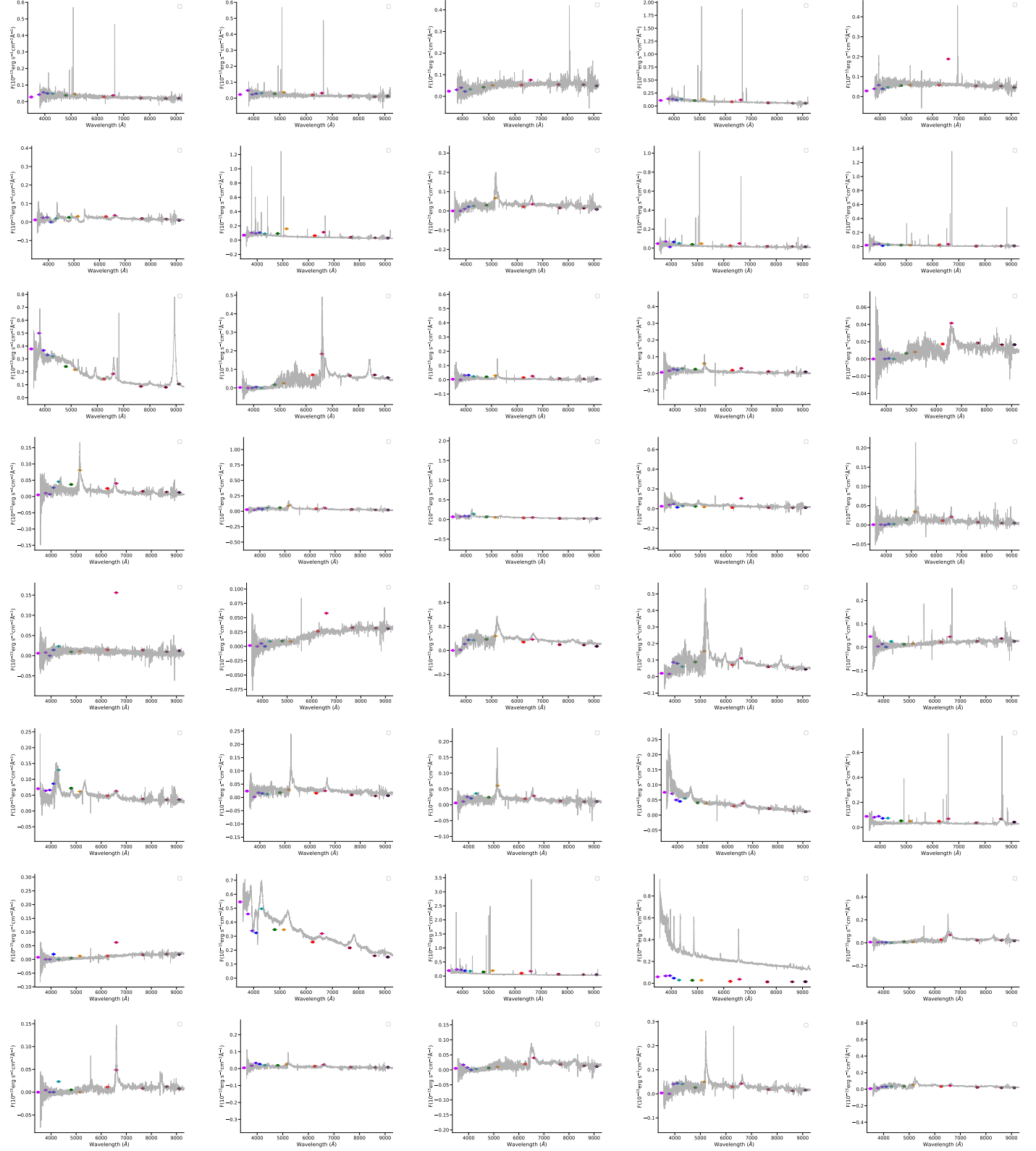


Table B2: –continued

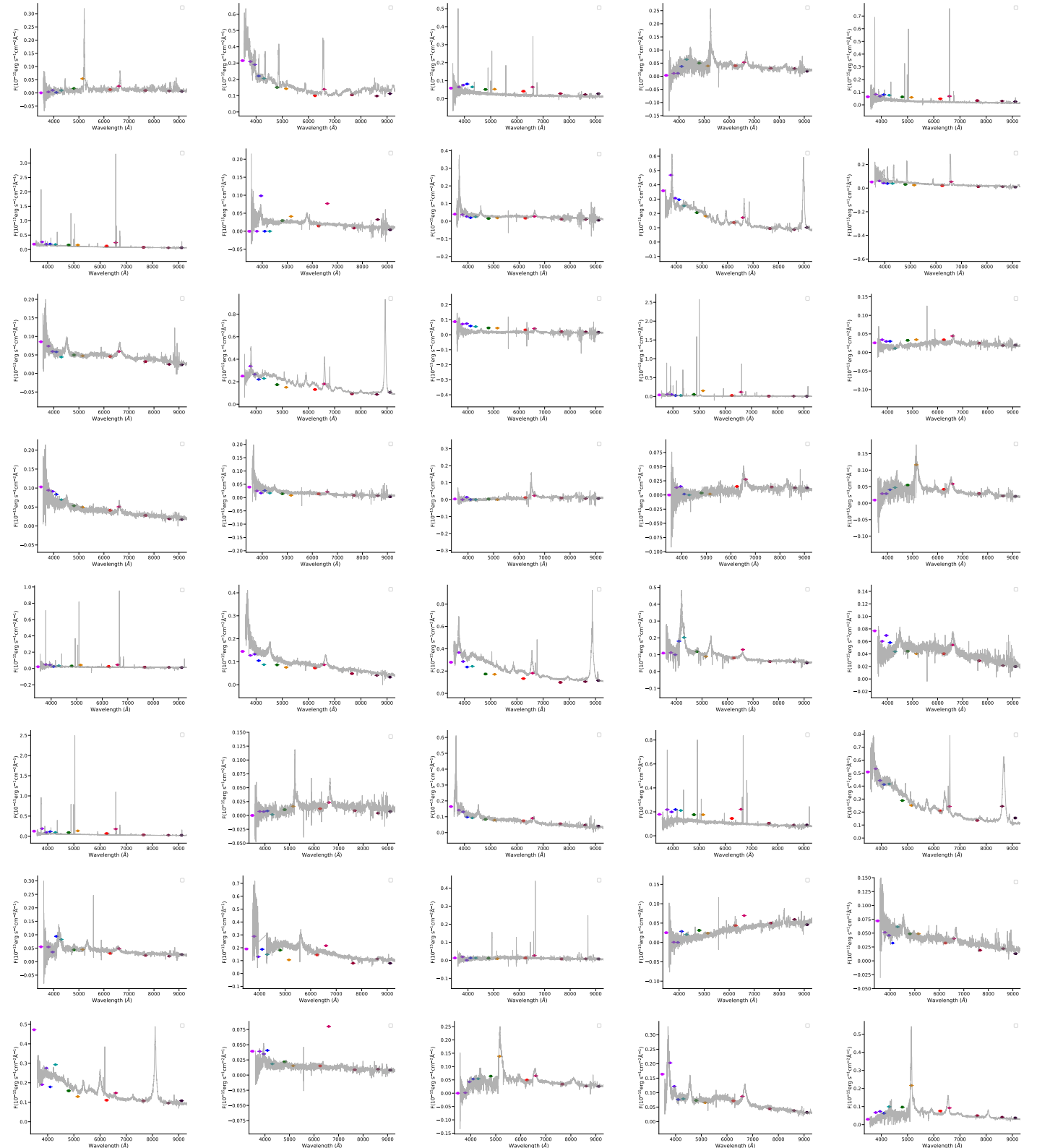


Table B2: –continued

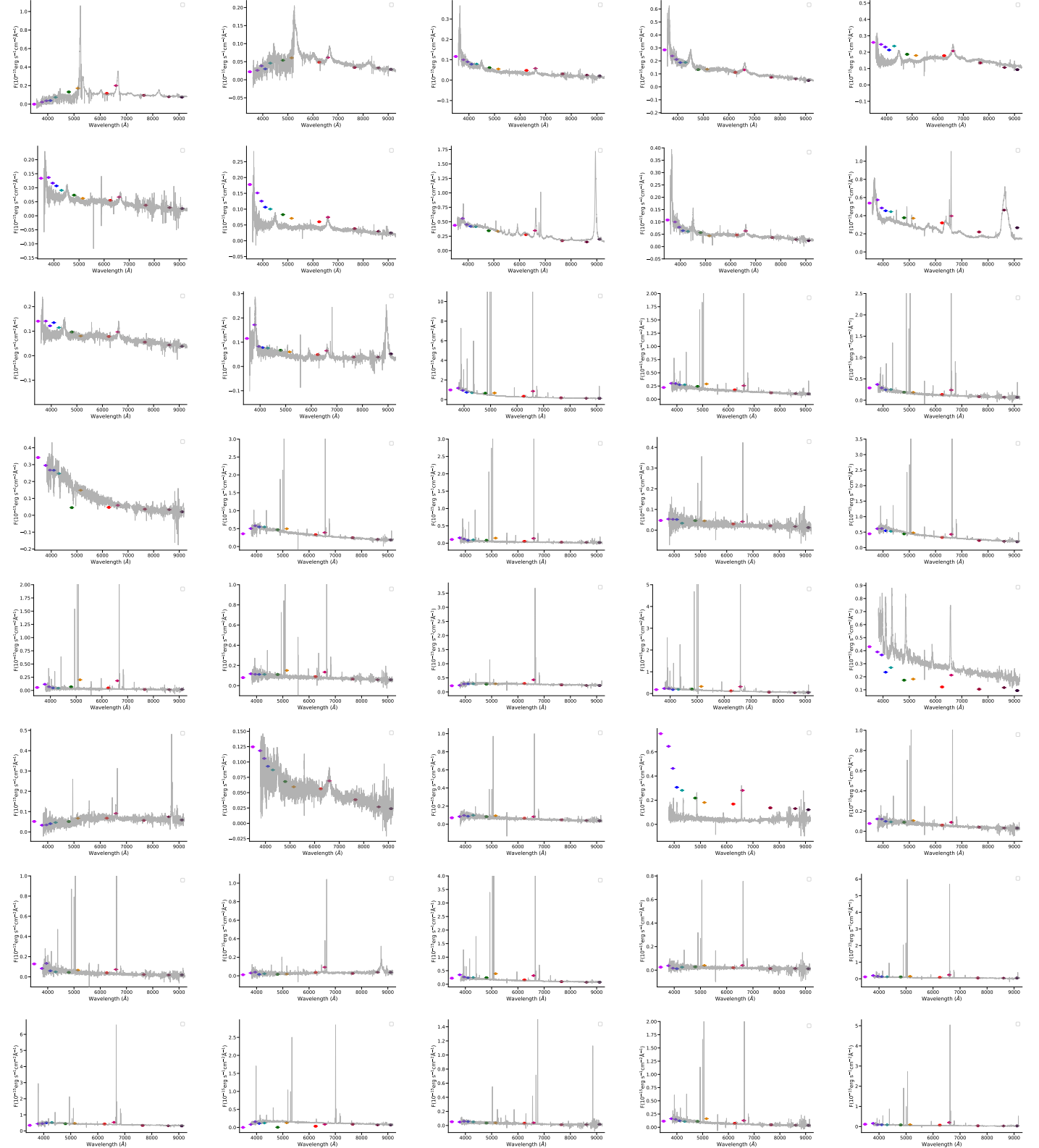


Table B2: –continued

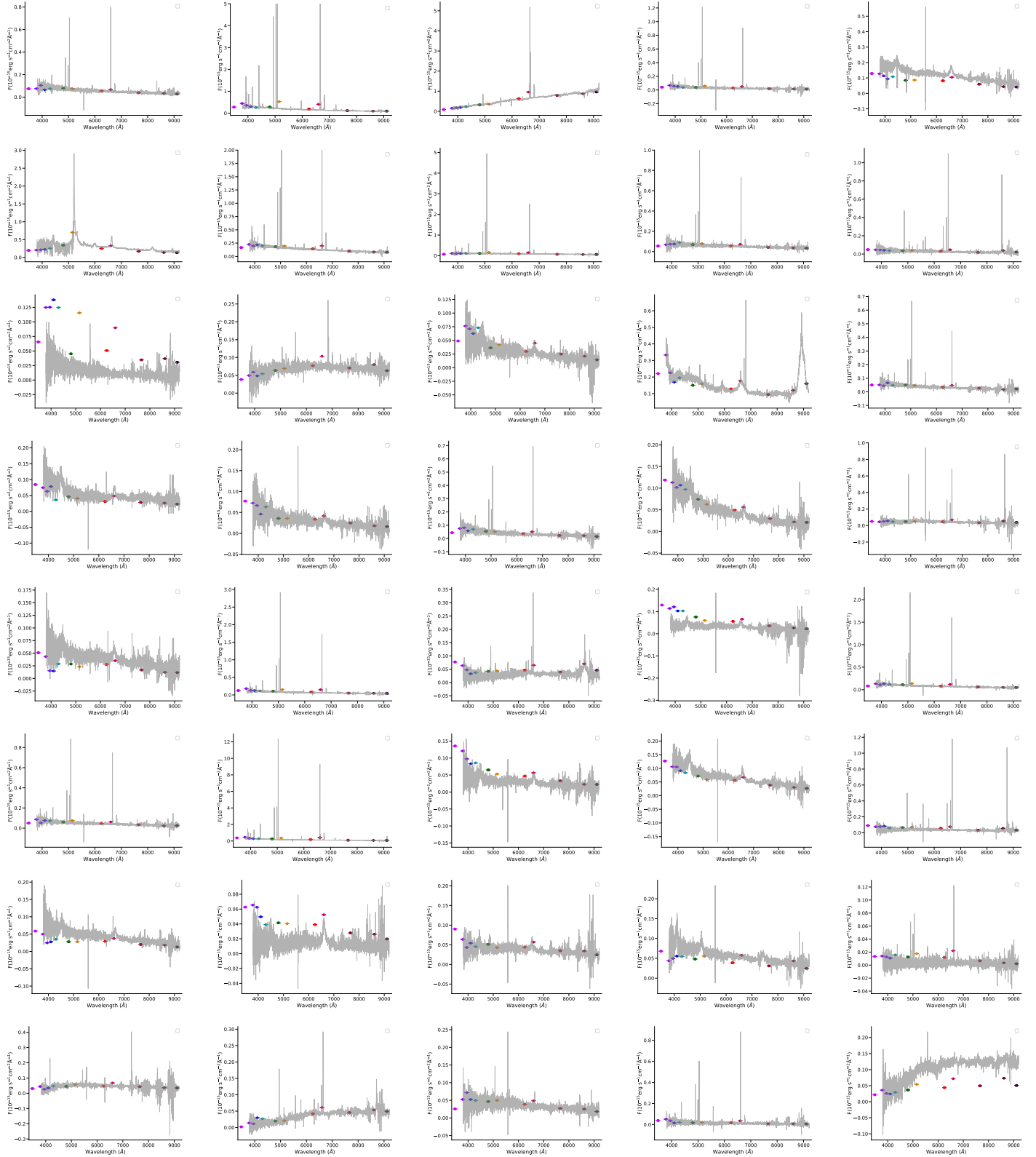


Table B2: –continued

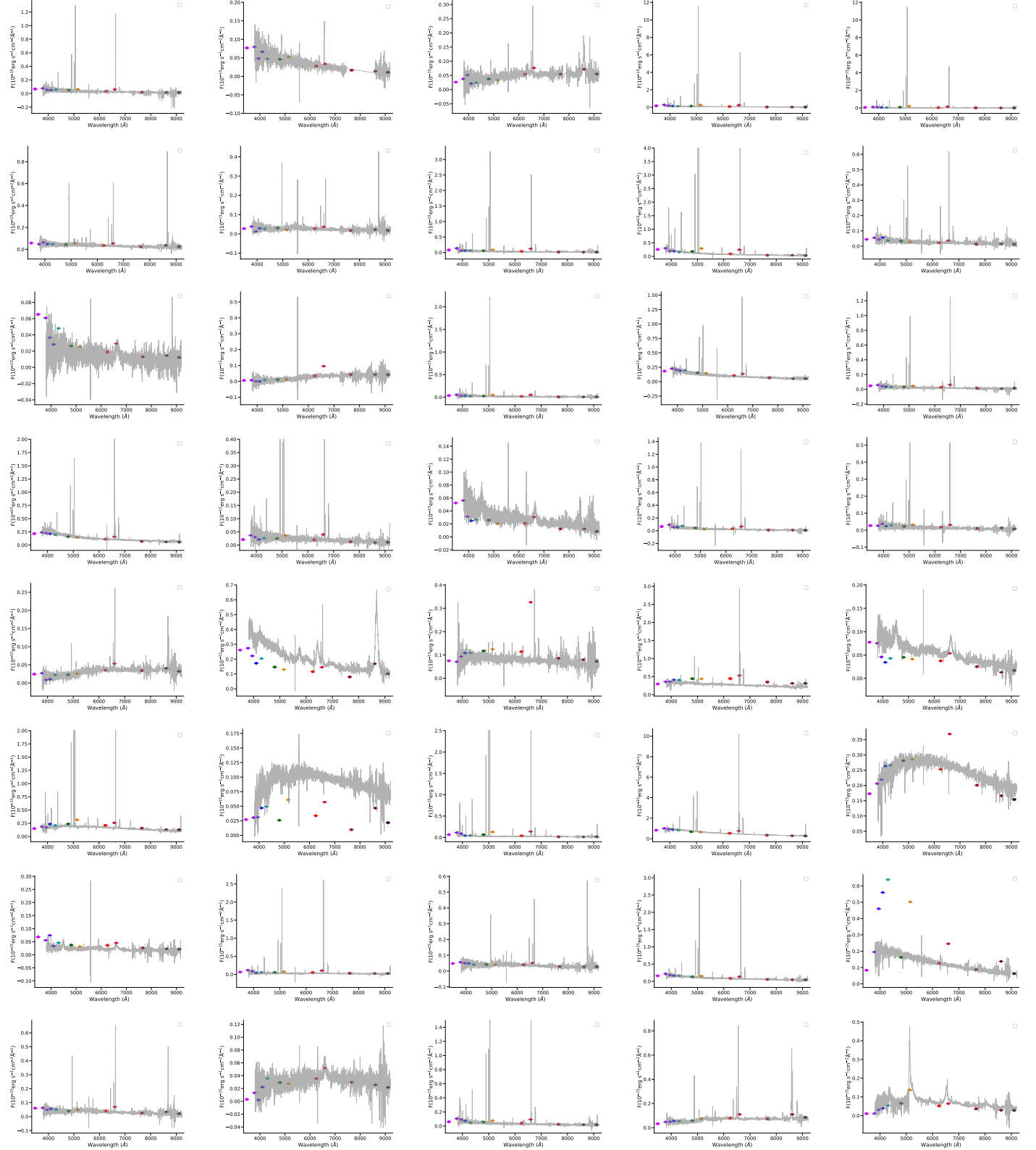


Table B2: –continued

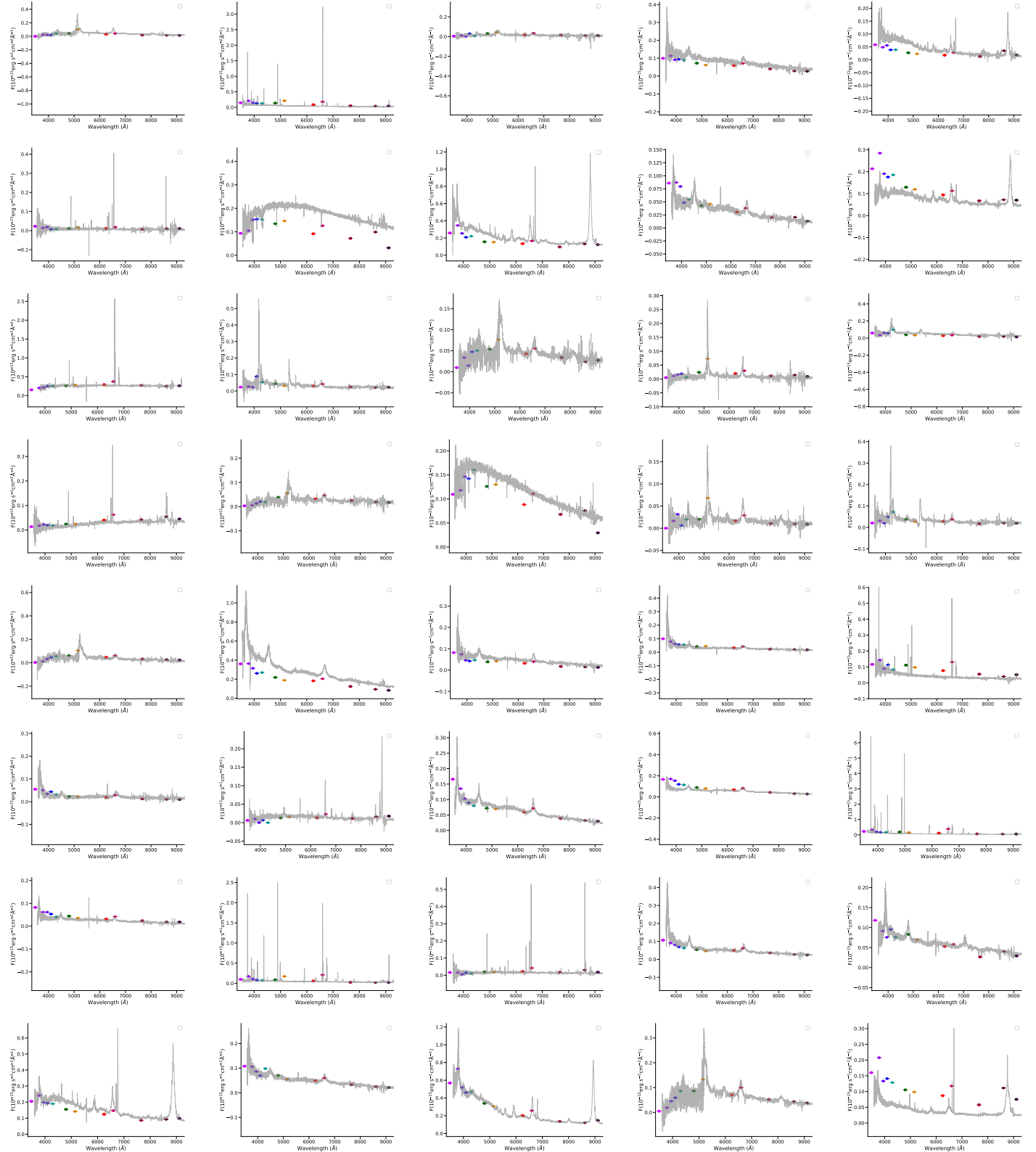


Table B2: –continued

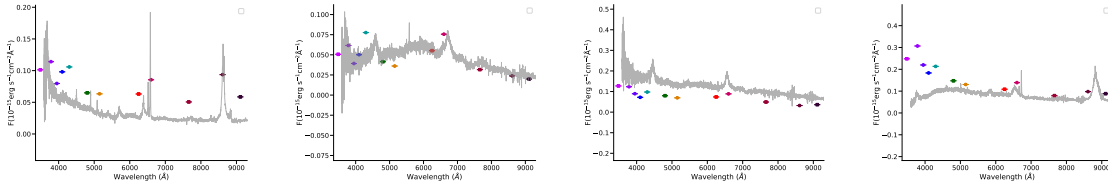


Table B3: Espectra from LAMOST DR6

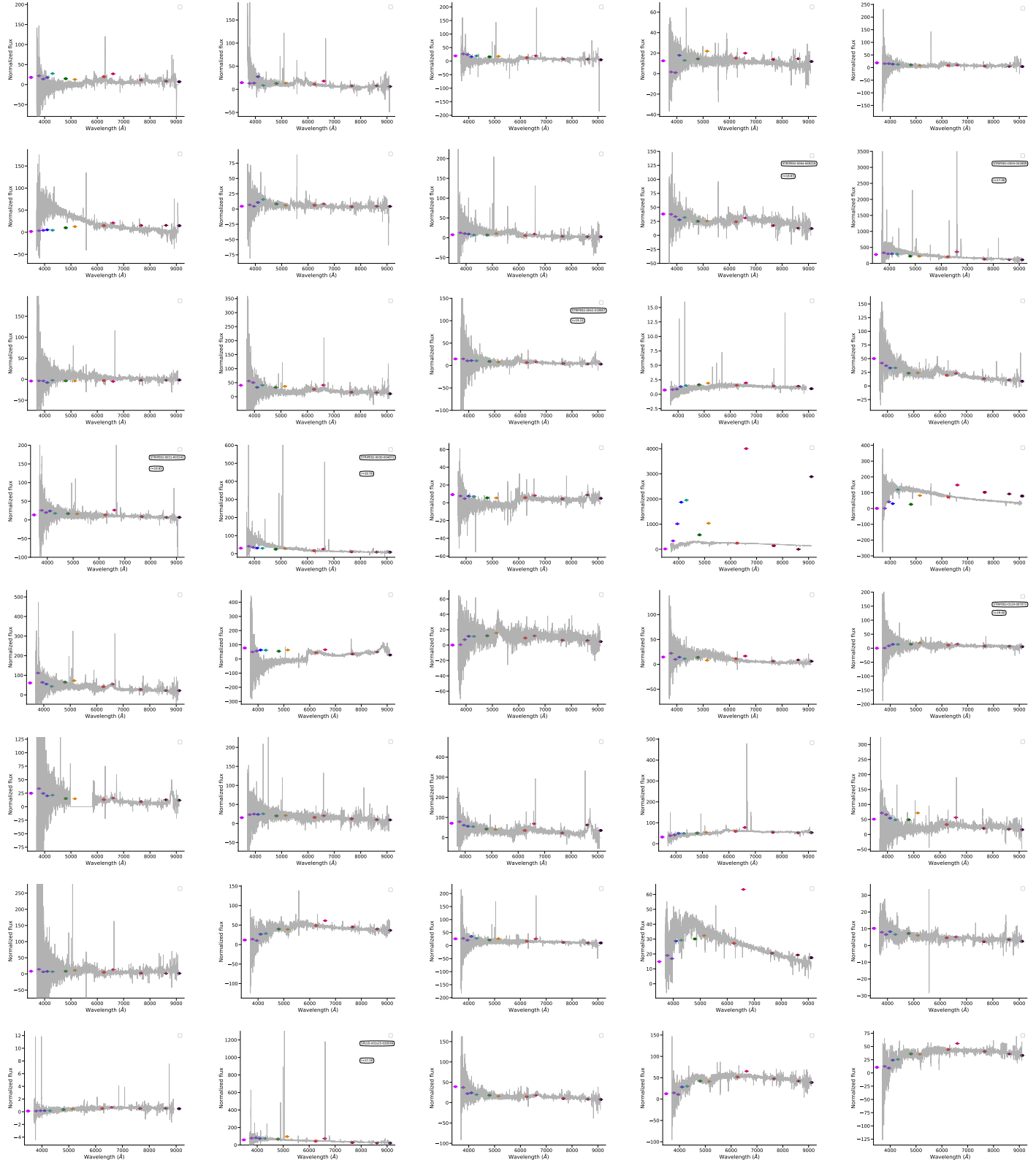


Table B3: –continued

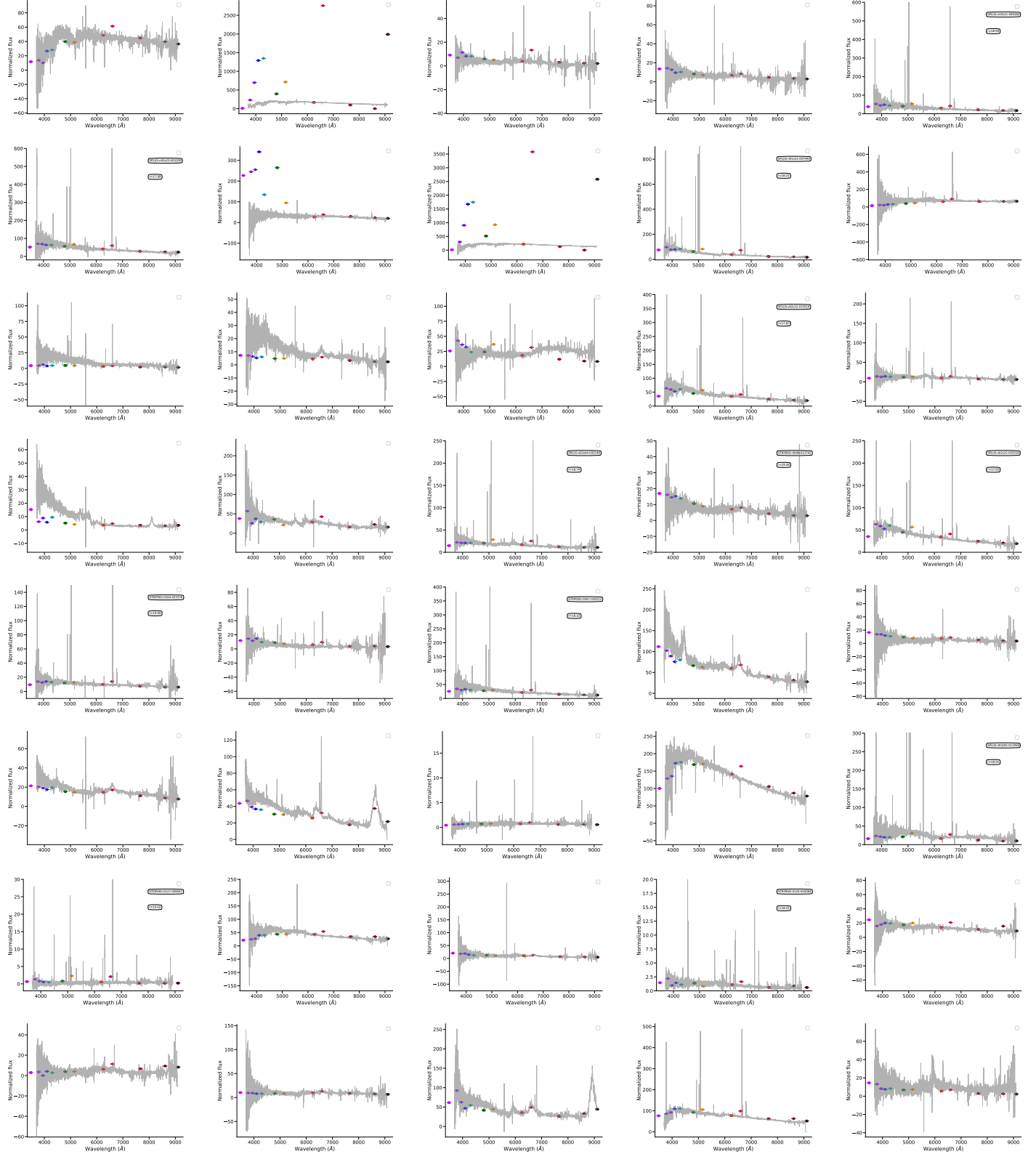
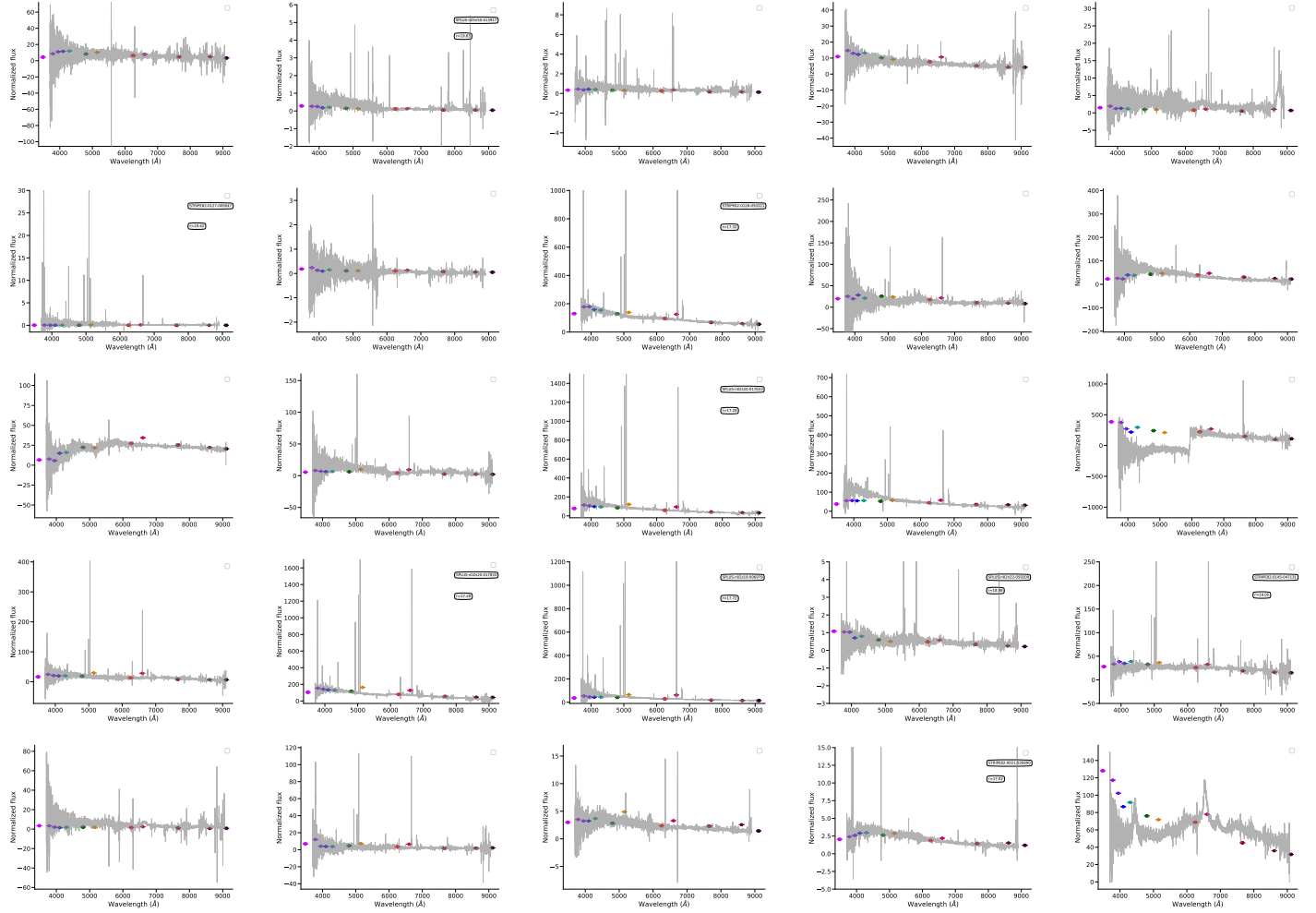


Table B3: –continued



This paper has been typeset from a  $\text{\TeX}/\text{\LaTeX}$  file prepared by the author.